DELIVERABLE D2.2

Optimization of the pre-conceptual design of the MSFR

Evaluation and Viability of Liquid Fuel Fast Reactor System EVOL

Contract (grant agreement) number: 249696

Author(s): Mariya Brovchenko (CNRS/IN2P3/LPSC), Elsa Merle-Lucotte (Grenoble INP / PHELMA, CNRS/IN2P3/LPSC), Hervé Rouch (INOPRO IAO), Fabio Alcaro (POLITO), Manuele Aufiero (POLIMI), Antonio Cammi (POLIMI), Sandra Dulla (POLITO), Olga Feynberg (KI), Lodewijk Frima (TU Delft), Olivier Geoffroy (INOPRO IAO), Daniel Heuer (CNRS/IN2P3/LPSC), Victor Ignatiev (KI), Jan-Leen Kloosterman (TU-Delft), Danny Lathouwers (TU Delft), Axel Laureau (CNRS/IN2P3/LPSC), Lelio Luzzi (POLIMI), Bruno Merk (HZDR), Piero Ravetto (POLITO), Andrei Rineiski (KIT), Pablo Rubiolo (Grenoble INP/PHELMA, CNRS/IN2P3/LPSC), Li Rui (KIT), Maté Szieberth (BME), Shisheng Wang (KIT), Bogdan Yamaji (BME) *et al*

Date of issue of this report: version of 09/24/2013

Outline

1. Introduction

In the frame of the EVOL project, the first objective of the WP2 “Design&Safety” addresses the improvement of the core geometry of the MSFR. Since the partners of WP2 (and of the MARS project) use different numerical tools for the reactor analysis, a comparative evaluation of the existing codes was necessary as a first step. This evaluation comprises two sets of benchmark: the first one focused on the neutronics aspects of the reactor, while the second one is oriented towards the system thermal-hydraulic behavior to further optimize the reactor design.

The neutronic benchmark was carried out using different reactor working parameters with two aims: firstly, to compare the results of the different codes at various working conditions. Secondly, to use these results to perform an initial optimization of the core parameters which would allow defining a reference design to be used for the second set of benchmark studies. Special emphasis was given in the neutronic benchmark, to the adequacy of the codes to correctly account for the effects of the presence of a liquid fuel and a fast neutron spectrum in the core of the MSFR. As already mentioned, further reactor design optimization will be performed during the thermal-hydraulic benchmark.

The objective of the thermal-hydraulic (T&H) benchmark is to compare the results from different team, using different T&H models and different softwares. As we know from previous results, a too simple core shape induces recirculation and very hot but local temperature spots. We also know from hydraulic experience in nuclear field that some instabilities may appear in such flow. We then had the choice between the two following procedures:

- doing the benchmark on a simple geometry, and compare results with high temperature spots and an unstable flow;
- working on the core shape in order to be able to do the benchmark on an optimized shape, with a lower maximum temperature in the core flow and a more stable salt flow.

The EVOL project schedule was written following the first procedure which is more logical in term of project management: the idea was first to define a benchmark and then to perform the optimization. However, comparing results with very high salt temperatures is not efficient. Furthermore, if the salt flow is unstable, the comparison may be done using full transient simulation models which are much more computer intensive.

Following the design objective, which is to get a core shape with no hot spot and no dynamic instabilities, we kept the benchmark for stationary T&H softwares, but did it on a shape chosen from the on-going work for core optimization.

This deliverable thus reports on these two benchmarks to optimize the MSFR. In particular Section 2 provides the characteristics of the MSFR used in the studies (core and the main fuel circuit systems). Section 3 provides the details of the neutronic benchmark, including the definition, the tools used for the calculations and the results from static and evolution calculations. Finally section 4 deals with the thermal-hydraulic benchmark.

2. MSFR presentation

Starting from the Oak-Ridge National Laboratory Molten Salt Breeder Reactor project [Whatley et al., 1970], an innovative concept called Molten Salt Fast Reactor or MSFR [Nuttin et al., 2005; Mathieu et al., 2006 and 2009; Forsberg et al., 2007; Merle-Lucotte et al., 2008 and 2009] has been proposed. This concept results from extensive parametric studies in which various core arrangements, reprocessing performances and salt compositions were investigated with a view to the deployment of a thorium based reactor fleet on a worldwide scale. The primary feature of the MSFR concept versus that of other older MSR designs is the removal of the graphite moderator from the core (graphite-free core), resulting in a breeder reactor with a fast neutron spectrum and operated in the Thorium fuel cycle as described below. The MSFR has been recognized as a long term alternative to solid fuelled fast neutron systems with a unique potential (excellent safety coefficients, smaller fissile inventory, no need for criticality reserve, simplified fuel cycle…) and has thus been officially selected for further studies by the Generation IV International Forum since 2008 [GIF, 2008 and 2009; Boussier et al., 2012; Renault et al., 2009].

2.1. Concept overview

The reference MSFR is a 3000 MW_{th} reactor with a fast neutron spectrum and based on the Thorium fuel cycle as previously mentioned. In the MSFR, the liquid fuel processing is an integral part of the reactor where a small sample of the molten salt is set aside to be processed for fission product removal and then returned to the reactor. This is fundamentally different from a solid-fuelled reactor where separate facilities produce the solid fuel and process the Spent Nuclear Fuel. The MSFR can be operated with widely varying fuel compositions thanks to its on-line fuel control and flexible fuel processing: its initial fissile load may comprise ^{233}U, ^{235}U enriched (between 5% and 30%) natural uranium, or the transuranic (TRU) elements currently produced by PWRs.

In the MSFR concept, the nuclear fission reactions take place within the flowing fuel salt in the cavity where a critical mass is attained. The core cavity can be decomposed on three free volumes: the active core, the upper extraction volume and the lower injection volume. The salt's thermal-hydraulic behavior is closely coupled to its neutronic behavior, because the salt's circulating time (4s) and the lifetime of the precursors of delayed neutrons (around 10s) are of the same order of magnitude. A sketch of the reactor layout is presented in Figure 2.1.

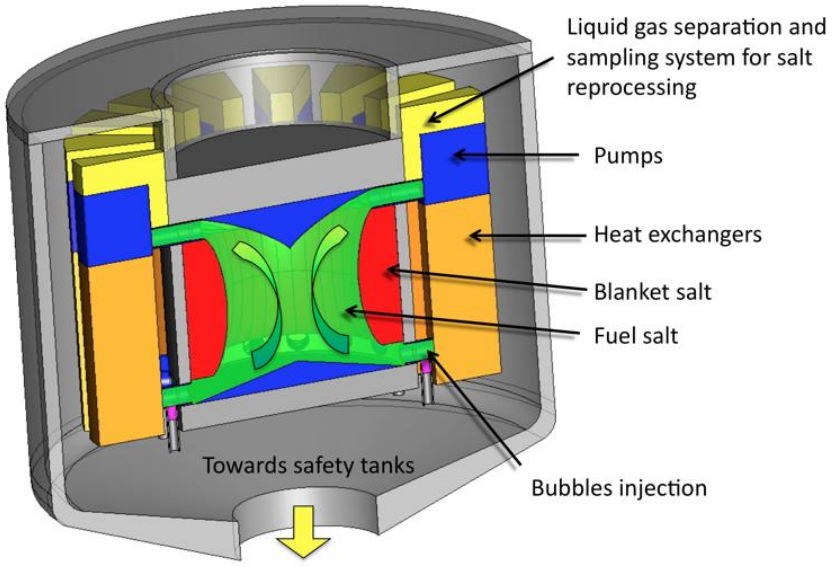

Figure 2.1: Conceptual design of the MSFR

Optimization studies have been performed prior the beginning of the EVOL project, relying on neutronic considerations (feedback coefficients and breeding capacities), material

damages and heat evacuation efficiency, and resulting in MSFR configurations with a total fuel salt volume of 18 m^3, half of the salt (9 m^3) located in the core and half in the external circuits as explained above. Based on these preliminary studies and for the purpose of the current analysis the core cavity was assumed to have a cylindrical shape with a height to diameter ratio (h/d) equal one (to minimize the neutron leaks and thus improves the breeding ratio). A more complete description of the design is given in the next subsections. More details on the whole system will be given in the deliverable 2.8.

2.2. Systems description of the MSFR fuel circuit

In order to initiate the work and the discussions on possible ranges for the reactor parameters, basic drawings have been developed from the preliminary conceptual design. Figure 2.2 illustrates one of the possible geometrical configurations. During normal operation, the fuel salt circulates in the core and in 16 external modules, so called fuel loops. Each of them contains a pump, a heat exchanger and a bubbling system (external modules). The time circulation of the fuel salt is of the order of a few seconds, depending on the specific core power and the salt temperature rise (ΔT) in the core. The principal reactor systems which have an impact on the core optimization will be discussed in detail in the followings paragraphs.

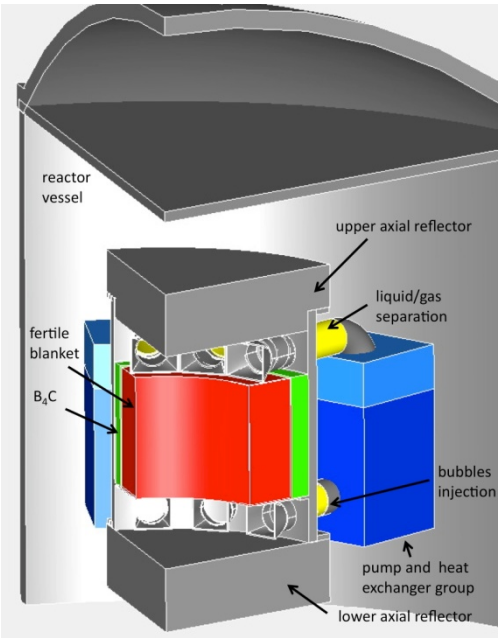

Figure 2.2: Example of a 3-D layout for the Molten Salt Fast Reactor (MSFR)

- **Core:** The core active region is defined as the salt volume where most nuclear fissions take place. It includes the flowing salt in the central cavity, the injection zone (in the bottom part of the core) and the extraction zone (top of the core). In the MSFR core there is no solid moderator or any internal support structure except for the wall materials. As previously mentioned, the reference concept is designed for a nominal power of 3 GWth, with a salt temperature rise preliminary fixed at $\Delta T = 100$ K. The operating temperatures chosen in the initial simulations were 650°C (inlet temperature) and 750°C (outlet temperature). The lower limit due to the salt's melting point (565°C) while the upper limit is imposed by the structural materials performance (limit around 800°C - see materials constraints in WP4). The core working parameters were defined after performing various parametric studies seeking for low neutron losses, low reflector irradiation and minimal fissile inventory, while maintaining a fuel salt volume in the heat exchangers large enough to ensure that salt cooling by $\Delta T = -100$ K is feasible. The resulting core shape is roughly a cylinder, with 1/2 of the entire salt volume

inside the core, the rest being located in the external fuel loops. This core geometry has to be further optimized to guaranty a stable flow in the core (see section 3).

- **Fuel Salt:** The choice of the fuel salt composition relies on several parametric reactor studies (chemical and neutronic considerations, burning capabilities, safety coefficients, and deployment capabilities). The optimal fuel salt composition is a binary fluoride salt, composed of LiF enriched in ^{7}Li to 99.995 % and a heavy nuclei (HN) mixture initially composed of fertile thorium and fissile matter (see WP3). This salt composition leads to a fast neutron spectrum in the core. With a fusion temperature of 565°C, the mean operating temperature has been chosen at around 700°C (see above). The fission products created during operation can be soluble or insoluble in the salt. To maintain the physico-chemical and neutronic characteristics of the salt, it is necessary to clean the salt, i.e., to extract the fission products. It is important to stress that due to the fast neutron spectrum of the MSFR the impact of the fission products on the neutronic economy is relatively small and thus the control of the physico-chemical properties is clearly the main aim of the reprocessing unit (see WP3). The temperature of the salt depends strongly on the operation of the pumps and the cooling in the heat exchangers.

- **Upper and Lower Reflectors:** The lower and upper walls of the core are neutronic reflectors. A NiCrW hastelloy has been selected (see section 2.3.1 for its composition and WP4 for more details) as a structural material candidate for the reflectors walls (and for all other internal walls in contact with the fuel salt). The upper reflector is submitted to mechanical, thermal (the fuel salt's mean temperature in the extraction area is around 750°C with possible spatial and time dependent fluctuations) and radiation constraints. The combination of high temperature and high radiation levels seems to be the biggest challenge for the proposed alloy so that the surface of the upper reflector may require a thermal protection. Due to the significant lower inlet temperature, the lower reflector is under reduced thermal stress. Its specificity is to be coupled to the draining system. Optimized shapes of these reflectors will be studied to insure the most stable thermal flow in the core.

- **Fertile Blanket:** This component serves as radial reflector and as a neutron shield to protect the external components of the fuel loops (pipes, heat exchangers). In addition to this protection function, the fertile blanket is used to improve the breeding capabilities of the reactor. The walls of the blanket containment are made of a Ni-based alloy for corrosion resistance and have an external layer of B_4C on the outer wall to further reinforce the neutronic shielding. The salt in the blanket is of the same type as the one in the core but with 22.5 mol% of Th and without any initial fissile material. Since the thorium present in the fertile salt is exposed to the core neutron flux, it will generate the ^{233}U fissile element. A small fraction of the ^{233}U produced in the blanket will fission so that fission products are produced in the blanket and will need to be extracted. In addition, the power arising from the ^{233}U fissions (13MW) and from the captures on thorium (24MW) will heat-up the fertile salt in the blanket. It has been found that this heat cannot be evacuated through the blanket walls by a natural convection mechanism of the fertile salt. Therefore a fertile blanket external cooling system will be necessary. If breeding is not required, the MSFR design could be simplified by replacing the fertile blanket by an inert reflector, identical to the axial reflectors. Optimized shapes of the fertile blanket may also be studied to improve the thermal flow in the core.

- **Heat Exchanger (x16):** Each heat exchanger (HX) unit has to extract about 187 MW during normal operation. The HX design is challenging since a very compact design is needed (to reduce the volume of the fuel salt outside the core) but on the other hand the maximum compactness achievable has to be limited by considerations on the HX pressure drop, the maximum velocity allowed for the salt (erosion) and the thermodynamics properties of the working fluids. A preliminary design has been developed based using a plate heat exchanger type which allow a reasonable compromise between compactness (exchange surface) and

pressure drop. This preliminary design is adequate for the purpose of the current benchmarks but will require further studies (in particular related to the geometry, materials and fabrication) to allow for a better optimization. The design of this component impacts the heating ΔT in the core when both reactor power and total fuel volume fixed.

- **Pump (x16):** The salt is circulated in the reactor by sixteen pumps located in each of the fuel loops. The fuel salt flow rate is about 0.28 m^3/s to guaranty an adequate temperature rise in the core for the current core power level. The power of the pumps has an impact on the circulation time of the salt and thus on the heating in the core.
- **Pipes:** The piping system allows the circulation of salt between the core and the HX and pumps. The pipes are sized (diameter and length) according to two main constraints: reduce the fuel salt volume outside the core and limit the maximum salt speed in the pipes (to avoid erosion). Varying the pipes diameter impacts the circulation period of the fuel salt in the whole system, and thus its heating in the core if the power is fixed. Other considerations that will have to be analyzed in the future include optimization of the pressure drop, thermal fatigue (in particular in the upper pipes), pipe vibration, welding, seismic behavior, access for inspection, thermal shielding, etc.
- **Reactor Vessel:** The core and the reactor systems (components of fuel loops such as pipes, pumps, HX, etc.) described before are contained inside a reactor vessel which is filled with an inert gas (argon). As in the original experimental reactor MSRE, the inert gas has a double function: it is used to cool down the reactor components by maintaining the gas temperature at about around 400°C; and it allows for sampling to early detect a possible salt leak. Note fixing the gas temperature at 400°C will guarantee that in the event of a small fuel salt leak, the salt should solidify since its melting temperature is equal to 565°C. The reactor vessel parameters (geometrical and material) do not directly impact the core performance (and thus are not needed for the optimization) but will be necessary for the safety analysis.

2.3. Data used for the simulations of the MSFR

2.3.1. Structural materials

The reflectors are made of a Ni-based alloy. The density of the Ni-based alloy, whose composition is detailed in Table 2.2, is equal to 10 (data given by WP4). This material will not be submitted to a high neutron flux; hence the choice of its composition is not too constrained.

Ni	W	Cr	Mo	Fe	Ti	C	Mn	Si	Al	B	P	S
79.432	9.976	8.014	0.736	0.632	0.295	0.294	0.257	0.252	0.052	0.033	0.023	0.004

Table 2.2: Composition (at%) of the Ni-based alloy considered for the simulation of the structural materials of the core

Concerning the neutronics protection, we have considered the composition of natural boron: 19.8% of ^{10}B and 80.2% of ^{11}B. The B_4C density is equal to 2.52016 (data used in SIMMER, given by KIT).

2.3.2. Physicochemical properties of the molten salts used in the MSFR

New measurements of the physico-chemical properties of fluoride salts have been performed in the frame of the MARS and the ISTC #3749 projects, the properties for a salt of LiF (78 mol%)-ThF_4 (22 mol%) are listed in Table 1. The third column summarizes the values used in these studies, at a mean temperature of 700°C (halfway between the low and the high operating temperatures). During reactor operation, fission products and new heavy nuclei are produced in the salt up to some mole% only, we have considered that they do not impact these salt physicochemical properties. The same data are used in the simulations for the fertile salt.

	Formula	Value at 700°C	Validity Range, °C
Density ρ (g/cm^3)	$4.094 - 8.82 \cdot 10^{-4} (T_{(K)}-1008)$	4.1249	[620-850]
Kinematic Viscosity ν (m²/s)	$5.54 \cdot 10^{-8} \exp\{3689/T_{(K)}\}$	$2.46 \cdot 10^{-6}$	[625-846]
Dynamic viscosity μ (Pa.s)	$\rho_{(g/cm3)} \cdot 5.54 \cdot 10^{-5} \exp\{3689/T_{(K)}\}$	$10.1 \cdot 10^{-3}$	[625-846]
Thermal Conductivity λ (W/m/K)	$0.928 + 8.397 \cdot 10^{-5} \cdot T_{(K)}$	1.0097	[618-747]
Calorific capacity C_p (J/kg/K)	$(-1.111 + 0.00278 \cdot T_{(K)}) \cdot 10^3$	1594	[594-634][a]

Table 2.1: Physicochemical properties used for the fuel and fertile salt in the Benchmark, measured for the salt 78%mol LiF-22%mol ThF_4 [Ignatiev et al., 2012]

Note: For the thermal-hydraulic benchmark calculations, since the optimized solution has not yet been defined, the salt will reach high temperatures out of the validity ranges of Table 2.1. In a first time, constant values will be used for each property, corresponding to the maximum temperature of the validity ranges. For example, the heat capacity will be taken equal to1410 J/kg K corresponding to the measured value at 634°C. In the future, these correlations will have to be extended to a larger temperature range to allow their utilization in accidental conditions (for the safety studies). In the case where data was not available, conservative values will be used outside the validity range.

[a] In fact, we have to extrapolate the formulas up to 700°C.

3. Neutronic benchmark of the MSFR

A first benchmark has been defined on a simple geometry to compare all neutronic calculations and check the effects of all possible assumptions. The choice of a simple geometry allows saving computer time and being able to compare all code solutions and all assumptions. The knowledge from this starting point will be crucial to be able to interpret next results, sometimes obtained from only one or two simple modeling solutions but on more complex geometries. Working on such "real" geometries, and design it, is the main final objective of EVOL.

The neutronic benchmark was thus carried out using different reactor working parameters with two aims: firstly, to compare the results of the different codes at various working conditions. Secondly, to use these results to perform an initial optimization of the core parameters which would allow defining a reference design to be used for the second set of benchmark studies. Special emphasis was given in the neutronic benchmark, to the adequacy of the codes to correctly account for the effects of the presence of a liquid fuel and a fast neutron spectrum in the core of the MSFR. As already mentioned, further reactor design optimization are currently performed during the second (thermal-hydraulic) benchmark.

3.1. Presentation of the neutronic benchmark

3.1.1. Geometry used in the benchmark

As shown in Fig. 3.1, the core is a single cylinder (the diameter being equal to the height) where the nuclear reactions occur within the flowing fuel salt. The core is composed of three volumes: the active core, the upper plenum and the lower plenum. The fuel salt considered in the simulations is a binary salt, LiF - (Heavy Nuclei)F_4, whose (HN)F_4 proportion is set at 22.5 mole % (eutectic point), corresponding to a melting temperature of 565°C. The choice of this fuel salt composition relies on many systematic studies (influence of the chemical reprocessing on the neutronic behavior, burning capabilities, deterministic safety evaluation and deployment capabilities). This salt composition leads to a fast neutron spectrum in the core.

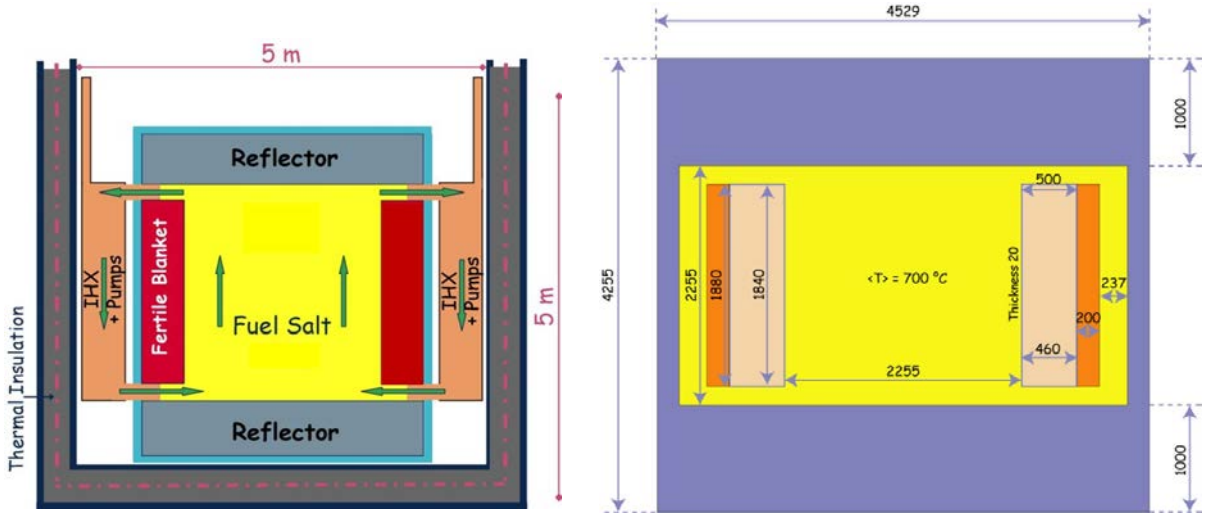

Figure 3.1 (Left): Simplified to scale vertical scheme of the MSFR system including the core, blanket and fuel heat exchangers (IHX) – (Right): Model of the core as used for the neutronic simulations (dimensions given in mm) with the fuel salt (yellow), the fertile salt (pink), the B_4C protection (orange) and the reflectors and 20mm thick walls in Ni-based allow (blue)

As previously mentioned, the radial reflector is a fertile blanket (~50 cm thick) filled with 7.3 m^3 of a fertile salt LiF-ThF_4 with molar 22.5% of ^{232}Th. This fertile blanket improves the global breeding ratio of the reactor thanks to a ^{233}U extraction in an around six months period, i.e. 100% of the ^{233}U produced in the blanket is extracted in 192 days (40 liters per day as shown in the lower part of Fig 3.1). This fertile blanket is surrounded by a 20cm thick neutronic protection of B_4C which absorbs the remaining neutrons and protects the heat exchangers. The thickness of this B_4C protection

has been determined so that the neutron flux arriving from the core through it is negligible compared to the flux of delayed neutrons emitted in the heat exchangers.

The radial blanket geometry is an angular section toron of 188 cm high and 50 cm thick. The 2 cm thick walls are made of Ni-based alloy (see composition in Table 4). A single volume of fertile salt is considered, homogenous and cooled to a mean temperature of 650°C. A temperature variation of the fertile salt of around 30 °C between the bottom and the top of the fertile blanket may be introduced to check its low impact on the reactor evolution.

3.1.2. Fuel salt initial composition

The core contains a fluoride fuel salt, composed of 77.5 molar % of LiF enriched in ^{7}Li (99.999 at%) and 22.5 molar % of heavy nuclei (HN) amongst which the fissile element. This HN fraction is kept constant during reactor evolution, the produced FPs replacing an equivalent proportion of the lithium. The neutronics benchmark focuses on the ^{233}U-started and the TRU-started MSFR. Deliverable 3.7 is dedicated to the evaluation of optimized initial fuel salt compositions, based on neutronics, chemical and material issues.

^{233}U-started MSFR

As detailed in Table 3.1, the initial fuel salt is composed in this case of LiF-ThF_4-$^{233}UF_3$, the initial fraction of ^{233}U being adjusted to have an exactly critical reactor.

<table>
<tr><td>Thermal power (MWth)</td><td colspan="5">3000</td></tr>
<tr><td>Electric power (MWe)</td><td colspan="5">1500</td></tr>
<tr><td>Fuel Molten salt initial composition (mol%)</td><td colspan="5">LiF-ThF_4-$^{233}UF_4$ or LiF-ThF_4-(Pu-MA)F_3
with 77.5 % LiF</td></tr>
<tr><td>Fertile Blanket Molten salt initial composition (mol%)</td><td colspan="5">LiF-ThF_4 (77.5%-22.5%)</td></tr>
<tr><td>Melting point (°C)</td><td colspan="5">565</td></tr>
<tr><td>Input/output operating temperature (°C)</td><td colspan="5">650-750</td></tr>
<tr><td rowspan="6">Initial inventory (kg)</td><td colspan="2">^{233}U-started MSFR</td><td colspan="3">TRU-started MSFR</td></tr>
<tr><td>Th</td><td>^{233}U</td><td>Th</td><td colspan="2">Actinide</td></tr>
<tr><td rowspan="4">38 300</td><td rowspan="4">5 060</td><td rowspan="4">30 600</td><td>Pu</td><td>11 200</td></tr>
<tr><td>Np</td><td>800</td></tr>
<tr><td>Am</td><td>680</td></tr>
<tr><td>Cm</td><td>115</td></tr>
<tr><td>Density (g/cm^3)</td><td colspan="5">4.1249</td></tr>
<tr><td>Dilatation coefficient (g.cm^{-3}/°C) [Ignatiev et al., 2012]</td><td colspan="5">8.82 10^{-4}</td></tr>
<tr><td>Core dimensions (m)</td><td colspan="5">Radius: 1.1275
Height: 2.255</td></tr>
<tr><td>Fuel Salt Volume (m^3)</td><td colspan="5">18
9 out of the core
9 in the core</td></tr>
<tr><td>Blanket Salt Volume (m^3)</td><td colspan="5">7.3</td></tr>
<tr><td>Total fuel salt cycle in the system</td><td colspan="5">4.0 s</td></tr>
</table>

Table 3.1: Characteristics of the MSFR simulated on the neutronics benchmark

TRU-started MSFR

The initial fuel salt is composed of LiF-ThF_4-(TRU)F_3. More precisely, the reference MSFR is started with a TRU mix of 87.5% of Pu (^{238}Pu 2.7%, ^{239}Pu 45.9% , ^{240}Pu 21.5%, ^{241}Pu 10.7%, and ^{242}Pu 6.7%), 6.3% of Np, 5.3% of Am and 0.9% of Cm, as listed in Table 3.2 and corresponding to the transuranic elements contained in an UOX (60 GWd/ton) fuel after one use in a standard LWR and

five years of storage. The amounts of TRU elements initially loaded in the TRU-started MSFR are given in Table 3.1.

Isotope	Proportion in the mix
Np 237	6.3 mole%
Pu 238	2.7 mole%
Pu 239	45.9 mole%
Pu 240	21.5 mole%
Pu 241	10.7 mole%
Pu 242	6.7 mole%
Am 241	3.4 mole%
Am 243	1.9 mole%
Cm 244	0.8 mole%
Cm 245	0.1 mole%

Table 3.2: Proportions of transuranic nuclei in UOX fuel after one use in PWR without multi-recycling (burnup of 60 GWd/ton) and after five years of storage

3.1.3. Fuel salt reprocessing considered for the evolution calculations

As displayed in Figure 3.2, the salt management combines a salt control unit, an online gaseous extraction system and an offline lanthanide extraction component by pyrochemistry.

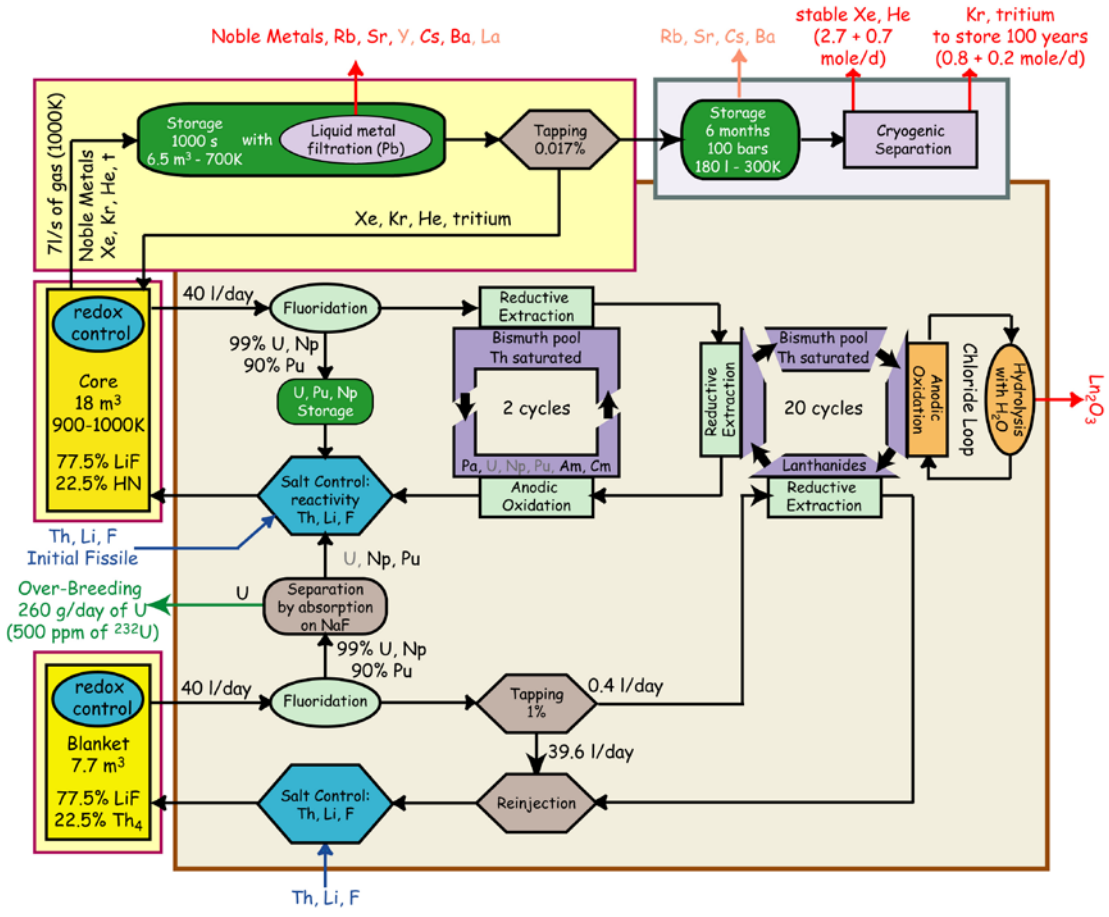

Figure 3.2: Overall scheme of the fuel salt management including the online gaseous extraction (top) and the offline reprocessing unit (bottom) – The yellow boxes surrounded by a red line represent the parts enclosed within the reactor vessel

The gaseous extraction system, where helium bubbles are injected into the core, removes all non-soluble fission products (noble metals and gaseous fission products). This on-line bubbling

extraction has a removal period $T_{1/2}$=30s in the simulations. The elements extracted by this system are the following: Z = 1, 2, 7, 8, 10, 18, 36, 41, 42, 43, 44, 45, 46, 47, 51, 52, 54 and 86.

A fraction of salt is periodically withdrawn and reprocessed offline in order to extract the lanthanides before it is sent back into the core. The actinides are sent back into the core as soon as possible in order to be burnt. With the online control and adjustment part, the salt composition and properties are checked.

The rate at which this offline salt reprocessing is done depends on the desired breeding performance. In the reference simulations, we have fixed the reprocessing rate at 40 litres per day whatever the fuel salt volume, i.e. the whole core is reprocessed in 450 days. In the simulation of the reactor evolution, this is taken into account through a 100% offline extraction of the following fission products in 450 days: Z = 30, 31, 32, 33, 34, 35, 37, 38, 39, 40, 48, 49, 50, 53, 55, 56, 57, 58, 59, 60, 61, 62, 63, 64, 65, 66, 67, 68, 69, 70

Thanks to this simplified view of the reprocessing, even if not totally realistic, a stationary state may be reached during the reactor evolution. In the following, the extraction efficiencies may be refined in cooperation with WP3.

As displayed in Figure 3.2, the fission products of the fertile blanket are slowly removed, with a rate of 0.4 litre of salt cleaned per day i.e. the whole fertile salt volume (7.3m^3) cleaned in 19250 days (52.7 years). The actinides, mostly ^{233}U, are extracted and then re-injected in the core at a rate of 40 litres of salt cleaned per day. Additionally, the gaseous fission products are extracted in the same way as in the core (see above).

3.1.4. Delayed neutron precursors

Mean values of abundances for the neutron precursors are considered here for fissions that are due to ^{233}U (90%) and ^{235}U (10%) with a spectrum located between a thermal and a fast one (50% of thermal spectrum and 50% of fast spectrum).

Group	1	2	3	4	5	6	7
Precursor	^{87}Br	^{137}I	^{88}Br	^{93}Rb	^{139}I	^{91}Br	^{96}Rb
Half-Life	55.9 s	24.5 s	16.4 s	5.85 s	2.3 s	0.54 s	0.199 s
Abundances							
^{233}U (fast)	0.0788	0.1666	0.1153	0.1985	0.3522	0.0633	0.0253
^{233}U (thermal)	0.0787	0.1723	0.1355	0.1884	0.3435	0.0605	0.0211
^{235}U (fast)	0.0339	0.1458	0.0847	0.1665	0.4069	0.1278	0.0344
^{235}U (thermal)	0.0321	0.1616	0.0752	0.1815	0.3969	0.1257	0.0270
Mean Value	0.0742	0.1679	0.1209	0.1915	0.3533	0.0684	0.0240

Table 3.3: Abundances of seven delayed neutron precursors for two uranium isotopes

3.1.5. Calculations performed

The following calculations were performed by the WP2 and ROSATOM partners for both a ^{233}U-started and a TRU-started MSFR:

- The amounts of fertile and fissile matters needed initially to have a reactivity equal to 1, together with their uncertainty

- The effective proportion of delayed neutrons in the salt (BOL and steady-state)
- The generation time of the neutrons
- The thermal feedback coefficients with its two contributions (Doppler / density) at BOL and steady-state
- The neutron spectrum (neutron flux as a function of the neutron energy) in the core
- The breeding ratio and the breeding gain
- The evolution of inventories of interest (U, Pu, minor actinides, fission products) as a function of the operation time, both for the ^{233}U-started and the TRU-started MSFR

The irradiation damages to the structural materials (displacement per atom (dpa), Helium production, W transmutation) have also been evaluated; these results will be included in the deliverable 2.4.

3.2. Tools used for the neutronics and evolution calculations

Since the partners of WP2 (and of the MARS project) use different numerical tools for the reactor analysis based on neutronic calculations, a comparative evaluation of the existing codes was necessary. In a first step, a list of the tools existing or to be developed and or adapted for the studies of a fast molten salt reactor has been drawn up, as shown in Tables 3.4a and 3.4b.

Contribution \ Partner	CNRS	TUD	KIT-IKET	KIT-INR	FZD - HZDR
Neutronic simulations	Yes	Yes	Yes		Yes
Code for neutronic simulations (name+short description)	MCNP - Probabilistic code	DALTON (3-D time dependent diffusion with precursor transport)	SIMMER-III (2D neutron transport with movable presursors)	SIM-MSR (1D kinetic with movable presursors)	DYN3D-MSR (3D neutron kinetics with precursor transport)
Neutronic simulations: include reactor evolution?	Yes - Neutronic code coupled to the REM in house code for materials evolution	Yes - Own made ORIGEN-like program LOWFAT	TRAIN (Burnup code)	no	HELIOS cell code with script based execution for reactor evolution calc.
Code availability (date) / validation (yes/no + on which system)	Used since 10 years / Tested on MSRE and MSBR	MSRE (Neutronic) + code-to-code (Burnup)	code available; validated within MOST & MOSART project	code available; validated within MOST & MOSART project	code available; validated within MOST project
Thermalhydraulic simulations		Yes	SIMMER & TRAIN for solid fuel	SIM-MSR	Yes
Tool for thermalhydraulic simulations (name+short description)		HEAT(CFD) (Fast MSR), THERM (Thermal MSR)	SIMMER-III (2D Eulerain fluid-dynamics code)	SIM-MSR	DYN3D-MSR (channel-type thermo-hydraulics model)
Code availability (date) / validation (yes/no + on which system)		Yes	Yes	yes	Yes; validated for channel-type thermal MSR
Neutronic-thermalhydraulic coupling	Yes (foreseen)	Yes	Yes	yes	Yes
Codes coupled (name+short description)	(MCNP+REM) to be coupled to a thermal-hydraulic code (not yet chosen: Trio-U or other code?)	DALTON-HEAT (Fast MSR) and DALTON-THERM (Thermal MSR)	SIMMER-III (Neutronics-Thermal-hydraulic coupled)	SIM-MSR (Neutronics-Thermal-hydraulic coupled)	DYN3D-MSR; coupled with CFD (ANSYS_CFX); to be adapted for fast MSR
Coupling availability (date) / validation (yes/no + on which system)	To be done in EVOL frame by end of 2011	DALTON-HEAT To be done in EVOL	Yes	yes	DYN3D-MSR/CFX to be done in EVOL
Other couplings or tools (+short description/details)	Neutronic-reprocessing coupling - Available since 2010 - Validation on-going	Chemistry (to be developed)	SIMMER-TRAIN interface under development	SIM-SFR	No

Table 3.4a: Numerical tools dedicated to neutronic and evolution calculations of the MSFR (part 1)

Contribution \ Partner	POLIMI	POLITO	INOPRO	BME
Neutronic simulations	Yes	YES		Yes
Code for neutronic simulations (name+short description)	SERPENT2 (Monte Carlo) ERANOS/EQL-3D (Deterministic)	DYNAMOSS - deterministic code		MCNP - Monte Carlo transport (modified for circulating fuel), SCALE - deterministic and Monte Carlo (KENO) transport
Neutronic simulations: include reactor evolution?	(S) Yes: purpose made extension of b-up routines (E) Yes: extension of EQL-3D procedure	No- only sort-term dynamics included (no burnup)		Yes - Trition module in SCALE
Code availability (date) / validation (yes/no + on which system)	(S) The extension is available since now upon request, will be implemented in the official version of SERPENT-2. Code-to-code assessment between the 2 codes.	Developed during MOST and ALISIA project, benchmarked during MOST project		Used for MSRE, MSBR and MOSART concepts
Thermalhydraulic simulations			Yes	Yes
Tool for thermalhydraulic simulations (name+short description)			Fluent (well known commercial code – LES available) and OpenFoam (open CFD code, under internal validations at INOPRO IAO – may allow adaptations of models)	ANSYS CFX 13 3D computational fluid dynamics code
Code availability (date) / validation (yes/no + on which system)			Use of INOPRO IAO License of Fluent. Open license for OpenFoam	Used for 12 years / Tested on LWRs (VVER-440, VVER-1000), used for MSRE, MOSART modelling: Validation: Construction of a MSFR mockup using water for PIV (particle image velocimetry) measurements - details of MSFR concept needed.
Neutronic-thermalhydraulic coupling	Yes	Yes		?
Codes coupled (name+short description)	Comsol model (finite element, 2D axial symmetric Neutron diffusion + CFD) OpenFOAM (finite volume, full-core 3D, Neutron diffusion + CFD)	DYNAMOSS - coupled neutronics-TH, solve multiG diffusion for neutrons and fluid equation for incombressible flow + Boussinesq approximation		
Coupling availability (date) / validation (yes/no + on which system)	OpenFOAM solver for steady-state analysis with multi-group diffusion available upon request (needs OpenFOAM 1.6-ext)	Developed during ALISIA project and tested (journal publications available)		
Other couplings or tools (+short description/details)				

Table 3.4b: Numerical tools dedicated to neutronic and evolution calculations of the MSFR (part 2)

After this inventory of the different numerical tools developed or used by the partners of WP2 and of the MARS project, the next step was an evaluation of their adequacy to simulate the core of the MSFR which combines both a liquid fuel and a fast neutron spectrum. This evaluation comprises two

sets of benchmark: the first one focused on the neutronics aspects of the reactor, while the second one will be oriented toward the system thermal-hydraulic behavior to further optimize the reactor design. Prior to that, the best design parameters to be used in the benchmarks and optimization studies of task 2.1 have been selected (see deliverable 2.1 released mid 2012).

3.2.1. CNRS/IN2P3/LPSC (LPSC)

Simulation of reactor evolution

The numerical simulations performed at LPSC/IN2P3/CNRS rely on the coupling of the MCNP neutron transport [Briesmeister, 1997] with a home-made materials evolution code REM [Heuer et al., 2010; Doligez et al., 2009; Nuttin, 2002; Mathieu, 2005].

The probabilistic MCNP code evaluates the neutron flux and the reaction rates in all the parts (called cells) of the simulated system. This requires a precise description of the geometry and the characteristics of all materials involved (temperature, density, elements, isotopes, proportions), together with the interaction cross-sections of each isotope present in the reactor.

These calculations are static, for a given and fixed state of the system. Following the reactor operation over time also requires simulating the temporal evolution of the system. The neutronic code thus has to be coupled with an evolution code, as shown in Figure 3.3.

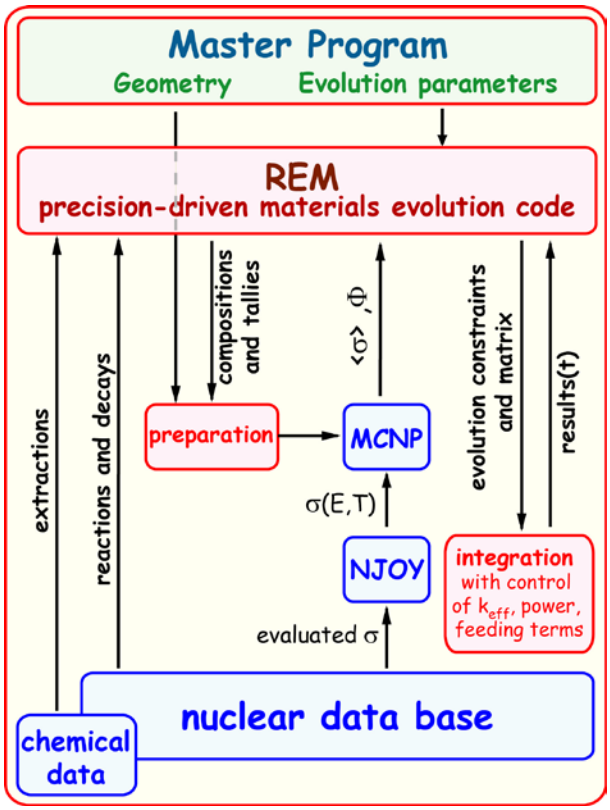

Figure 3.3: Coupling scheme of the MCNP neutron transport code with the in-house materials evolution code REM

The evolution code, REM, solves the Bateman equations to compute the evolution of the materials composition isotope by isotope within the cells as a function of the nuclear reactions and decays occurring in the system and of external parameters like fuel reprocessing or composition adjustment. The extraction by reprocessing of nucleus i out of the core is implemented through specific removal constants λ_{chem} equivalent to decay constants. The fuel adjustment of such reactors is performed during reactor operation through fertile or fissile supply. The classical Bateman equations have thus to be modified by adding two terms to take into account these MSR's fundamental characteristics compared to classical solid-fuel reactors:

$$\frac{\partial N_i}{\partial t} = \sum_{j \neq i} \lambda_{j \to i} N_j + X_j < \sigma_j \phi > N_j - \lambda_i N_i - < \sigma_i \phi > N_i - \lambda_{chem} N_i + A_i \quad \text{(Eq. 3.1)}$$

with A_i the fertile or fissile supply of nucleus i, and X_j the branching ratio for the reaction of nucleus j to nucleus I (fission yield for a fission product for example). Our simulations consider several hundreds of nuclei (heavy nuclei, fission products, structural materials…) with their neutron interactions and radioactive decays.

The nuclear cross section database firstly used for these calculations is ENDF/B-VI, which was chosen for the most conservative effect on the breeding gain of the MSFR. However, ^{7}Li and fluorine cross sections are extracted from JENDL-3 database. The benchmark calculations have also been performed with the JEFF-3.1 database.

The simulations of the reactor's evolution take into account the input parameters (power released, criticality level, chemistry...), by continuously adjusting the materials composition and thus the neutron flux of the system, via multiple interactions between the neutronic and the evolution tools. The REM code is indeed a precision-driven code, i.e. it has been designed to determine the reactor evolution while controlling the precision of the results at each step of this evolution. The resolution of the Bateman equations is constrained by several variables to keep the simulated reactor's physical parameters constant during the evolution. These include the total power (with a one percent or so precision) and the reactivity (with a huge precision of some ten pcms, much smaller than the computational uncertainty of this parameter under MCNP). The numerical integration of the Bateman equations is done using a Runge-Kutta method, as illustrated in Figure 3.4.

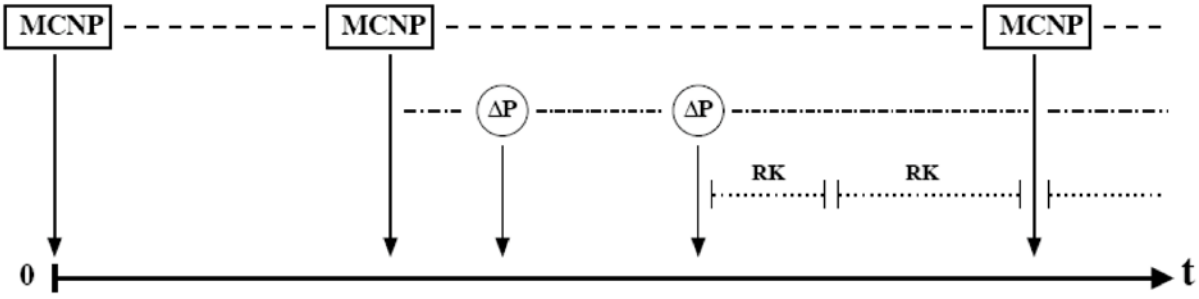

Figure 3.4: Scheme of the evolution procedure - Here'Δp' stands for the adjustment steps (total power and reactivity) and 'RK' represent the Runge-Kutta steps

Simulation of the whole system: coupling of neutronics and reprocessing

A tool coupling neutronics and reprocessing has been developed at LPSC [Heuer et al, 2010; Doligez, 2010]. The method developed in the previous paragraph calculates each nucleus population only inside the core. In order to calculate the nuclei populations inside the whole process, we partitioned the whole system (reactor, reprocessing unit…) into elementary sub-systems characterized by transfer functions from one sub-system to another. Just like the core extraction, those transfer functions have to characterize the kinetic of the considered operations and the thermodynamic equilibrium. There is thus at each step a competition between nuclear decays and chemical extraction. For instance, let's consider uranium just before the fluorination. There are three possibilities: nuclear decay, extraction by fluorine, or it could stay in the salt and thus could go to the next step which is the reductive extraction.

To couple the reprocessing and the core evolution, we add a dimension in equation 3.1. We have to add the location of each nucleus in the system as a new parameter. Consequently, the size of the matrix which was N (the number of nucleus) becomes N*x, where x is the number of elementary operations done in the reprocessing unit. Equation 3.1 becomes equation 3.2 where 'B' symbolizes the location of nucleus i in the sub-system B and 'B→C' the transfer from sub-system B to sub-system C:

$$\frac{\partial N_i^B}{\partial t} = \sum_{j \neq i} \left\{ \left(\lambda_{j \to i} + X_j < \sigma_{j \to i} \phi > \right) N_j^B \right\} + \sum_{C \neq B} \lambda_{Chem}^{C \to B} N_i^C - \lambda_i N_i^B - < \sigma_i \phi > N_i^B - \sum_{C \neq B} \lambda_{Chem}^{B \to C} N_i^B$$

(Eq. 3.2)

We are thus able to calculate the evolution of matter in each process of the system and to know isotopes concentrations, gamma or neutron flux or the residual heat (fundamental data for radioprotection) everywhere in the fuel circuit and the reprocessing unit.

The main issue in the reprocessing unit simulation is to determine the kinetic of each step of the process and consequently the transfer constants. As technological choices have not been fixed yet, only the available thermodynamic data have been used [Doligez, 2010].

3.2.2. Helmholtz-Zentrum Dresden-Rossendorf (HZDR)

For the simulations at HZDR, the HELIOS 1.10 code system with the internal 47 energy group library is used [Villarino, 1992]. The code is a 2D spectral code with wide unstructured mesh capabilities and a transport solver, based on the collision probability method [Helios, 2003]. It is written for the simulation of solid structure fuel assemblies, thus the possibility of online re-fuelling and online reprocessing is not foreseen.

To deal with these very special features of molten salt reactors, a python script has been developed. The script is based on the special features of HELIOS. All important information, which is not changed during the whole reactor operation, is stored in an expert input. The changing material configuration is given in the user input. Both inputs are merged in the pre-processor AURORA, which creates the complete input for the HELIOS run for the determination of the neutron flux distribution and the burn-up of the materials for a defined burn-up period. The results are evaluated in the post-processor ZENITH. Here it can be decided which isotopes will be fed back into the next user input which is created by the script (see Figure 3.5).

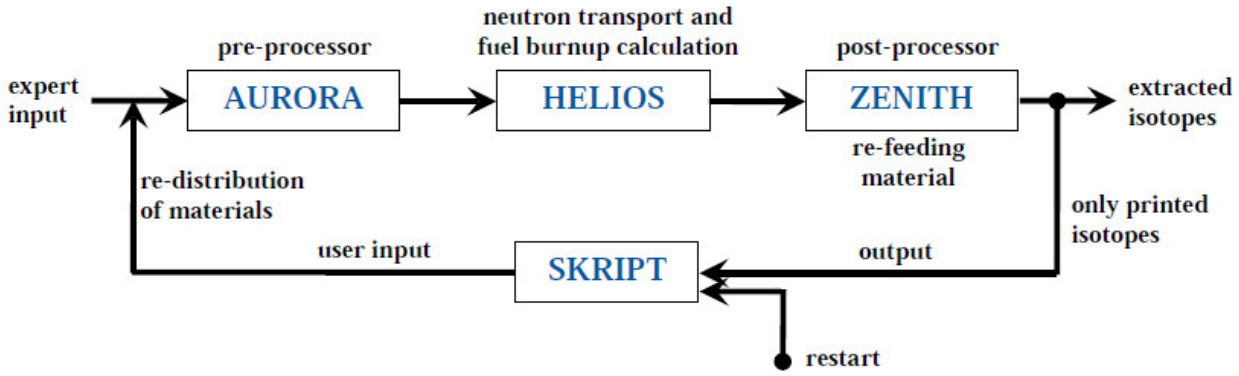

Figure 3.5: Description of the calculation cycle for the simulation of a MSR

Theoretically, it is possible precisely to simulate a molten salt reactor by using small time steps in this calculation loop. In a real MSR two different time scales for the salt reprocessing are used, due to the different extraction methods for the fission products. The helium bubbling, which has a halving time of ~ 30s for gaseous fission products, is used. The salt chemical reprocessing takes 450 days to have a throughput of 100% of the fuel salt volume. For the required long time investigation an approximation is used, only the second process is simulated and all fission products are extracted after an operation time of 450 days. The salt reprocessing is established inside the post-processor, only the isotopes which remain in the salt are forwarded to the script; the isotopes or a share of the isotopes which will be dropped are representing the isotope extraction in the salt processing system. Additionally, a defined amount of material with a given isotope vector, e. g. refill of thorium to the initial amount at each cycle and/or refill of a certain amount of fissile material, can be added to the individual isotopes and will be rewritten in the script to the new user input.

For the calculation of the benchmark a 2D model of the benchmark geometry in HELIOS has been built with (see Figure). It is a full 2D model for a quarter of the core using reflecting boundaries inside, vacuum boundaries outside and ~250 calculation regions like shown.

Due to the characteristics of the HELIOS code developed for solid fuelled systems, some approximations have to be accepted. There is no fuel salt movement in the 2D calculation system, thus an undesired burn-up distribution arises during the 450 day cycle. The materials are only re-distributed when a new user input is defined in each cycle over the script. The effect could be reduced by reducing the cycle time and a re-feed of a part of the fission products. HELIOS is a LWR code and a LWR spectrum is used for the weighting of the 47 group master library. Nevertheless, comparisons to SERPENT on the isotope accumulation during the burn-up have shown a good agreement for the major isotopes [Rachamin et al, 2013]. The approximations and the use of HELIOS seem to be adequate for the approximation level required for this kind of long term study and the approximations on geometry and modeling given by the used benchmark.

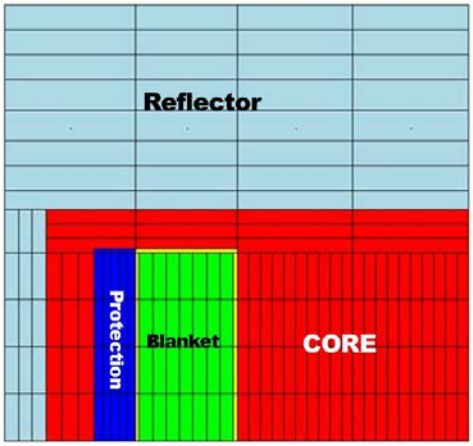

Figure 3.6: Description of the geometry modelized in HELIOS for the benchmark calculations

3.2.3. The Kurchatov Institute (KI or KIAE)

Description of the Calculation Scheme

The method that was used in our study is based on well-known Monte Carlo MCNP-4B code coupled by special developed interface with a ORIGEN2.1 code, which solves depletion equations. In the next part brief description and calculation scheme of coupled code complex MCNP-4B+ORIGEN2.1 is demonstrated.

The method of depletion calculation.

In order to define time variation of core reactivity and burn-up in MSR, the reactor operating time is divided on N user-specified finite intervals Δt_i with i=1,..,N. At the beginning of each time interval Δt_i for fuel composition obtained at the end of previous time interval (if i=1 then the start-up composition is used) the following neutronic characteristics are calculated by MCNP-4B code: multiplication factor, flux distribution and averaged one-group cross sections (averaged on neutron spectrum and active core volume) that would be used in depletion calculation on time interval Δt_i.

Taking into account the fuel salt flow rate and that mixing in primary circuit of MSR is high enough it is assumed that at given time the nuclear composition of fuel salt in primary circuit might be considered as constant in each point of fuel volume. To define one-group cross-section of j-nuclide for i-reaction averaged by the salt volume and neutron spectrum the following equation is used:

$$\frac{\iint \sigma_i^j(E)F(E,r)dEdr}{\iint F(E,r)dEdr} \quad \text{(Eq 3.5)}$$

where F(E,r) – neutron flux, $\sigma_i(E)$ – microscopic cross-section of j-nuclide for i-reaction from MCNP-4B data library.

Segment	Light element incl. structural materials	Actinide	Fission product
$\sigma_{n,\gamma}$ (daughter nucleus in stable state)	+	+	+
$\sigma_{n,\gamma}$ (daughter nucleus in metastable state)	+	+	+
$\sigma_{n,\alpha}$	+		+
$\sigma_{n,p}$	+		+
$\sigma_{n,2n}$ (daughter nucleus in stable state)	+	+	+
$\sigma_{n,2n}$ (daughter nucleus in metastable state)	+	+	+
$\sigma_{n,3n}$		+	
$\sigma_{n,fission}$		+	

Table 3.5: Types of cross-sections required for each segment in ORIGEN2.1 library

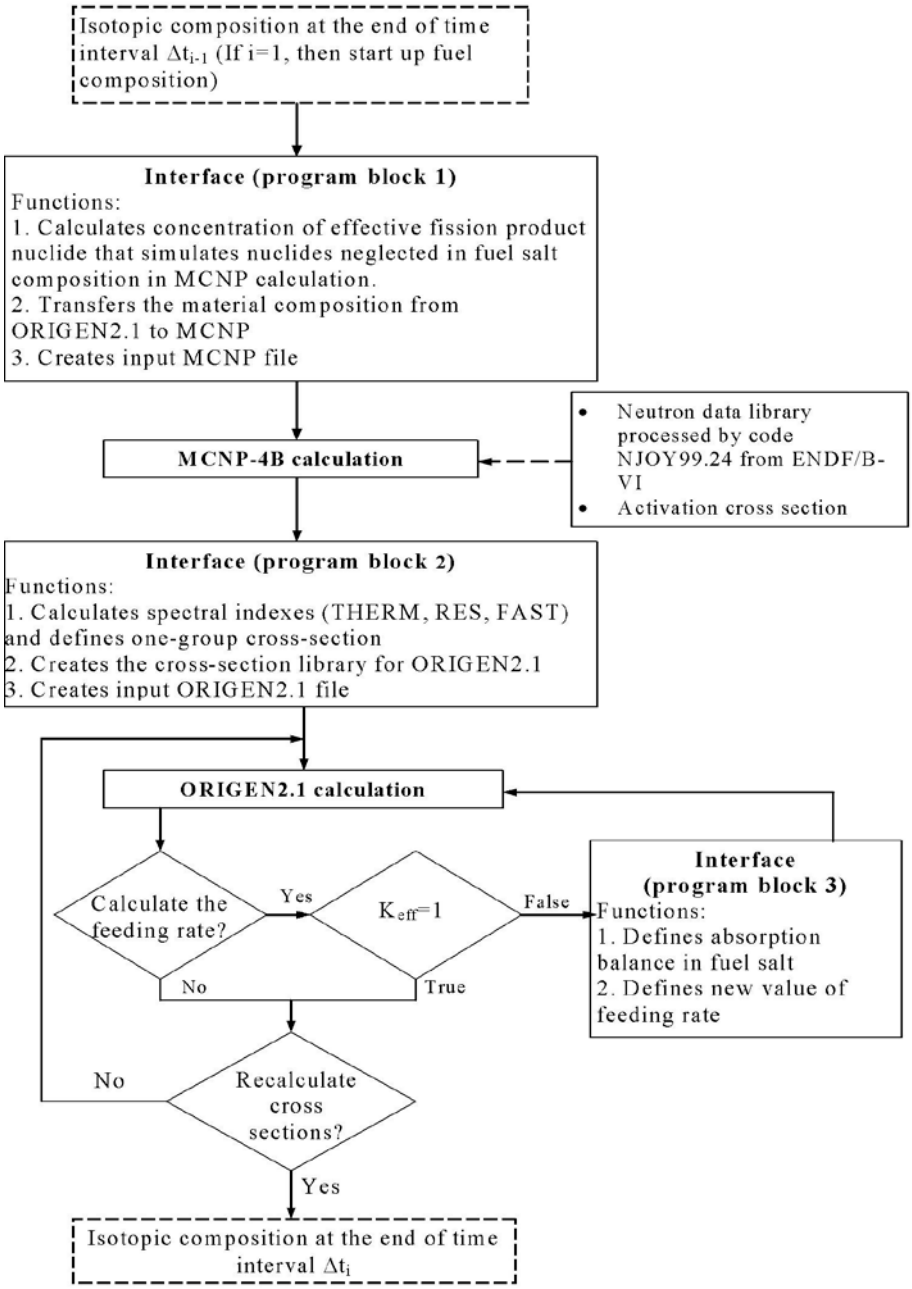

Figure 3.7: Schematic of MCNP-ORIGEN2.1 burn up calculation

Group	Nuclide	Data source
1. Data source	Th-232, Th-233, Pa-233, U-232, U-233, U-234, U-235, U-236, U-237, U-238, Np-237, Np-238, Np-239, Pu-236, Pu-238, Pu-239, Pu-240,Pu-241, Pu-242, Pu244, Am-241, Am-242m, Am-243, Cm-242, Cm-243, Cm-244, Cm-245, Cm-246, Cm-247, Cm-248, Bk-249, Cf-249, Cf-250, Cf-251, Cf-252	ENDF/B-VI
2.Fission products	Kr-83, Sr-90, Zr-93, Mo-95, Tc-99, Ru-101, Ru-103, Rh-103, Rh-105, Pd-105, Pd-107, Pd-108, Ag-109, Cd-113, In-115, I-127, I-129, I-135, Xe-131, Xe-135, Cs-133, Cs-134, Cs-135, Ba-137, Ba-138, La-139, Pr-141, Pr-142, Pr-143, Nd-143, Nd-145, Nd-147, Pm-147, Pm-148, Pm-148m, Pm-149, Sm-147, Sm-148, Sm-149, Sm-150, Sm-151, Sm-152, Eu-153, Eu-154, Eu-155, Eu-156, Gd-157	ENDF/B-VI
3. Nuclides of the intermediate salt		ENDF/B-VI
4. All other nuclides		ENDF/B-V

Table 3.6: Sources of neutron data files used for calculation of one-group cross sections

Burn-up calculation of nuclear composition on time interval Δt_i is carried out by code ORIGEN2.1 using the one-group cross-section obtained from MCNP-4B calculation at the beginning of the interval.

The standard libraries of one-group cross sections included in ORIGEN2.1 prepared for different type reactors consist of three segments: light-element cross-section library, actinide cross section library and fission products cross-section library. The types of cross-sections required for each segment in ORIGEN2.1 library are given in Table 3.5.

The standard neutron data library of MCNP-4B code contains data only for limited quantity of nuclides and doesn't embrace abundance of nuclides used in code ORIGEN2.1. Moreover, the neutron cross-section in standard MCNP-4B library for all nuclides (besides U-235, U-238, Pu-239) processed for material temperature 0, 293.6 or 300 K.

In order to achieve precise calculations of depletion in MSR, nuclear data processing code NJOY99.24 was integrated in the calculation scheme to build new MCNP data files for the given material temperature from the ENDF-B/VI data files.

Calculation of fuel depletion in MSR requires to take into account the special features of fuel cycle in MSR that include the possibility of fuel makeup and fission product clean up in reactor operation. The soluble fission product clean up might be organized in continuous or batch mode. The code ORIGEN2.1 allows user to take into account these peculiarities of a MSR.

In order to link MCNP with ORIGEN2.1 a fully automated tool was created which principle function is to transfer one-group cross-section and flux values from MCNP to ORIGEN2.1, and then transfer the resulting material compositions (after irradiation and/or decay) from ORIGEN2.1 back to MCNP in a repeated, cyclic fashion. This interface is written in Compaq Visual Fortran 6.0. Figure 3.7 shows a scheme of the burn up calculation.

3.2.4. Politecnico di Milano (POLIMI)

ERANOS-based EQL3D procedure and extension for the MSFR core physics simulation

Starting from a given core configuration with an initial fuel composition, the EQL3D procedure simulates the behavior of a reactor over multiple cycles of operation. The main assumptions are: constant core power, total actinide plus fission products (FPs) concentration and fuel management scheme [Fiorina et al. 2013]. Although primarily aimed at achieving the final

equilibrium state, the procedure is also able to capture with good fidelity the trend in the cycle-by-cycle transition from BOL (Beginning Of Life) to equilibrium.

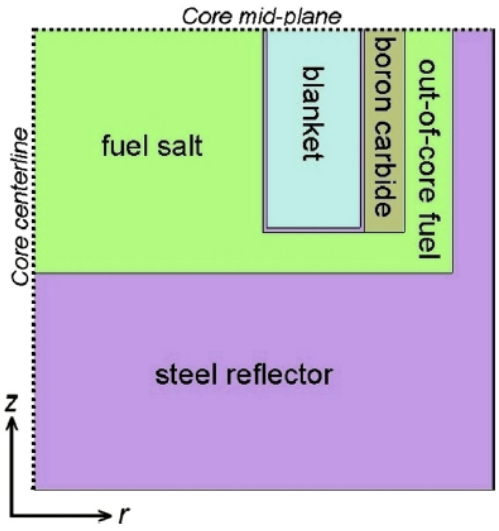

Figure 3.8: Simplified axial symmetric MSFR geometry adopted in POLIMI's simulations

The EQL3D procedure has been developed to analyze solid-fuel fast reactors. In order to study the performance of MSRs, the procedure has been modified to simulate on-line fuel reprocessing. This can be approximated by FP removal in amounts proportional to their quantity and simulated in EQL3D by adding to the physical decay constant of each FP a fictitious component. In a first time [Fiorina et al., 2012a,b], this additional time constant was unique and it enabled only to model the quick removal of non-soluble FPs through the helium bubbling system. The individual fictitious decay constant employed here generalizes the previous treatment to allow simulating the slow on-line extraction of soluble FPs. This provides more accurate results as well as the basic means to perform consistent comparisons among different MSFR feed options. For the analysis of the MSFR, EQL3D has also been modified to improve the treatment of the blankets [Fiorina et al., 2012a,b].

The lattice data for the core calculations have been generated using the ECCO cell code with JEFF 3.1-based 1968-group neutronic library. The core calculations have been performed using the transport BISTRO calculation scheme and 33-group energy collapsed lattice data from ECCO. Both ECCO and BISTRO are part of the ERANOS 2.2-N code system [Rimpault et al., 2002]. For symmetry reasons, a two-dimensional r-z geometry is analyzed and only the bottom half of the core is simulated. A schematic view of the geometry implemented in the BISTRO code is reported in Figure 3.8.

SERPENT-2 extension for on-line fuel reprocessing

SERPENT is a three-dimensional continuous energy Monte Carlo neutron transport code with group constant generation capabilities. The developed extension of SERPENT-2 code directly takes into account the effects of online fuel reprocessing on burn-up calculations and features a reactivity control algorithm [Aufiero et al. 2013a].

Equation 3.6 describes the rate of change of the concentration of a generic nuclide due to neutron induced reactions and decay processes:

$$\frac{dN_i}{dt} = \sum_j N_j \,\phi\cdot\sigma_{j\to i} - \sum_j N_i \,\phi\cdot\sigma_{i\to j} + \sum_j N_j \lambda_j b_{j\to i} - N_i \lambda_i \qquad \text{(Eq. 3.6)}$$

where N_i is the atomic density of the generic nuclide i, ϕ is the neutron flux, $\sigma_{j\to i}$ is the microscopic one-group transmutation cross-section of nuclide j to nuclide i, λ_i is the decay constant of the nuclide i, and $b_{j\to i}$ is the branching ratio from nuclide j to nuclide i.

During fuel isotopic evolution calculations, the total molar fraction of heavy metal (HM) fluorides is kept constant at 22.5%. For this purpose, fissioned isotopes are replaced with the HM feed material (e.g., thorium). This is achieved, in the extended SERPENT-2 version, by modifying the burn-up equations of the isotopes present in the feed vector, adding the following additional term to the Right-Hand Side (RHS) of Eq 3.6:

$$c_i \sum_{k=HM} N_k \, \phi \cdot \sigma_{k,f} \qquad \text{(Eq. 3.7)}$$

where $\sigma_{k,f}$ is the one-group fission cross-section of the HM nuclide k and c_i is the atomic fraction of the isotope i in the feed vector. As fission products are generated, lithium is progressively removed to keep constant the fraction of 22.5mol% of heavy nuclei. In this case, Eq. 3.6 becomes:

$$\frac{dN_{Li}}{dt} = \sum_j N_j \, \phi \cdot \sigma_{j\to Li} - \sum_j N_{Li} \, \phi \cdot \sigma_{Li\to j} + \\ + \sum_j N_j \lambda_j b_{j\to Li} - \sum_{k=HM} N_j \, \phi \cdot \sigma_{k,f} \cdot \left(\sum_{l=FP} FY_{k\to l} \right) \qquad \text{(Eq. 3.8)}$$

where $FY_{k\to l}$ is the fission yield for the production of the FP l from a fission of the HM k and $\sum_{l=FP} FY_{k\to l}$ is approximately 2 in most cases.

The removal of fission products is achieved by adding an explicit decay term to the burn-up equations. For the generic fission product l, we can add to RHS of Eq. 3.6 the term $-N_l.\lambda_{l,repro}$ where $\lambda_{l,repro}$ is the effective removal time constant of the particular chemical specie. As stated before, the atomic density of lithium is consequently increased. The following additional term is added to the RHS of Eq. 3.8:

$$\sum_{l=FP} N_l \lambda_{l,repro} \qquad \text{(Eq. 3.9)}$$

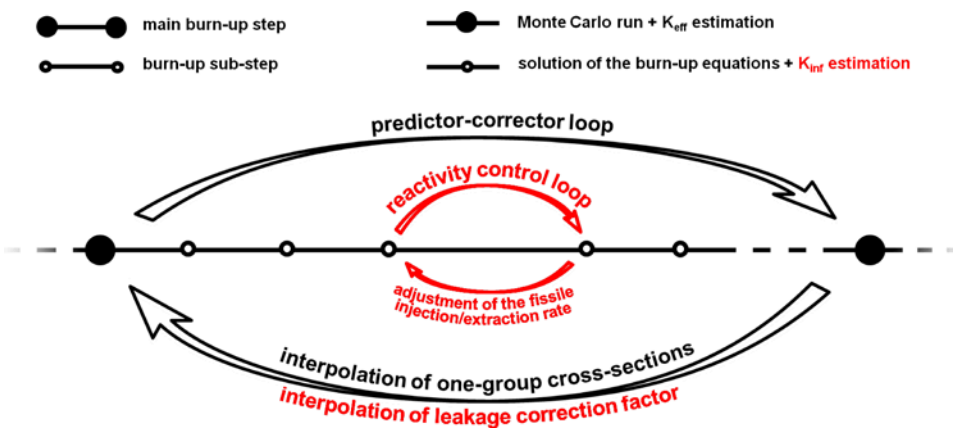

Figure 3.9: Simplified scheme of the reactivity control algorithm implemented in the extended SERPENT-2 version

The main reactor breeding parameters (i.e., conversion ratio, doubling time and instantaneous fissile material production/consumption rate) can be correctly estimated only if the proper composition,

which leads to system criticality, is adopted. For this purpose, the extended version of SERPENT-2 features a reactivity control that allows keeping the effective multiplication factor close to 1 during the whole simulation. This is performed by continuously adjusting the fissile-to-fertile ratio in the feed material. The scheme of the continuous reactivity control algorithm is sketched in Fig. 3.9.

3.2.5. Politecnico di Torino (POLITO)

The results produced by POLITO have been obtained by both deterministic and stochastic neutronic codes.

Stochastic calculations

The evaluations on MSFR concerning:

- the critical composition
- the neutron spectrum
- the characteristics of the delayed neutron families (including the beta effective WITHOUT the effect of fuel motion)
- the generation time
- the flux maps
- the reactivity coefficients

have been performed with the Monte Carlo code SERPENT [Leppanen, 2007]. The full geometry of the core and recirculation loop as described in the benchmark specifications have been modeled in SERPENT.

The SERPENT code has also been used for the generation of three-group cross sections [Fridman et al., 2011] for the core and blanket region, to be used in the following deterministic calculations.

The evaluation on MSFR concerning the Breeding Ratio (BR) has been performed using the code FISPACT [Eastwood et al., 2011], an inventory evolution code currently used for activation calculations. The BR, defined in the benchmark has been evaluated in POLITO calculations as:

$$BR = \frac{\mathrm{R_{dec}}\left[^{233}\mathrm{Pa}\right]}{\mathrm{R_{abs}}\left[^{233}\mathrm{U}\right]} \approx \frac{\mathrm{R_{cap}}\left[^{232}\mathrm{Th}\right]\eta_{U3}}{\mathrm{R_{abs}}\left[^{233}\mathrm{U}\right]}$$

Where the breeding yield of ^{233}U (η_{U3}) has been evaluated as:

$$\eta_{U3} = \frac{\mathrm{R_{cap}}\left[^{232}\mathrm{Th}\right] - \mathrm{R_{abs}}\left[^{233}\mathrm{Th}\right] - \mathrm{R_{abs}}\left[^{233}\mathrm{Pa}\right]}{\mathrm{R_{cap}}\left[^{232}\mathrm{Th}\right]}$$

All the reaction rates have been obtained from the FISPACT code, providing as input the neutron spectrum obtained by the previous SERPENT calculations, properly recast in the XMAS format requested by the code.

Deterministic calculations

The three-group cross sections generated with SERPENT have been used for additional neutronic evaluation with the DYNAMOSS code [Dulla, 2005]. This code, based on a multigroup diffusion model in cylindrical r-z geometry, has been specifically developed for the study of circulating fuel system, therefore allowing evaluating the physical effects associated to the movement of the precursors in the system. The integral parameters for kinetic models have been properly defined and implemented [Dulla et al., 2004]. The parameters evaluated with the DYNAMOSS code are

- the effective fraction of delayed neutrons accounting for the fuel motion:

$$\tilde{\beta}_i = \frac{\left\langle \mathcal{E}_{i,0}^{\dagger} \middle| \hat{\mathrm{M}}_i \phi \right\rangle}{\mathcal{F}} \qquad \mathcal{F} = \sum_{i=1}^{R} \left\langle N_0^{\dagger} \middle| e_i \right\rangle + \left\langle N_0^{\dagger} \middle| \hat{\mathrm{M}}_p \phi \right\rangle$$

where the delayed fission production ($\widehat{\mathrm{M}}_i\phi$) is weighted on the importance of the delayed emissivities ($\varepsilon_{i,0}^{\dagger}$), to account properly of the change of importance of the delayed neutron precursors due to the fuel motion. The normalization is performed dividing by the total fission importance $\mathcal{F}$;

- the effective prompt neutron generation time, equal to 0.87 μs, is calculated by:

$$\ell_p = \frac{\left\langle N_0^{\dagger} \,|\phi\right\rangle}{\mathcal{F}} \qquad\qquad \mathcal{F} = \sum_{i=1}^{R} \left\langle N_0^{\dagger} \,|e_i\right\rangle + \left\langle N_0^{\dagger} \left|\hat{\mathrm{M}}_p\phi\right.\right\rangle$$

λ [s^{-1}]	β [pcm]	β_{eff} [pcm]	$\tilde{\beta}$ [pcm]
0.0125	23.4 ± 0.005	22.4 ± 0.1	7.0
0.0283	46.1 ± 0.01	44.8 ± 0.2	14.1
0.0425	40.9 ± 0.005	39.6 ± 0.2	12.7
0.1330	63.0 ± 0.009	61.4 ± 0.2	20.8
0.2925	99.8 ± 0.01	96.7 ± 0.3	36.8
0.6665	15.7 ± 0.01	15.2 ± 0.1	7.3
1.6348	21.5 ± 0.007	20.9 ± 0.1	14.6
3.5546	4.6 ± 0.002	4.5 ± 0.1	4.0
0.3278	315.1 ± 0.02	305.7 ± 0.5	117.3

Table 3.7: Delayed neutron production with β the physical beta value (from SERPENT), β_{eff} the effective beta (from SERPENT, not accounting for fuel motion) and $\tilde{\beta}$ the effective beta (from DYNAMOSS, accounting for fuel motion)

3.2.6. Technical University of Delft (TU-Delft)

The TU Delft model comprises of three coupled modules [Warmoeskerken et al., 2012; Van der Linden, 2012]: HEAT is an in-house developed CFD-program; DALTON, also in-house developed, calculates the neutronics and SCALE determines cross sections. The Neutronics Benchmark is modeled axisymmetrically by coupling these three modules, taking geometry and material properties into consideration. More information about the MSFR neutronic calculations may be found in [Frima, 2013].

Computational Fluid Dynamics

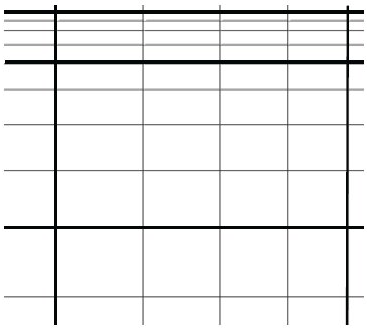

Figure 3.10: Part of the finer staggered HEAT mesh (264 x 312 cells), here displayed in gray, lies exactly on top the coarser DALTON mesh (68 x 78 cells), displayed as black

HEAT is the Computational Fluid Dynamics program. For the benchmark calculations, HEAT is programmed with a 264 x 312 staggered grid with rectangular cells. The mesh becomes finer near the walls. Figure 3.10 displays part of the mesh for both HEAT and DALTON. Reynolds Averaged Navier Stokes (RANS) equations with Boussinesq's hypothesis and the standard k-ε model form the basis of the (incompressible) flow model. The density is constant over space, although the buoyancy is modeled up to first order as a body force (see equation 3.10). T_{ref} is the reference temperature.

$$f_{b_z} \approx -\rho_f(T_{ref}) g_z \beta_\rho(T_{ref})(T - T_{ref}) \qquad \text{(Eq. 3.10)}$$

Energy transport is modeled only in the fluid. Therefore no energy transfer is modeled between fluid and structural materials; the only way energy leaves the system is via the heat

exchanger (see Figure 3.11). The heat sink depends both on velocity and temperature difference and occupies 36% of the out-of-core region. The Nusselt number is determined according to the Dittus-Boelter correlation. The pump is modeled as a body force and the pressure difference amounts to approximately 27 kPa. In the fertile blanket, the flow is also neglected. Heat transfer in this blanket is not modeled.

Neutronic calculations

DALTON is the in-house developed program calculating the neutronics. It uses a grid of 68 x 78 cells (thus four times coarser in each direction than HEAT) and the mesh of DALTON exactly overlaps HEAT's mesh. DALTON solves the neutron flux with the multi group diffusion equation, using nine energy groups and six precursor groups. Table 3.8 gives the energy boundaries of the flux and table 3.9 the decay constants and delayed neutron production of the precursor groups.

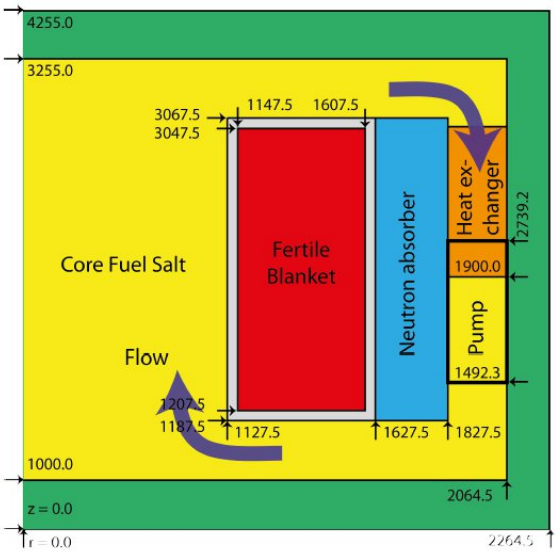

Figure 3.11: Model geometry of the MSFR (picture not to scale)

Boundary	Neutron energy (eV)
1	$2.000 \cdot 10^{7}$
2	$1.400 \cdot 10^{6}$
3	$5.730 \cdot 10^{5}$
4	$7.300 \cdot 10^{4}$
5	$2.290 \cdot 10^{3}$
6	$1.860 \cdot 10^{2}$
7	$5.200 \cdot 10^{1}$
8	$3.325 \cdot 10^{1}$
9	$1.290 \cdot 10^{1}$
10	$1.000 \cdot 10^{-5}$

Table 3.8: Boundaries of the nine energy groups

i	decay constant $[s^{-1}]$	ν_{d_i} x 100
1	0.0129 ± 0.0002	0.053 ± 0.003
2	0.0311 ± 0.0005	0.197 ± 0.012
3	0.134 ± 0.003	0.175 ± 0.025
4	0.331 ± 0.012	0.212 ± 0.013
5	1.26 ± 0.12	0.047 ± 0.014
6	3.21 ± 0.26	0.016 ± 0.006

Table 3.9: Six precursor groups with their characteristic decay time and delayed neutron production

Using the flow field provided by HEAT, DALTON takes into account precursor transport. Decay heat, however, is not modeled, i.e. all fission energy is considered prompt and thus released at the exact fission location. Equation 3.11 presents the differential equation describing precursor time evolution.

$$\frac{\partial C_k}{\partial t} + \vec{u} \cdot \nabla C_k = \nabla \cdot D_{eff} \nabla C_k + \beta_k \sum_{g=1}^{G} \nu \Sigma_{fg} \phi_g - \lambda_k C_k \qquad \text{(Eq. 3.11)}$$

Cross-sections

This model uses SCALE 6 to determine cross sections. In the first step, the cross sections are calculated for the mixture of nuclides using INFHOMMED, part of SCALE's CSASI routine in 238 neutron groups. It is done for several temperatures, each 100 K apart. In a second step, XSDRN, also part of SCALE, collapses these cross sections into 9 energy groups, taking geometry in 1 dimension into account. This process creates libraries of cross sections at 100 K intervals. In a final step, the proper library is chosen (depending on geometry) and the cross section at the proper temperature is interpolated using the weights of equation 3.12:

$$\omega_2 = \frac{\sqrt{T} - \sqrt{T_1}}{\sqrt{T_2} - \sqrt{T_1}} \quad \omega_1 = 1 - \omega_2 \qquad \text{(Eq. 3.12)}$$

3.3. Static calculations: results and comparisons

3.3.1. Effective reactivity (k_{eff}) corresponding to the initial compositions provided

First, a calculation of the effective multiplication coefficient k_{eff} for the compositions provided in the benchmark and reminded in Table 3.10.

^{233}U-started MSFR		TRU-started MSFR		
Th	^{233}U	Th	Actinide	
38 281 kg 19.985 %mol	4 838 kg 2.515 %mol	30 619 kg 16.068 %mol	Pu	11 079 kg 5.628 %mol
			Np	789 kg 0.405 %mol
			Am	677 kg 0.341 %mol
			Cm	116 kg 0.058 %mol

Table 3.10: Initial composition of the ^{233}U-started and TRU-started MSFR as provided for the benchmark calculations

The results of this calculation (see Table 3.11) show some important discrepancies that may be understood by looking more deeply the reaction rates corresponding to each reactor calculation. As can be concluded with Table 3.12 (for the ^{233}U-started MSFR composition), the choice of the database impacts the results, especially for the capture rates of ^{233}U and ^{232}Th. As shown in Figures 3.12 and 3.13, the (n,γ) cross-sections of ^{233}U and ^{232}Th show some noticeable discrepancies between the different databases. It also impacts the neutron spectrum as detailed in section 3.3.5.

Using JEFF-3.1 database, LPSC and POLIMI calculations are globally in good agreement even if some small discrepancies may be noticed on the ^{6}Li reaction rates.

Composition	LPSC ENDF-B.6	LPSC JEFF-3.1	POLITO analog JEFF-3.1.1	POLITO implicit JEFF-3.1.1	POLIMI SERPENT JEFF-3.1	POLIMI SERPENT ENDF-B7	POLIMI ERANOS JEFF-3.1
^{233}U-started	**1.02141**	**0.97628**	**0.99211**	**0.99206**	**0.99406**	**0.98301**	**1.01707**
Δk	3 pcm	84 pcm	11 pcm	4.3 pcm	40 pcm	41 pcm	-
TRU-started	**1.00273**	**1.00817**	**1.02873**	**1.02878**	**1.01651**	**1.01955**	**1.0143**
Δk	2 pcm	72 pcm	12 pcm	4 pcm	44 pcm	45 pcm	-

Table 3.11: Multiplication coefficient evaluation by different partners with different data bases for initial composition given in table 3.10

Reaction rate R = NσΦ [mol/day]	LPSC ENDF-B.6	LPSC JEFF-3.1	POLITO SERPENT JEFF-3.1.1	POLIMI SERPENT JEFF-3.1
Mean flux Φ [n/cm^2/s]	**3.38 10^{+15}**	**3.57 10^{+15}**	**3.499 10^{+15} ±2.1 10^{+11}**	**3.56 10^{+15}**
Fission Rate ^{233}U	**13.1**	**13.1**		**13.3**
(n,γ) Rate ^{233}U	**1.56**	**1.36**		**1.37**
Fission Rate ^{232}Th	**0.23**	**0.25**		**0.24**
(n,γ) Rate ^{232}Th	**15.1**	**15.9**		**15.8**
(n,t) Rate ^{6}Li	**0.154**	**0.157**		**1.9 10^{-3}**
(n,p) Rate ^{6}Li	**4.0 10^{-5}**	**3.9 10^{-5}**		
(n,γ) Rate ^{6}Li	**5.9 10^{-6}**	**6.0 10^{-6}**		
(n,γ) Rate ^{7}Li	**6.9 10^{-3}**	**7.6 10^{-3}**		**6.85 10^{-3}**
(n,γ) Rate ^{19}F	**0.15**	**0.13**		**0.12**
(n,α) Rate ^{19}F	**0.29**	**0.29**		**0.29**
(n,γ) Rate TOTAL	**16.8**	**17.3**		**17.29**
Fission Rate TOTAL	**13.3**	**13.3**		**13.55**
Statistic uncertainty	**< 2 %**	**< 2 %**		**0.1 – 5 %**

Table 3.12: Reaction rates in the fuel only, extracted from the evaluation by different partners with different data bases for initial composition of ^{233}U-started MSFR given in table 3.10

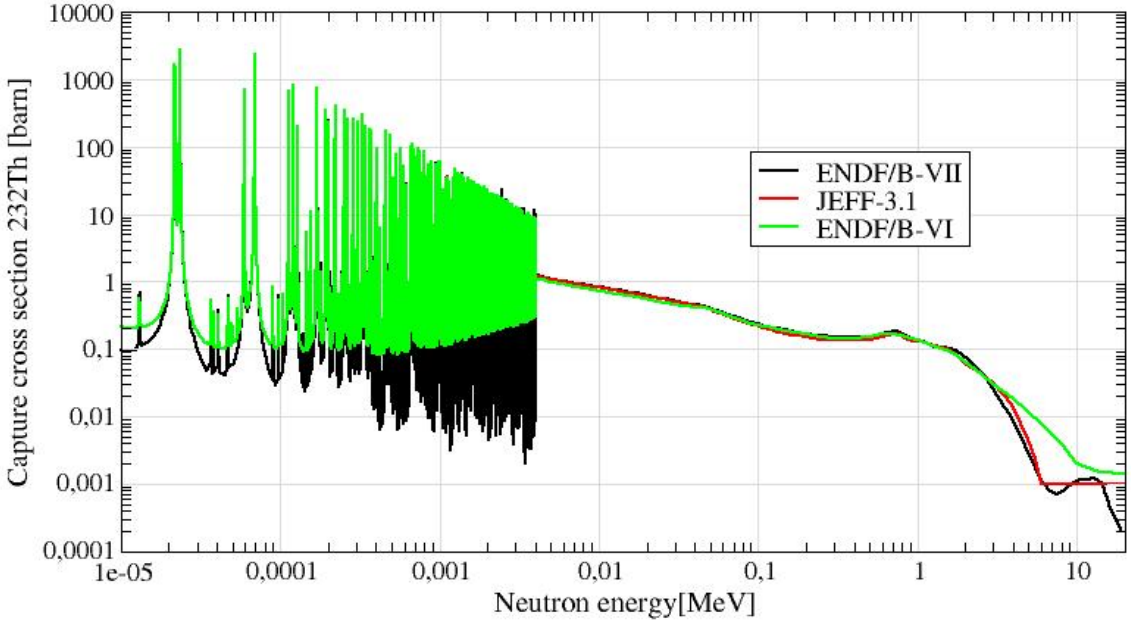

Figure 3.12: (n,γ) cross-section of ^{232}Th for the different databases used in the neutronic benchmark calculations

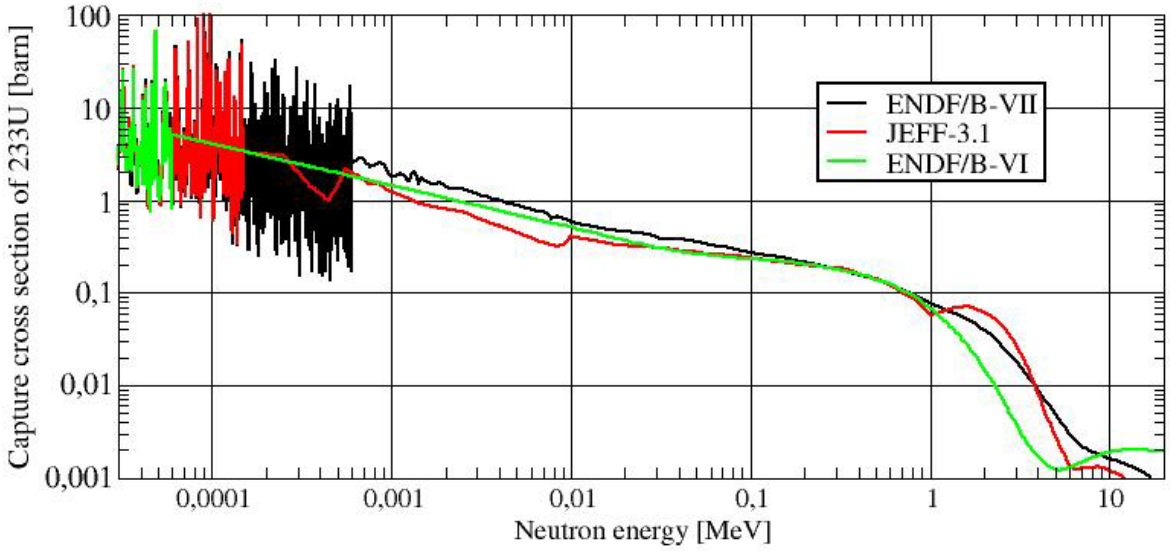

Figure 3.13: Neutron capture cross section of ^{233}U for different databases

3.3.2. Adjustment of the critical amount of initial fissile matter

The adjustments of the initial fissile amount have been performed either for $k_{prompt}=1$ or $k_{eff}=1$ depending on the partner, the precision Δk corresponding to each evaluation being indicated in the Table 3.13 for the ^{233}U-started MSFR, and in Tables 3.14. Again, some differences are observed, especially for ^{233}U-started MSFR. Those are partly due to the different data bases used for this evaluation by each partner, as already mentioned.

The critical inventories adjusted by each partner are quite similar despite the various calculation tools and databases used. We have to notice that the amount of ^{233}U is the most sensitive to these differences between the calculations, the differences on its evaluation being mainly due to the database used. In particular, the (n,γ) cross-sections of ^{233}U and ^{232}Th show some noticeable discrepancies between the different databases (see Figures 3.12 and 3.13).

^{233}U-started MSFR				
Element	LPSC ENDF-B6	TU Delft ENDF-B7	POLITO JEFF-3.1.1	KI ENDF-B5,6
$k_{effective} = 1$				
Th	19.985 %mol	19.886 %mol	19.948 %mol	-
^{233}U	2.515 %mol	2.614 %mol	2.551 %mol	-
Δk	5 pcm	-	12/4.6 pcm	-
$k_{prompt} = 1$				
Th	19.98 %mol	-	-	20.02 %mol
^{233}U	2.52 %mol	-	-	2.48 %mol
Δk	56 pcm	-	-	609 pcm

Table 3.13: ^{233}U started MSFR initial composition adjusted for $k_{effective} = 1$ or $k_{prompt} = 1$

TRU-started MSFR			
Element	LPSC ENDF-B6 $k_{effective}$	POLITO JEFF-3.1.1 $k_{effective}$	KI ENDF-B5,6 k_{prompt}
Th	16.068 %mol	16.3803 %mol	16.2 %mol
Pu	5.628 %mol	5.3547 %mol	5.50 %mol
Np	0.405 %mol	0.386 %mol	0.400 %mol
Am	0.341 %mol	0.324 %mol	0.33 %mol
Cm	0.058 %mol	0.055 %mol	0.057 %mol
Δk	3 pcm	15/4.7 pcm	153 pcm

Table 3.14: TRU started MSFR initial composition adjusted for $k_{effective} = 1$ or $k_{prompt} = 1$

3.3.3. Delayed neutron fraction

In Tables 3.15 to 3.17, the following definitions are used:

- β_0 is the physical fraction of delayed neutrons.
- β_{eff} is the fraction taking into account the importance of the delayed neutrons for the fission compared to the prompt neutrons ($E_n^{Delayed} < E_n^{Prompt}$).
- β_{circ} is the fraction of delayed neutrons accounting the motion of the fuel salt.

^{233}U-started composition	LPSC ENDF/ B6	POLITO JEFF-311 (see section 3.2.5)	POLIMI SERPENT			POLIMI ERANOS JEFF-3.1	TU Delft ENDF-B7
			JEFF-3.1		ENDF-B7		
			Nominal flow rate	Uniform sampling			
β_0 [pcm]	330	315.00 ± 0.04	310		325	-	310
β_{eff} [pcm]	320	305.00 ± 0.76	305		317.8	318.1	290
β_{circ}/β_{eff}	0.529	0.3837	0.479	0.407	-	0.540[b]	0.430
β_{circ} [pcm]	169.46	117.3	146	124	-	171.9[b]	124.6

Table 3.15: Initial delayed neutron fraction for the ^{233}U-started MSFR

TRU-started composition	LPSC ENDF/B 6	POLITO JEFF-311 (see section 3.2.5)	POLIMI SERPENT			POLIMI ERANOS JEFF-3.1	TU Delft ENDF/B7
			JEFF-3.1		ENDF/B 7		
			Nominal flow rate	Uniform sampling			
β_0 [pcm]	342.6	343.00 ± 0.05	334		331	-	-
β_{eff} [pcm]	312.76	301.00 ± 0.74	302		301.9	302.1	-
β_{circ}/β_{eff}	0.529	-	0.487	0.391	-	0.552[b]	-
β_{circ} [pcm]	165.45	-	147	118	-	166.7[b]	-

Table 3.16: Initial delayed neutron fraction for the TRU-started

Steady state composition	LPSC ENDF/B6	POLITO JEFF-311 (see section 3.2.5)	POLIMI SERPENT			POLIMI ERANOS JEFF-3.1	TU Delft ENDF/B7
			JEFF-3.1		ENDF/B7		
			Nominal flow rate	Uniform sampling			
β_0 [pcm]	359.7	-	331		356	-	322
β_{eff} [pcm]	342.63	-	319.9		340.8	334.2	307
β_{circ}/β_{eff}	0.529	-	-	-	-	0.537[b]	0.435
β_{circ} [pcm]	181.25	-	-	-	-	179.5[b]	133.64

Table 3.17: Delayed neutron fraction of the MSFR at steady-state

As expected, the TRU-started MSFR composition has the smallest fraction of delayed neutrons, while ^{233}U-started MSFR composition the highest delayed neutron fraction according to all participants. It is clear that the circulation of the fuel salt has an important influence on the delayed neutron fraction. The correction factor is of around 0.5 with different evaluation methods. This corresponds to the proportion of the fuel salt volume in the core.

[b] Values calculated with a simplified correction method and not with ERANOS

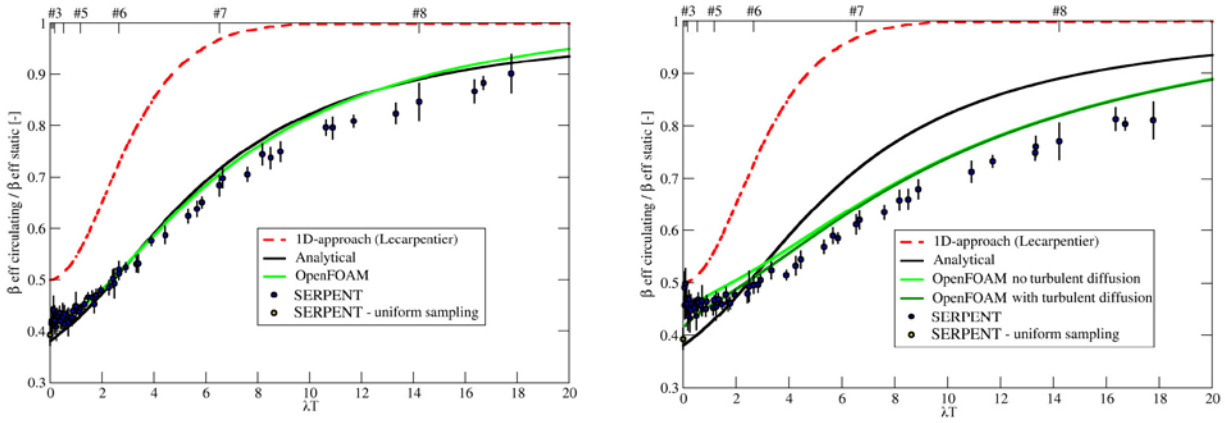

Figure 3.14: On the left with the uniform velocity field in the core, on the right with (k-ε) turbulence model [Aufiero et al. 2013b]

Some more precise evaluations have been performed by POLIMI with JEFF-3.1, as detailed in [Aufiero et al. 2013b]. Figure 3.14 shows the influence of the different methods and models used to estimate the loss of the delayed neutrons due to the circulation of the fuel. We can observe that the flow distribution, for example with or without the recirculation of the fluid near the blanket wall (nominal flow or uniform sampling, see Tables 3.15 to 3.17), influences the factor calculation by up to 20-30%. The recirculation trends to increase the delayed neutron fraction in the core.

3.3.4. Generation time

The results are presented in Table 3.18. The definitions used by each partner for the determination of the generation time are the following:

- **ERANOS**: weighted with adjoint flux
- **POLIMI SERPENT** and **LPSC**: implicit prompt lifetime
- **POLIMI SERPENT:** weighted with adjoint flux (based on the Iterated Fission Probability method)
- **TU-Delft**: lifetime evaluated as

$$\Lambda = (\frac{\bar{1}}{v})\frac{1}{\overline{\nu\Sigma_f}} = \frac{\int \frac{1}{v}\phi d^3rdE}{\int \phi d^3rdE}\frac{\int \phi d^3rdE}{\int \nu\Sigma_f\phi d^3rdE}$$

- **POLITO Analog:** average time between neutron emission and absorption (cannot account for leaked neutrons)
- **POLITO Implicit:** computed according to the following formula

$$t_{gen} = \frac{k_{eff}}{\bar{\nu}\,\nu\Sigma_f}$$

According to different definitions used by the partners, there is a global agreement regarding the prompt lifetime calculation. POLIMI's evaluations with SERPENT are in a very good agreement with the results of LPSC using MCNP and of TU Delft, especially for the initial compositions. Adjoint-weighted generation times were calculated by POLIMI with ERANOS and Serpent codes, for the TRU-started composition the generation time is much lower, almost half compared to the ^{233}U-started composition.

[µs]	LPSC	POLITO SERPENT analog	POLITO SERPENT implicit	POLIMI ERANOS (adjoint-weighted gen. time)	POLIMI SERPENT		TU Delft
					(implicit prompt lifetime)	(adjoint-weighted gen. time)	
^{233}U-started MSFR	1.2	0.9694	0.9706	1.13	1.204	1.09	1.15
TRU-started MSFR	0.9	0.7816	0.7827	0.64	0.93	0.65	-
Steady State	1.2	-	-	0.96	0.90	-	1.04

Table 3.18: Neutron generation time evaluation

Calculations performed by POLITO using an analog and an implicit methods are in a very good agreement with each other, but these values are slightly lower (around 20%) compared to the other evaluations. This may come from the evaluation here of the "prompt neutron reproduction time" which differs from both the generation time and the average prompt lifetime of other partners.

3.3.5. Thermal feedback coefficient

In the benchmark, the idea was to calculate the two contributions of the feedback coefficient (Doppler and density coefficients), together with the total value and its uncertainty. LPSC calculations were performed with a ΔT of 100K (neutronic calculations at 925 K and 1025 K). Similarly, Kurchatov Institute's calculations were performed at 900 and 1000 K. The results from POLITO were calculated at 900K and 1200K (data available by default in SERPENT). At POLIMI the evaluations were carried out using three different data bases: ENDF/B-6.8, ENDF/B-7 and JEFF-3.1. The Doppler coefficient was estimated by a comparison of two Monte Carlo runs with fuel temperature at 900 K and 1200 K. The density coefficient was calculated reducing the fuel density by 5% (from nominal value). The results are presented in Tables 3.19 to 3.23.

KI (ENDF-B6)	Density	Doppler	Uncertainty	TOTAL
^{233}U-started MSFR	-2.8	-4.7	+/- 0.2 pcm/K	-7.5
TRU-started MSFR	-2.7	-1.6	+/- 0.2 pcm/K	-4.3
Steady State	-2.5	-3.4	+/- 0.2 pcm/K	-5.9

Table 3.19: Thermal feedback coefficient evaluated by KI in pcm/K

LPSC (ENDF-B6)	Density	Doppler	TOTAL
^{233}U-started MSFR	-3.6	-2.6	-6.3 +/- 0.1 pcm/K
TRU-started MSFR	-2.2	-1.5	-3.8 +/- 0.1 pcm/K
Steady State	-3.2	-2.2	-5.4 +/- 0.3 pcm/K

Table 3.20: Thermal feedback coefficient evaluated by LPSC in pcm/K

POLIMI	^{233}U started			TRU started		
	ENDF-B7	ENDF-B6	JEFF 3.1	ENDF-B7	ENDF-B6	JEFF 3.1
Doppler	-1.63 ± 0.06	-1.78 ± 0.06	-1.64 ± 0.06	-3.73 ± 0.07	-3.77 ± 0.06	-3.84 ± 0.07
Density	-2.75 ± 0.06	-2.78 ± 0.06	-2.92 ± 0.06	-3.55 ± 0.07	-3.20 ± 0.07	-3.45 ± 0.07

Table 3.21: Thermal feedback coefficient evaluated with SERPENT by POLIMI in pcm/K

POLITO (JEFF-31)	Density	Doppler	Total
^{233}U-started	analog: -3.42±0.048 implicit: -3.41±0.018	analog: -3.15±0.048 implicit: -3.13±0.018	analog: -6.52±0.057 implicit: -6.53±0.022
TRU-started	analog: -2.85±0.041 implicit: -2.82±0.013	analog: -1.29±0.040 implicit: -1.31±0.013	analog: -4.11±0.066 implicit: -4.15±0.022

Table 3.22: Thermal feedback coefficient evaluated by POLITO in pcm/K

For TU-Delft, the total feedback coefficient is calculated by using the steady state flow and setting the entire reactor first at 650°C and then at 750°C. The total feedback coefficient is calculated by taking the difference between the two corresponding reactivity values and dividing by 100. As for other partners, the Doppler feedback coefficient is calculated by holding the density constant when calculating the cross-sections. The density feedback coefficient is calculated while only varying the density.

TU Delft	Density/Void	Doppler	Total
^{233}U-started	-2.58	-4.39	-6.97
TRU-started			
Steady State (100 yrs)			-5.27

Table 3.23: Thermal feedback coefficient evaluated by TU-Delft

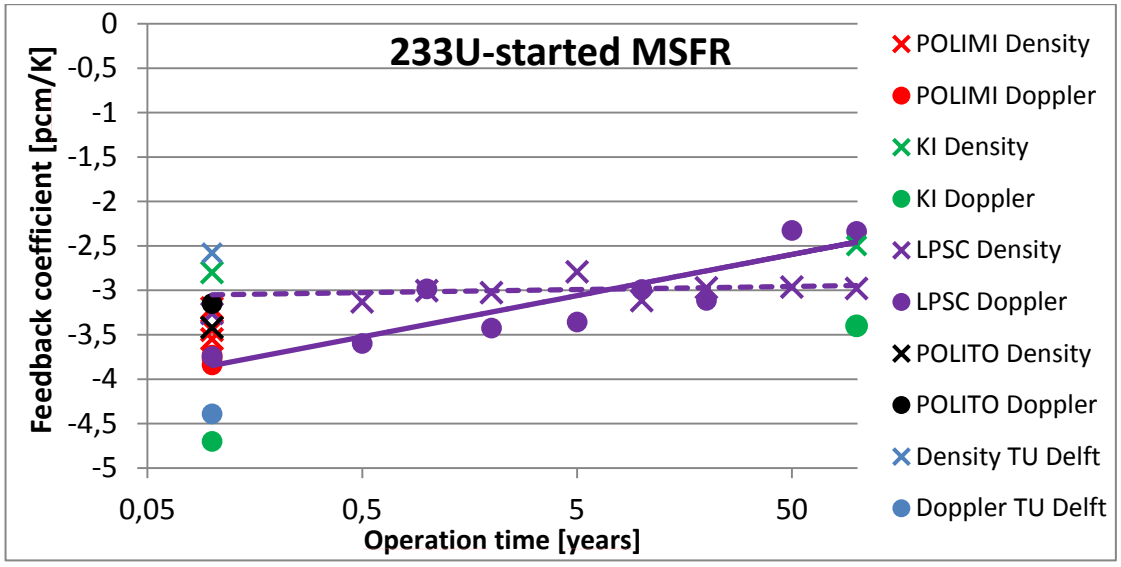

Figure 3.15: Feedback coefficient evaluations for the ^{233}U-started MSFR as a function of the reactor evolution time

The results are summarized in Figures 3.15 and 3.16 that show an overall good agreement for all compositions in the case of the initial composition of the fuel salt. The density coefficient (corresponding to the void coefficient) evaluations during reactor evolution, especially for the initial transuranic composition, are in a very good agreement for different codes and different databases. For the ^{233}U-started MSFR as its initial composition, the choice of the database has an influence on the density coefficient but has a negligible impact for the Doppler coefficient calculation. The evaluations of the Doppler effect for the initial transuranic composition are consistent within different codes and different data bases used. Only two calculations were available for the steady state composition comparison. Those show some differences for the Doppler and density coefficient calculations, while keeping the total feedback coefficient consistent. Also, the evolution of the feedback coefficient evaluated by LPSC and KI shows the same tendencies, especially for the ^{233}U-started MSFR. This effect will be investigated for the deliverable 2.3 on the sensitivities.

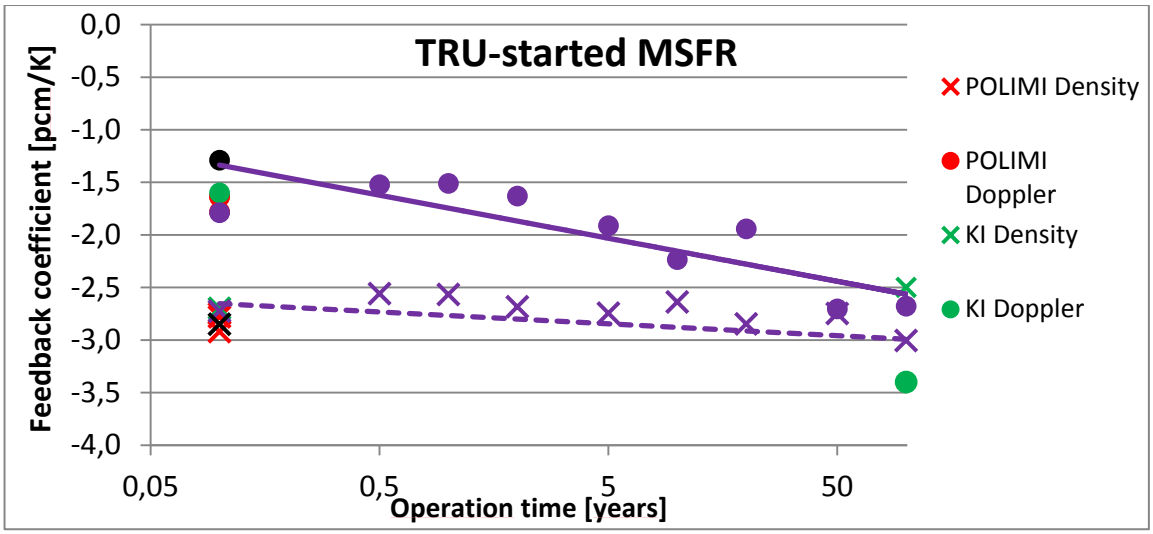

Figure 3.16: Feedback coefficient evaluations for the TRU-started MSFR as a function of the reactor evolution time

As expected, it is to point out that the initial transuranic composition presents the smallest negative feedback coefficient. These evaluations performed by all partners confirm that the total feedback coefficient as well its two contributions are negative, which is very positive for a good reactor intrinsic stability, see the deliverables 2.5 and 2.6 respectively on the safety analysis and transient calculations for more details.

3.3.6. Neutron spectrum of the MSFR

This fuel salt composition of the MSFR with 22.5 mole% of heavy nuclei leads to a fast neutron spectrum in the core, as shown in Figure 3.17 where the fast neutron spectrum of the simulated reference MSFR is compared to the spectra of 2 solid-fuel reactors: a Sodium-cooled Fast neutron Reactor (SFR) and a thermal Pressurized Water Reactor (PWR). The large Na capture cross-section appears clearly on the red curve at 2.8 keV, while the inelastic scattering cross-section of fluorine and lithium (see Figure 3.18) shows on the green curve between 0.1 MeV and 1 MeV.

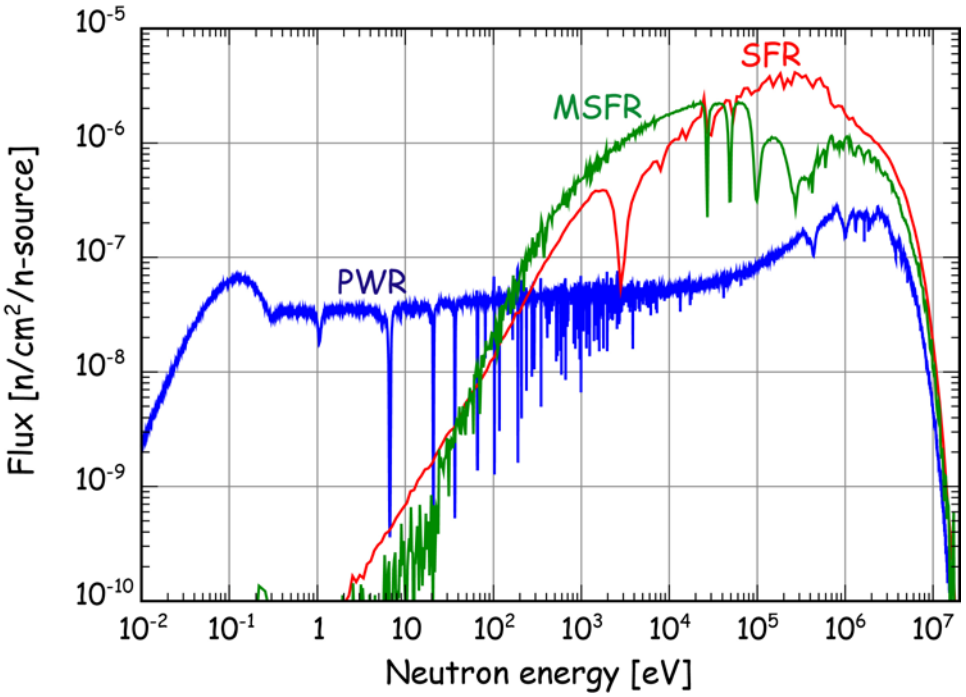

Figure 3.17: Fast neutron spectra of the reference MSFR (green curve) and of a Na-cooled fast neutron reactor (FNR-Na – red curve) compared to the thermalized spectrum of a pressurized water reactor (PWR – blue curve)

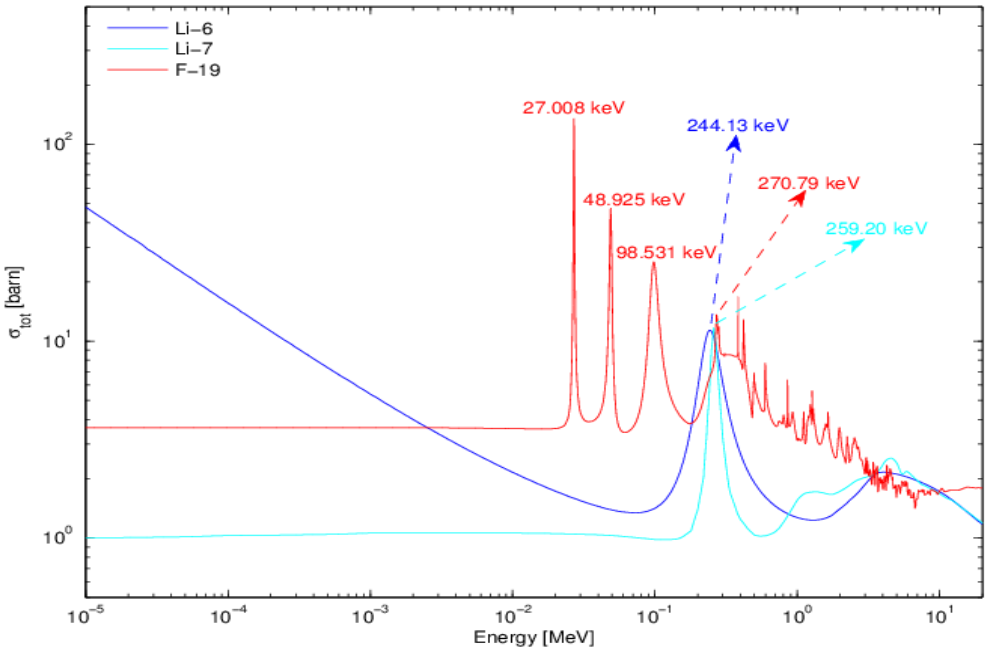

Figure 3.18: Scattering neutron cross section of ^{19}F, ^{7}Li and ^{6}Li

First, the neutron spectrum calculation has been evaluated with different tools using a continuous neutron energy and with the same database. The evaluations from POLITO (SERPENT), LPSC, POLIMI (SERPENT) with JEFF-3.1 are represented in Figure 3.19. The agreement between the curves is almost perfect. Some differences may be observed at lower energy (0.0001-0.01 MeV), that are due to the use of different energy steps at POLITO compared to LPSC and POLIMI. Some differences may also be observed around 0.1 MeV, that are due to the different options of reconstruction methods in the unresolved resonances region used for the cross section calculations. Finally, the calculations performed at Kurchatov Institute with ENDF/B-6 fit perfectly with LPSC's and POLIMI's calculations despite of the different databases used.

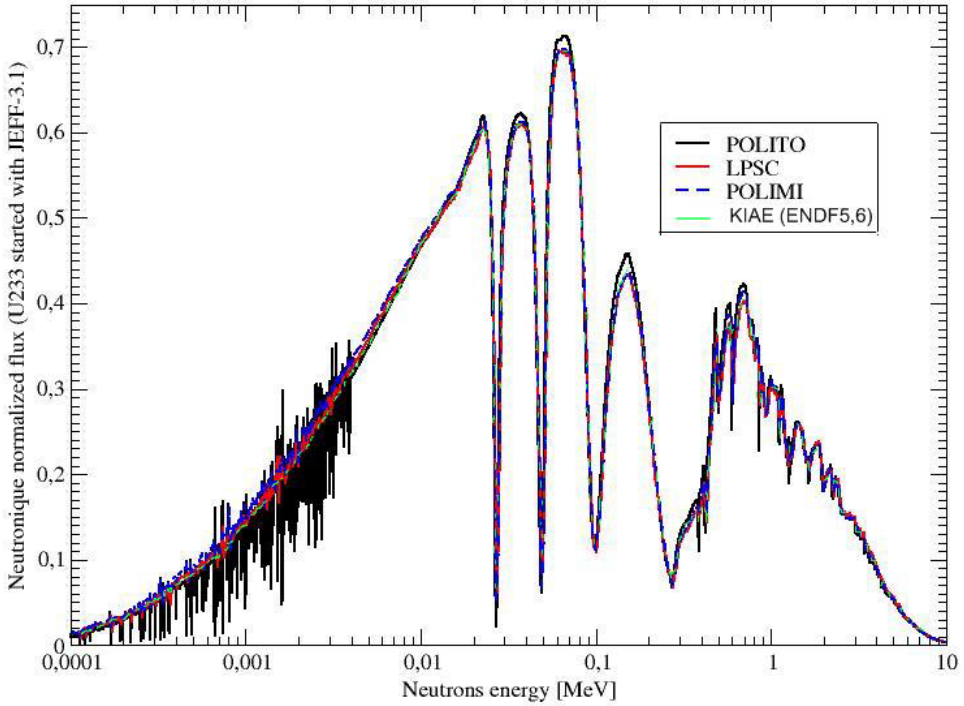

Figure 3.19: Neutronic normalized flux comparison of tools performing with continuous neutron energy spectrum

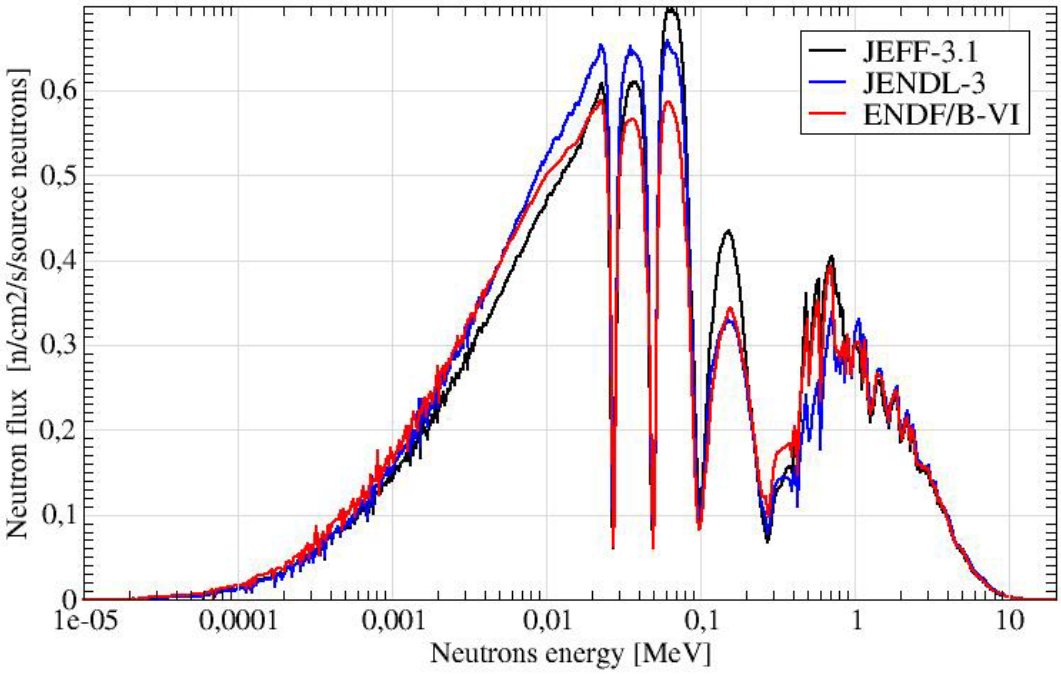

Figure 3.20: Neutronic flux comparison using different databases: JEFF-3.1, ENDF/B-6.8 and JENDL-3 evaluated with SERPENT (POLIMI) and MCNP (LPSC)

Figure 3.20 presents the sensibility study of the neutronic spectrum to the data basis used. An influence is observed using JEFF-3.1, ENDF/B-6.8 and JENDL-3 (only for Li and F isotopes, other isotopes from ENDF/B-6.8) databases. These differences may be partly explained when studying the fluoride diffusion cross section (see Figure 3.21). This cross section is evaluated differently within the databases JENDL-3, JEFF-3.1 or ENDF/B-6.8.

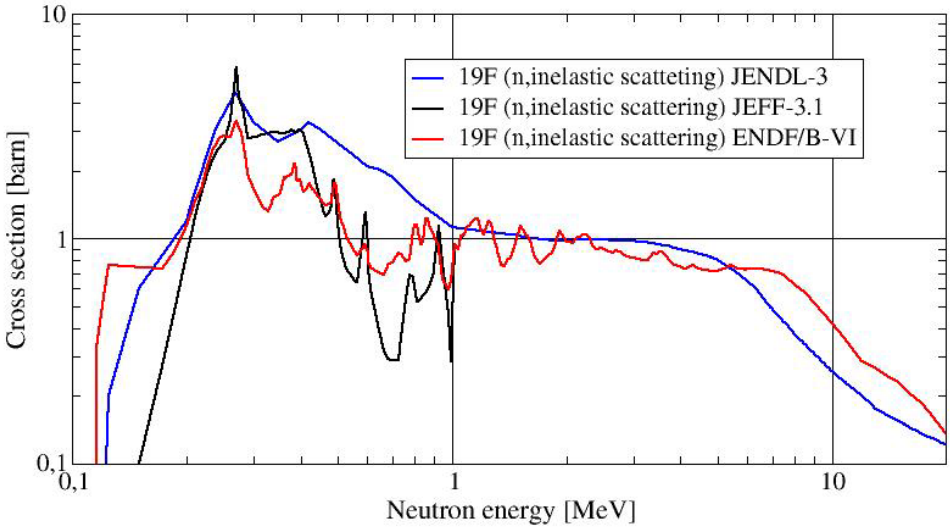

Figure 3.21: Inelastic scattering neutron cross section of ^{19}F from the databases JEFF-3.1, ENDF/B-6.8 and JENDL-3

The MSFR neutron spectrum used in the deterministic codes, ERANOS (POLIMI), HELIOS (HZDR) and DALTON (TU Delft), are shown in Figure 3.22. The evaluated spectra show an overall good agreement. The evaluation with ERANOS presents a neutron increase at low energy (10^{-8} MeV – 10^{-6} MeV), that is probably due to the choice of the numerical tolerance in the calculation, since the flux value is very low in this region. The calculation performed with HELIOS presents a more significant thermal neutron contribution compared to other codes. Indeed, the volume within the flux was calculated by including the fuel salt in the core but also the reflectors, and this adds a more important thermal neutron contribution.

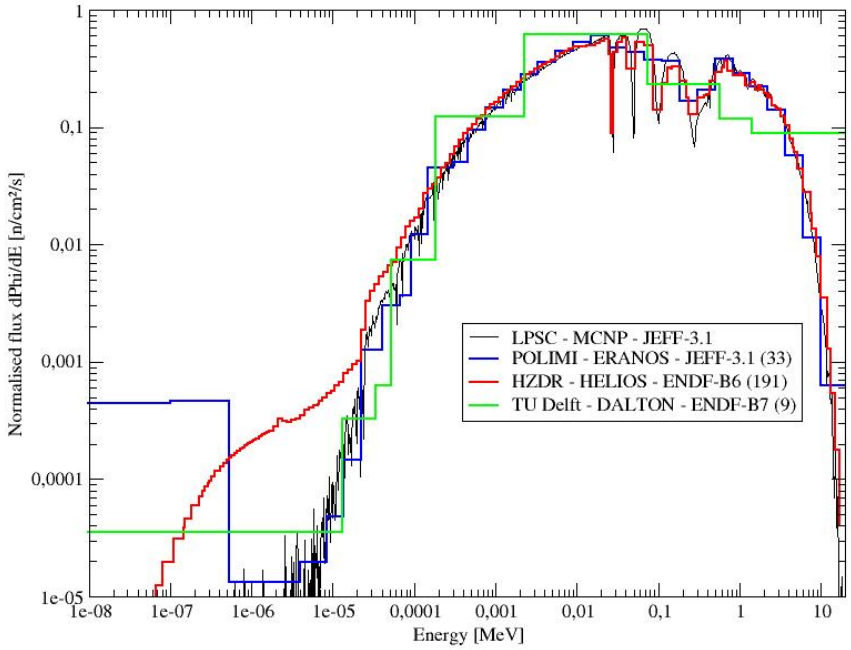

Figure 3.22: Neutron flux comparison of tools performing with discrete neutron energy spectrum

Moreover, the neutron flux distribution in the core and the fertile blanket is represented in Figure 3.23. Due to the homogeneity of fuel composition, the typical cosine/Bessel shape is obtained for the flux distribution in the core. The neutron flux in the fertile blanket is one order of magnitude lower than in the core. The neutron flux in the fertile blanket is also affected by the fuel salt circulating out of the core, as shown in Figure 3.23.

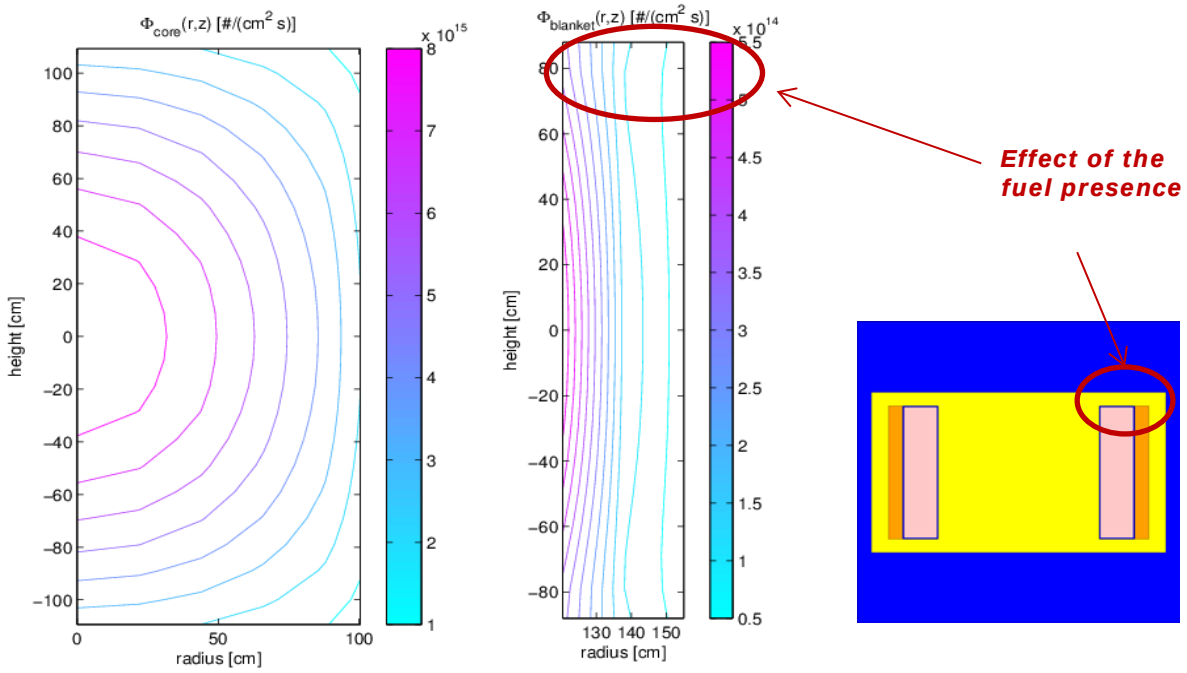

Figure 3.23: Neutron flux distribution in the core and the fertile blanket (evaluated with SERPENT, POLITO)

The neutron spectrum was also studied at different radial positions to identify some spatial effects. As shown in Figure 3.24, the neutron spectrum is very similar for different radial positions, but it becomes slightly more thermal next to the reflector. This effect is observed for both initial compositions.

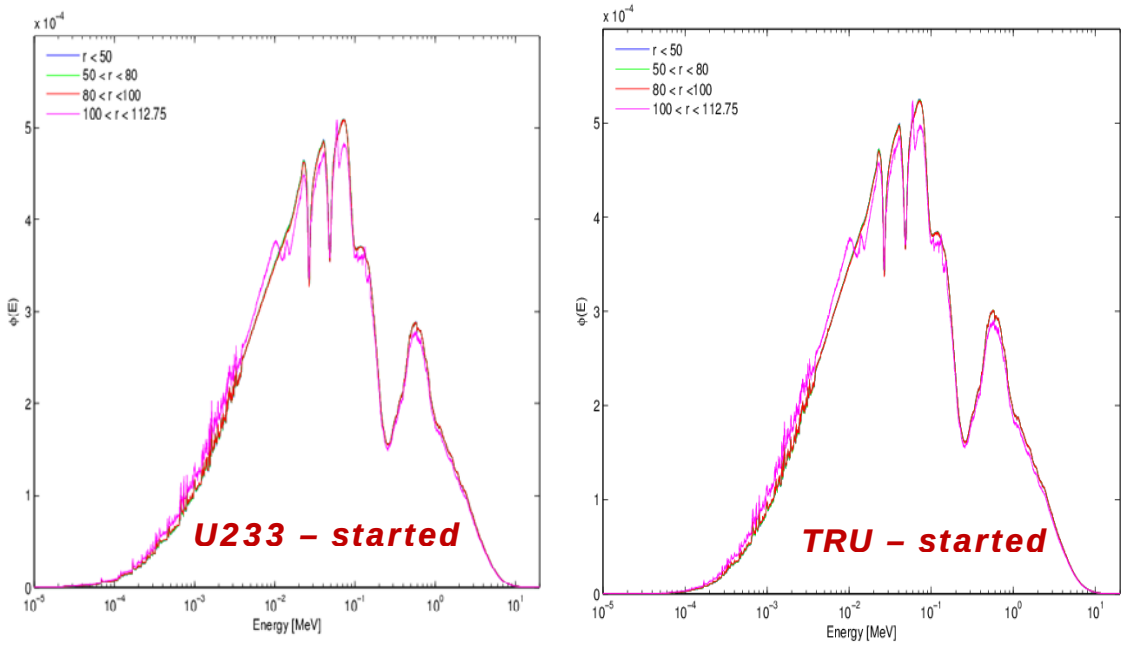

Figure 3.24: Neutron spectrum comparison for different radial positions (performed with SERPENT, POLITO)

Finally, the neutron spectrum was calculated for the different compositions of the MSFR: ^{233}U-started, TRU-started MSFR initial composition and steady state composition, as presented in Figure 3.25. The TRU-started composition has the faster spectrum and the ^{233}U-started composition the more thermal one, but all three curves are very close. The impact of the fuel salt composition is quite small.

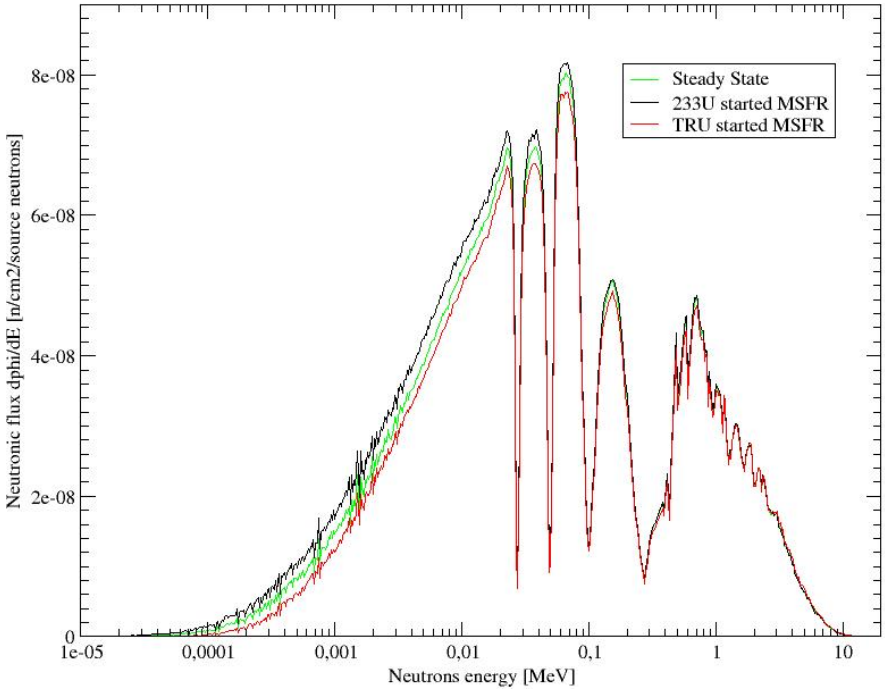

Figure 3.25: Neutron spectrum comparison for different compositions (performed with MCNP, LPSC)

3.4. Results (evolution calculations)

3.4.1. Steady state composition and evolution of the heavy nuclei inventories

The utilization of TRU elements to start the reactor increases the initial amounts of minor actinides compared to the ^{233}U-started MSFR. But at steady-state, the fuel salt compositions of TRU-started and ^{233}U-started MSFRs are identical, the initial TRU being converted into ^{233}U, as shown in Figure 3.26.

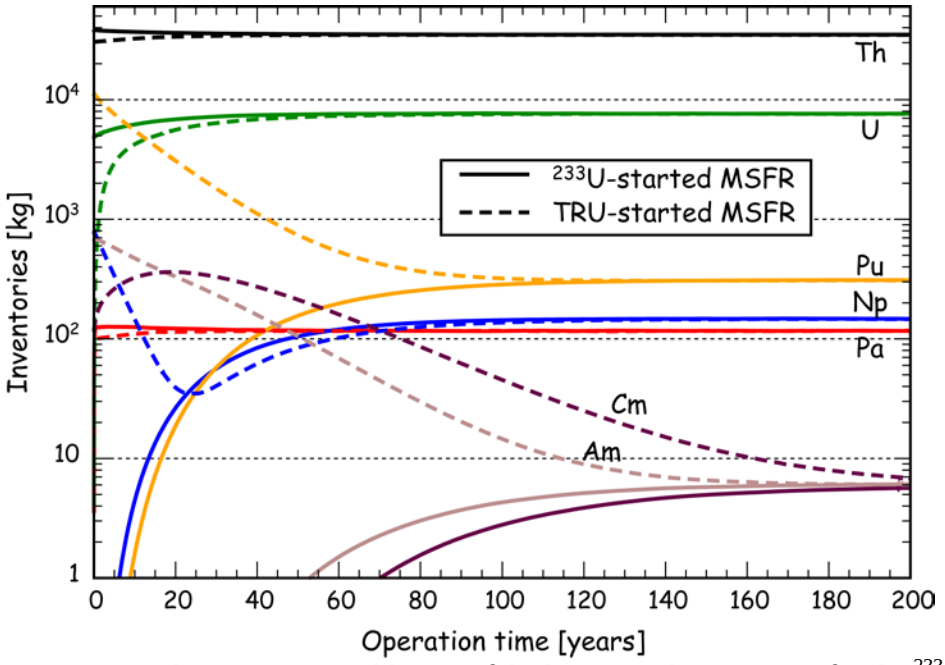

Figure 3.26: Time evolution up to equilibrium of the heavy nuclei inventory for the ^{233}U-started MSFR (solid lines) and for the TRU-started MSFR (dashed lines) – LPSC calculations

Th, Pa, U and Np reach their equilibrium composition quickly, while a few dozen years are necessary to burn 90% of the Pu initial load and around a century for the Am and Cm elements. The

in-core Cm inventory reaches a maximum of 390 kg (with 265 kg of ^{244}Cm) after 26 years of operation.

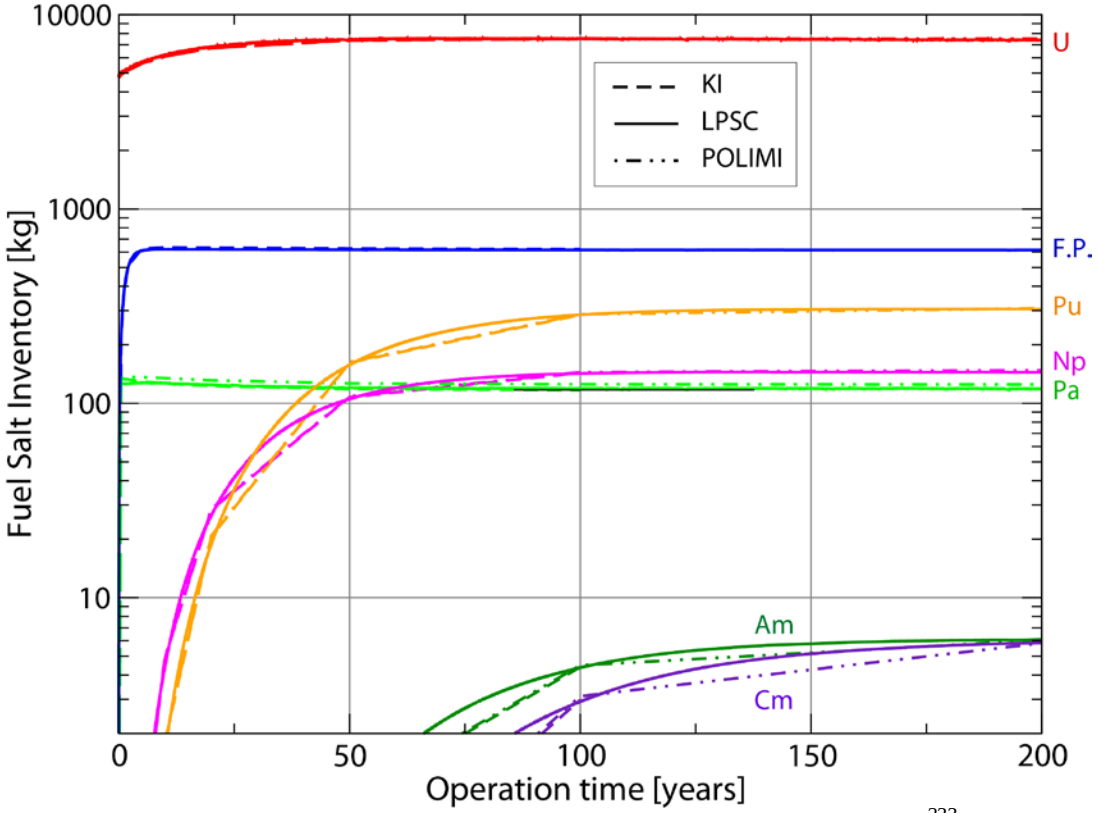

Figure 3.27: Time evolution of the trans-Th elements and fission products for the ^{233}U-started MSFR evaluated by different tools with the same database ENDF/B-6

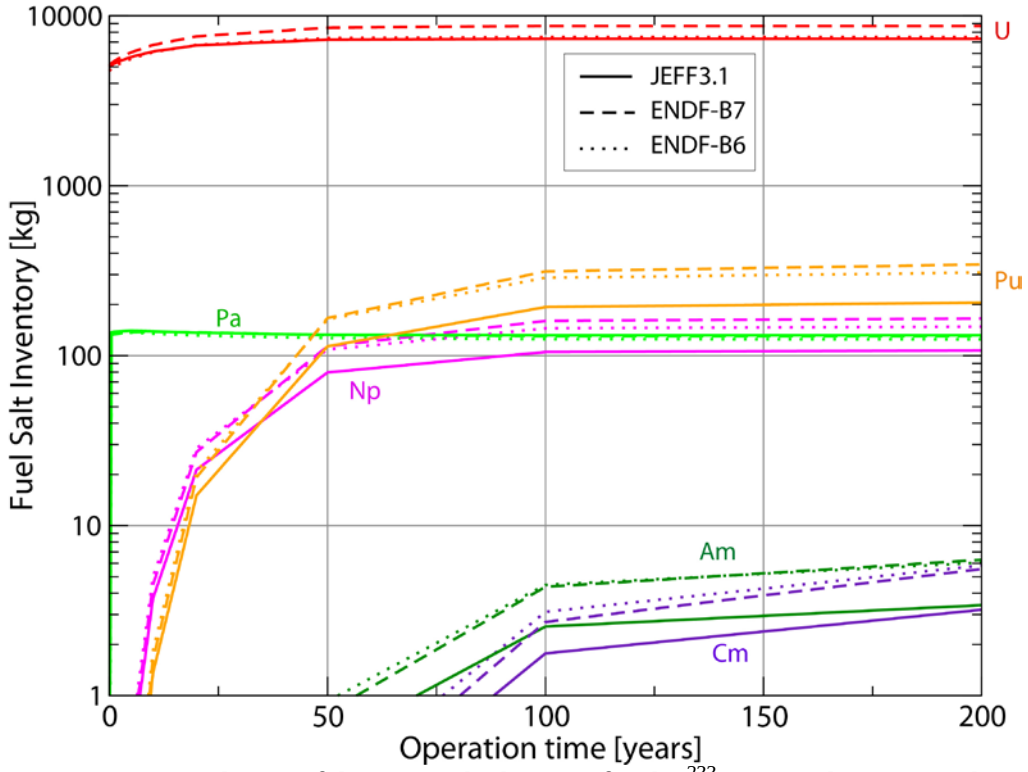

Figure 3.28: Time evolution of the trans-Th elements for the ^{233}U-started MSFR evaluated by POLIMI (SERPENT tool) with the different databases

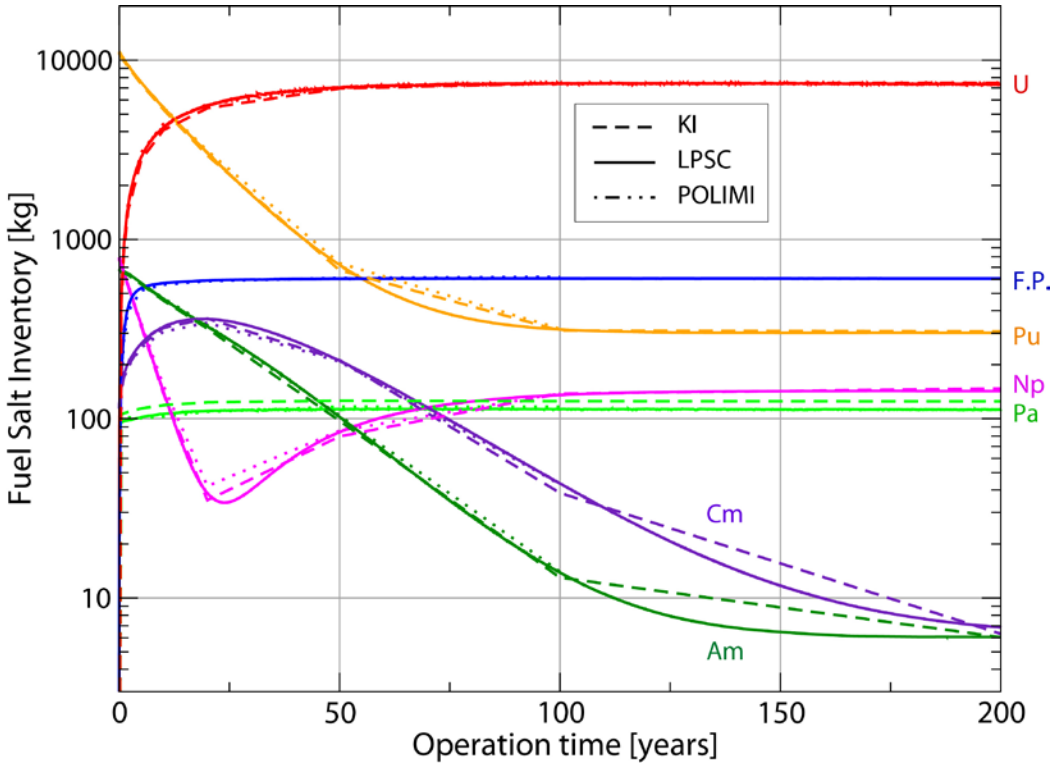

Figure 3.29: Time evolution of the trans-Th elements and fission products for the TRU-started MSFR evaluated by different tools with the same database ENDF/B-6

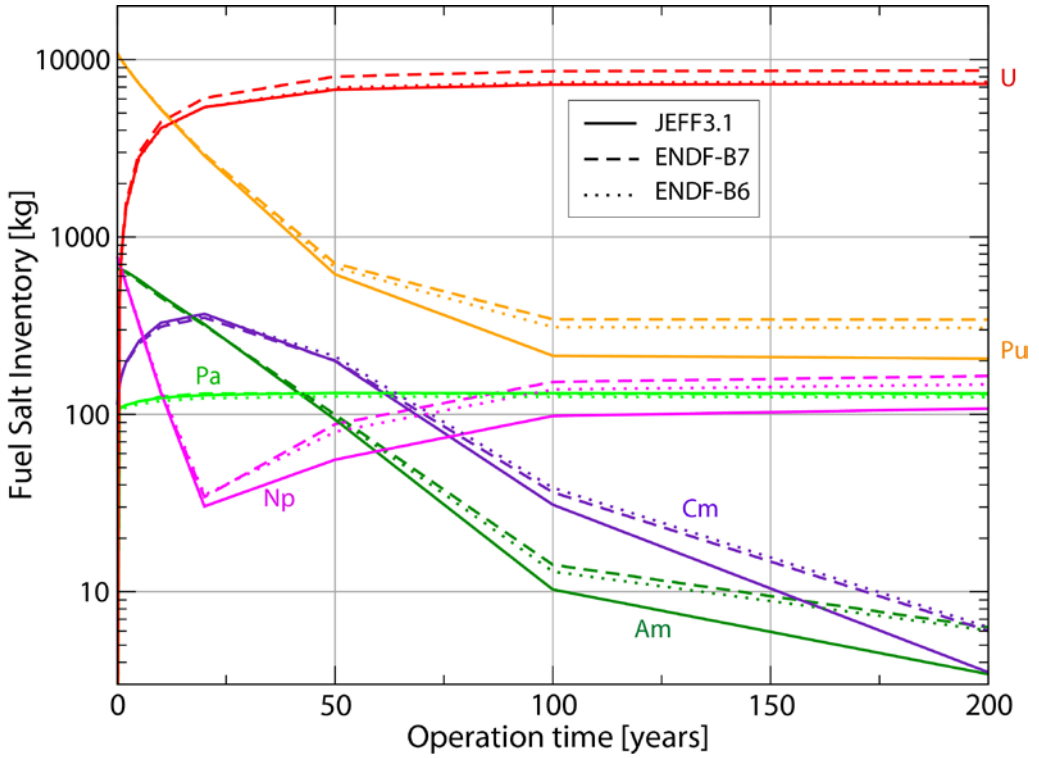

Figure 3.30: Time evolution of the trans-Th elements for the TRU-started MSFR evaluated by POLIMI (SERPENT tool) with the different databases

As observed in Figures 3.27 and 3.29, the results obtained with different tools but with the same database are in very good agreement for actinides and fission products inventory evolution, both for the ^{233}U-started and TRU-started MSFRs. The choice of the database has an important impact on the inventories evolution (see Figures 3.28 and 3.30). Detailed studies of the evolution of some specific nuclei are presented in the following sections.

3.4.2. Fuel salt evolution for the ^{233}U-started MSFR

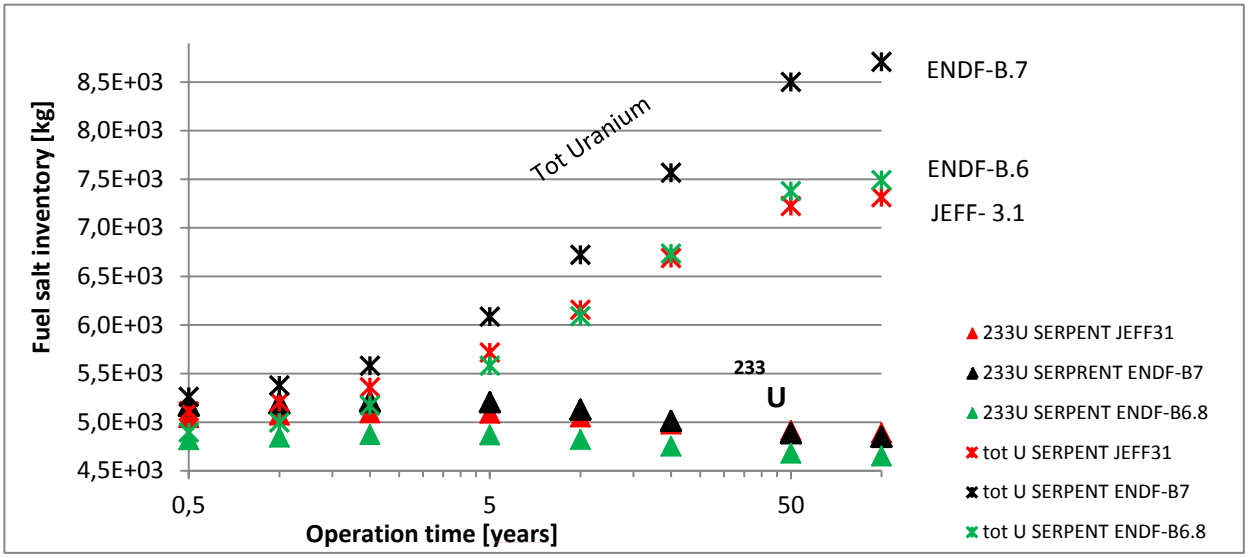

Figure 3.31: Fuel salt inventory in uranium and ^{233}U with ENDF/B-6, ENDF/B-7 and JEFF-3.1 data bases (performed with SERPENT, POLIMI)

First, the evolution calculations were performed for the ^{233}U-started MSFR. Figure 3.31 shows the ^{233}U and the total uranium inventory evaluated with different data basis: ENDF/B-6, ENDF/B-7 and JEFF-3.1. The uranium amount seems to be dependent on the database used. ENDF/B-7 data basis shows the most important difference on the uranium inventory that is higher than with other data bases. This difference may be partly explained by looking at the neutron capture cross section of ^{233}U, evaluated in different databases, as shown in Figure 3.13. Indeed, in the range of 0.001 MeV - 0.1 MeV the cross section are evaluated differently, and ENDF/B-7 evaluation is seems to be the highest one regarding the neutron capture.

Since the data basis seems to have an impact on the uranium inventory in the fuel salt, the tool comparison was performed while using the same data basis. Figures 3.32, 3.33 and 3.34 show the tool comparison used by LPSC, POLIMI (ERANOS and SERPENT), TU Delft and KI. One can observe that the uranium and ^{233}U inventories are in a very good agreement especially for longer operation time. ^{233}U inventory evaluated with the deterministic code ERANOS is however slightly lower compared to the evaluation with the other tools.

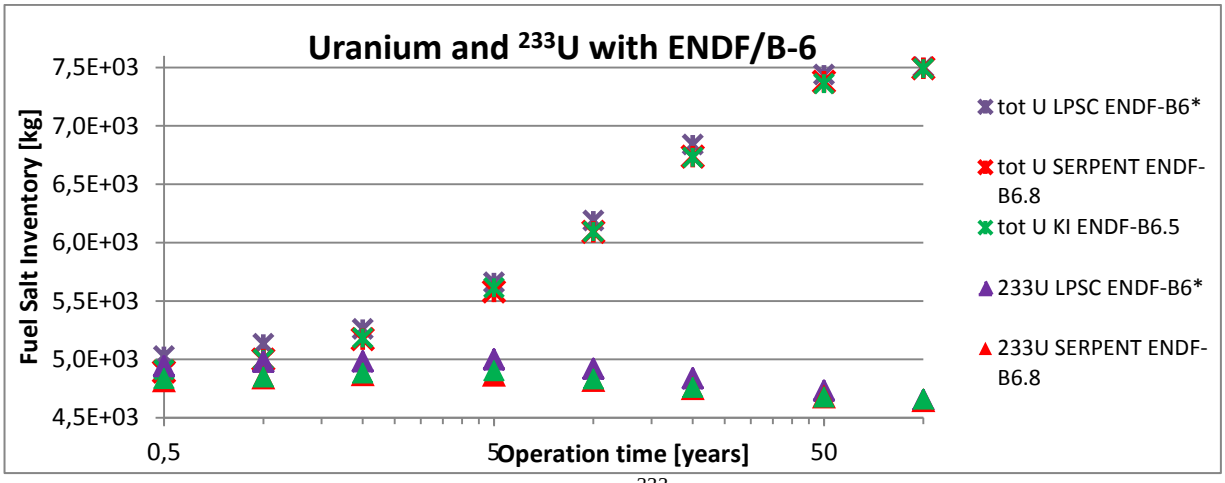

Figure 3.32: Fuel salt inventory in uranium and ^{233}U with ENDF/B-6 data basis performed by POLIMI (SERPENT), LPSC and KI

^{232}U and ^{231}Pa isotopes inventories were also compared as presented in Figure 3.35 evaluated using the ENDF/B-6 and ENDF/B-7 databases. The evaluations of ^{232}U inventory are in a good

agreement. The stockpile of ^{231}Pa evaluated at Kurchatov Institute is lower compared to those calculated at LPSC and POLIMI (SERPENT). Similarly, with the ENDF/B-7 database, the evaluations of POLIMI (SERPENT) are lower than that of TU-Delft. These effects will be studied for deliverable 2.3.

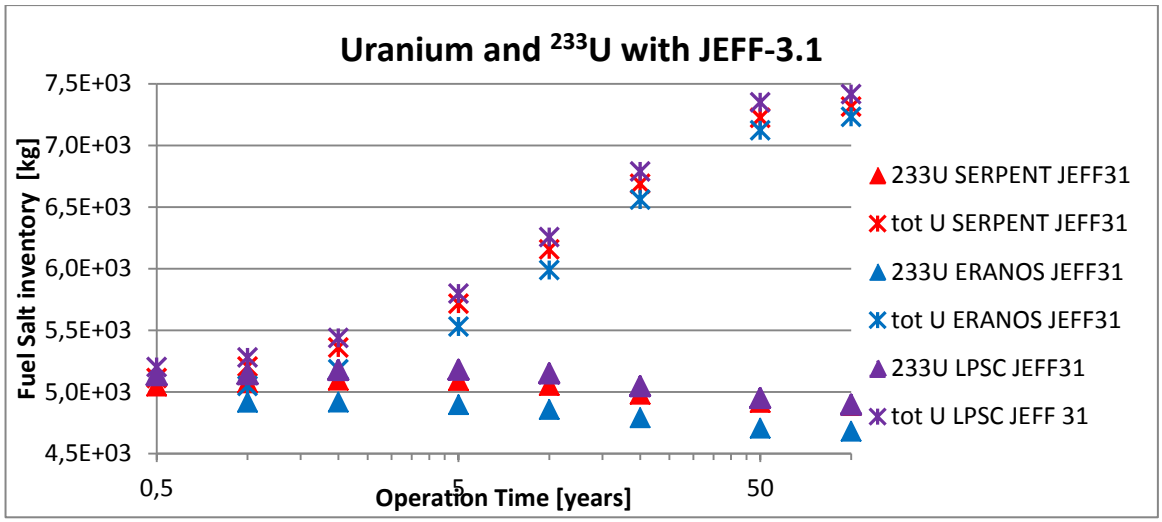

Figure 3.33: Fuel salt inventory in uranium and ^{233}U with JEFF-3.1 data basis performed by POLIMI (SERPENT), POLIMI (ERANOS) and LPSC

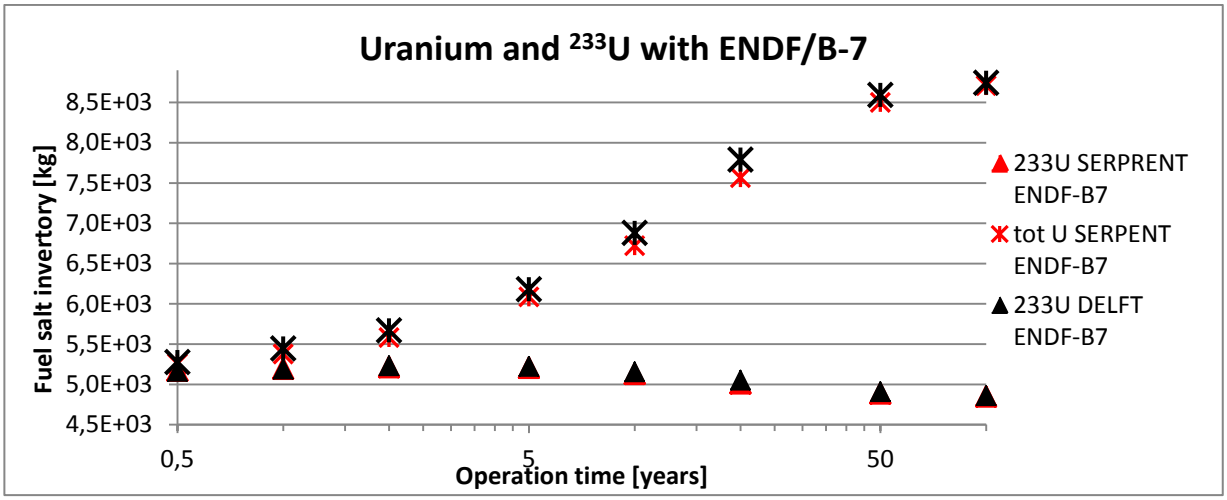

Figure 3.34: Fuel salt inventory in uranium and ^{233}U with ENDF/B-7 database performed by POLIMI (SERPENT), TU Delft

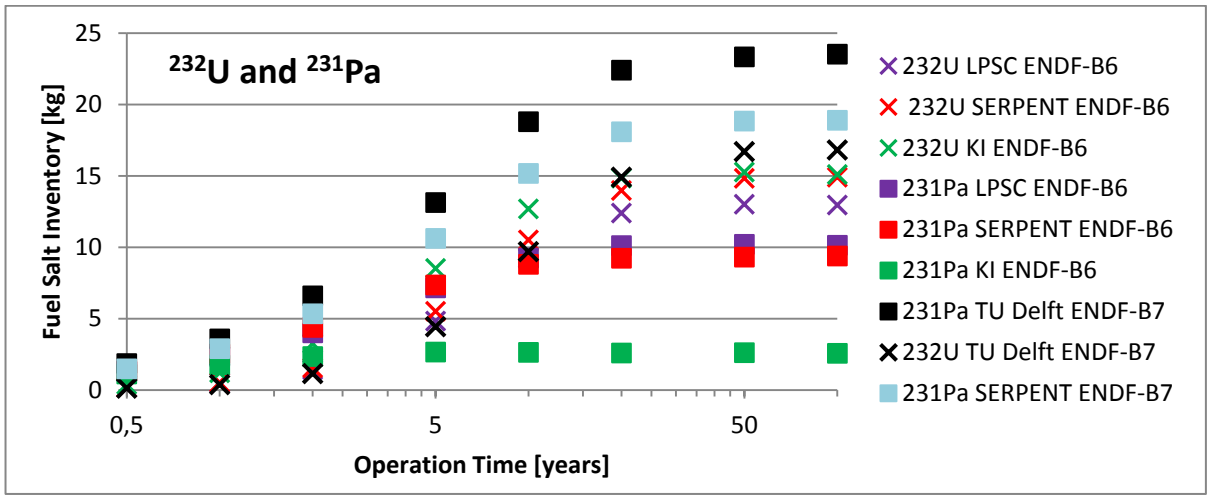

Figure 3.35: Fuel salt inventory in ^{232}U and ^{231}Pa

The inventories of different plutonium isotopes calculated with SERPENT (POLIMI) with different databases are presented in Figure 3.36. Similarly to uranium isotopes, the choice of the database only has an influence on the plutonium isotopes inventories. Different simulations performed by the partners with the same database (ENDF-B6) are thereby in a very good agreement as shown in Figure 3.37.

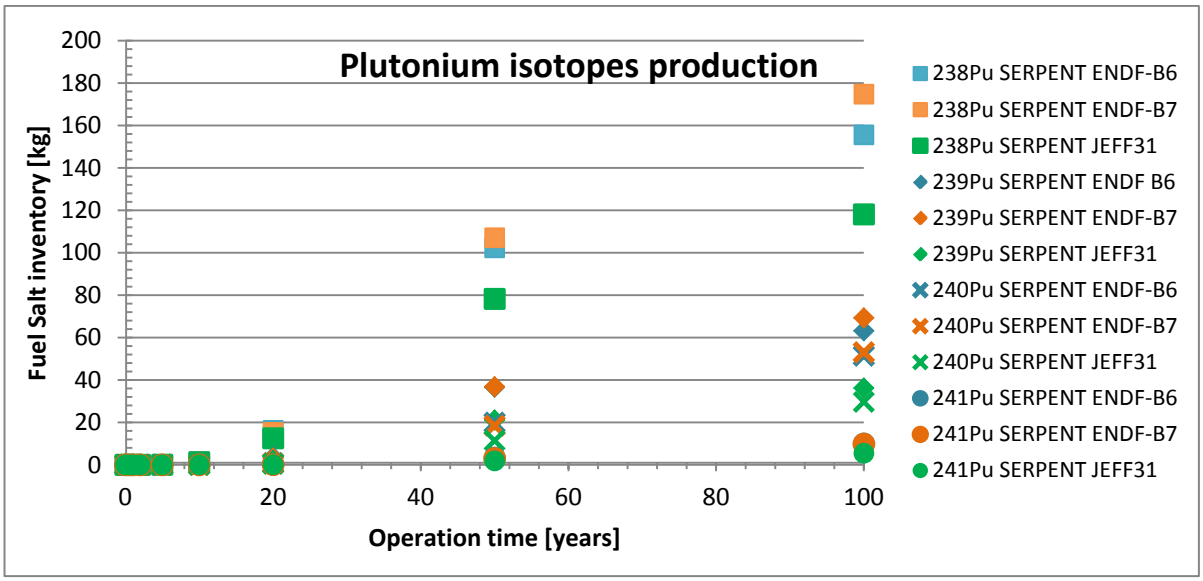

Figure 3.36: Evolution of the Plutonium isotopes in the fuel salt according to POLIMI (SERPENT)

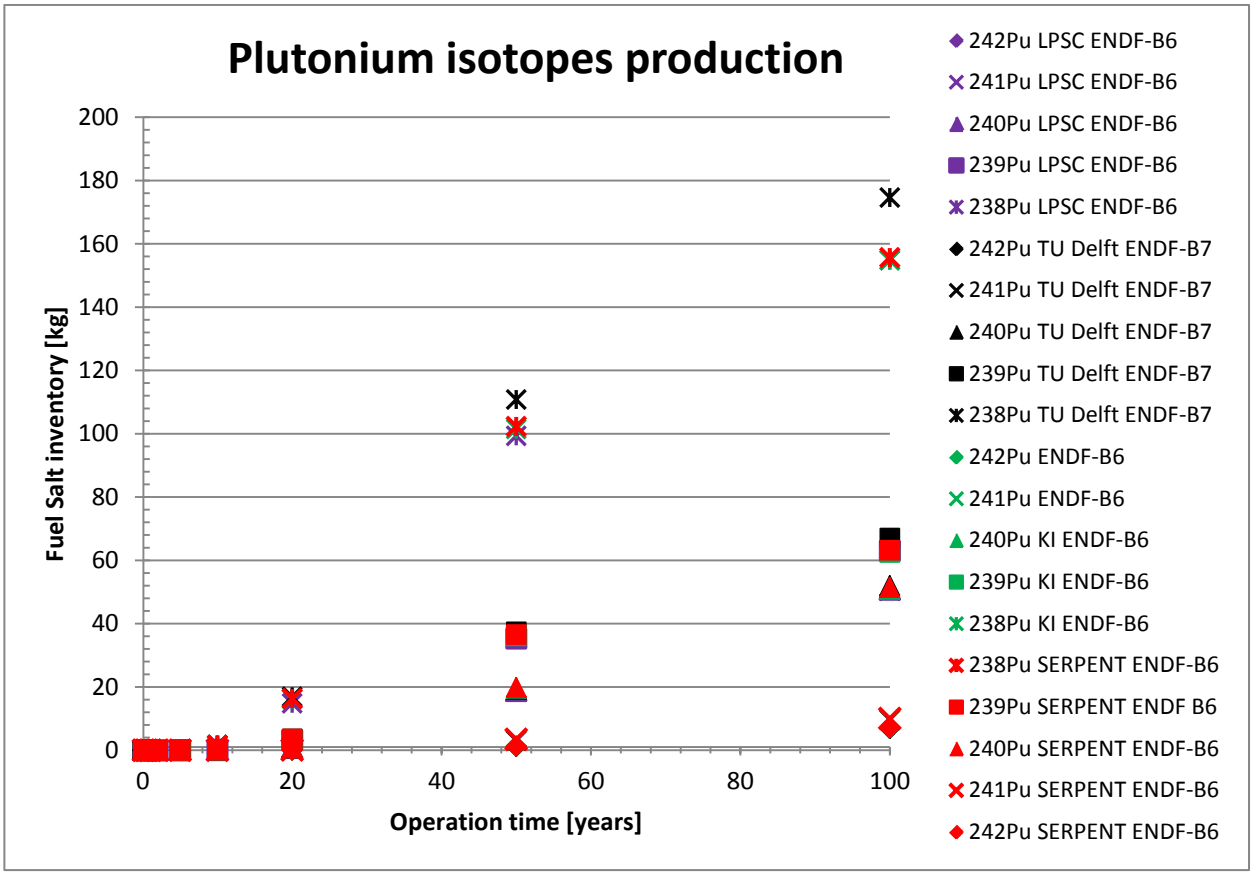

Figure 3.37: Evolution of the Plutonium isotopes in the fuel salt using the ENDF-B6/7 databases

3.4.3. Fuel salt evolution for the TRU-started MSFR

For the TRU-started MSFR simulations, the evolution of the minor actinides inventory in core has been calculated and is presented in Figure 3.38. This transuranic elements inventory considered here included the Pu, Np, Am and Cm elements. This inventory is reduced from 12 tonnes to some

hundreds of kilograms at steady state. The different simulations show a very good agreement on this minor actinides burning. When considering the plutonium inventory, as shown in Figure 3.39, similar conclusions are found.

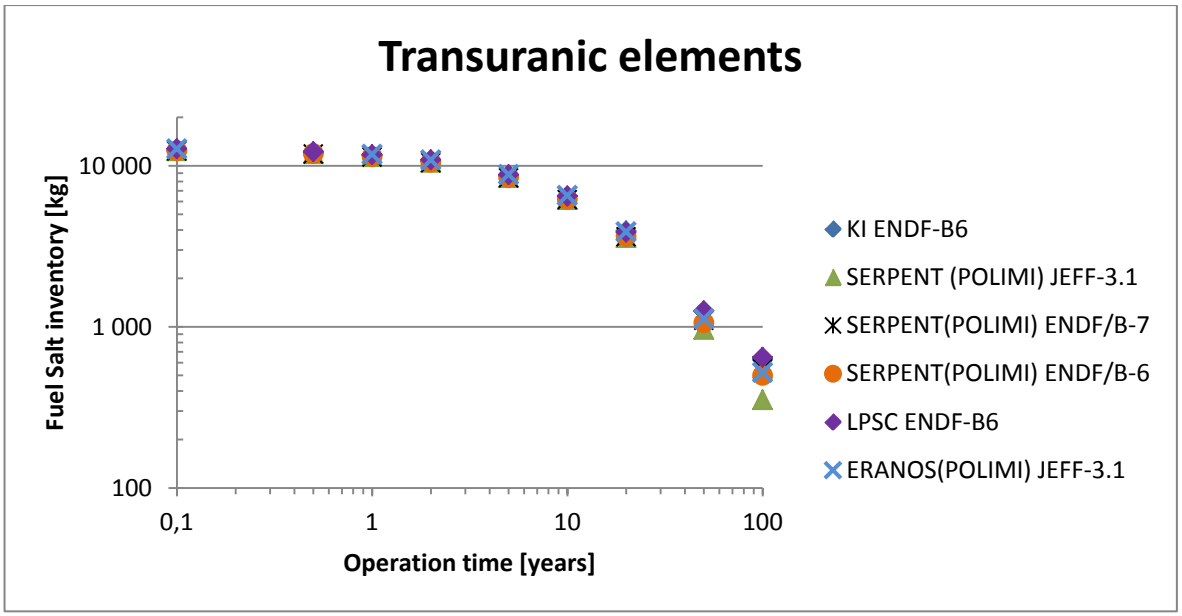

Figure 3.38: Fuel salt inventory in transuranic elements during reactor evolution

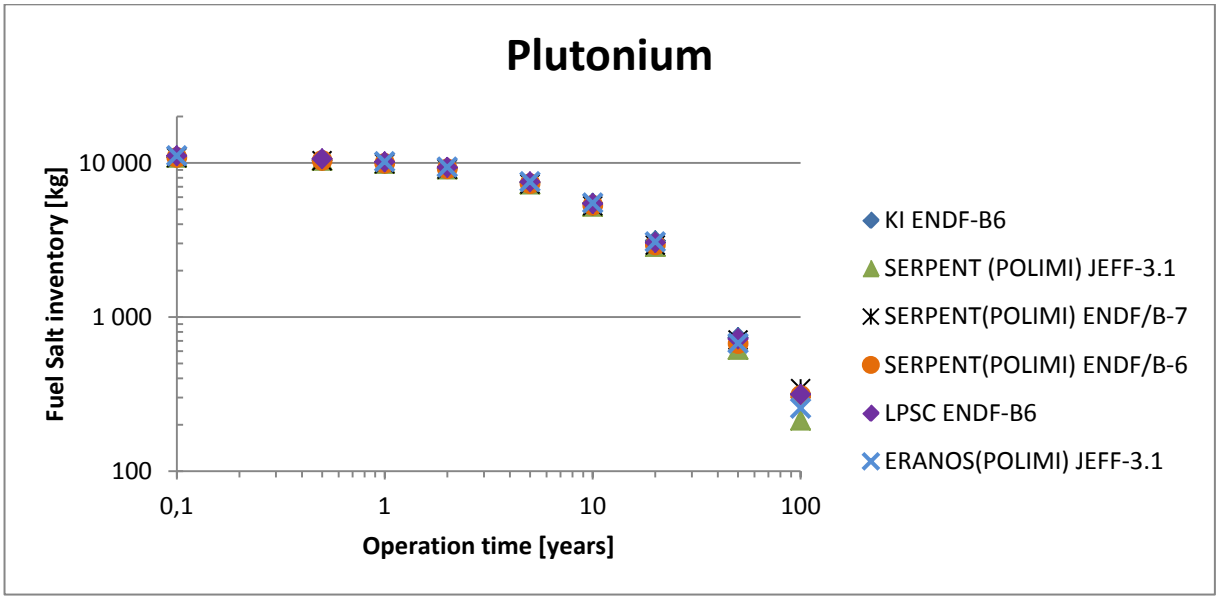

Figure 3.39: Fuel salt inventory in Plutonium during reactor evolution

During TRU-started MSFR operation, the uranium quantity increases as presented in Figure 3.40. As observed previously, the database used for the calculation has only a small impact on the uranium inventory of the fuel salt. Thereby, the ^{233}U inventory is in a very good agreement for different databases, see Figure 3.41.

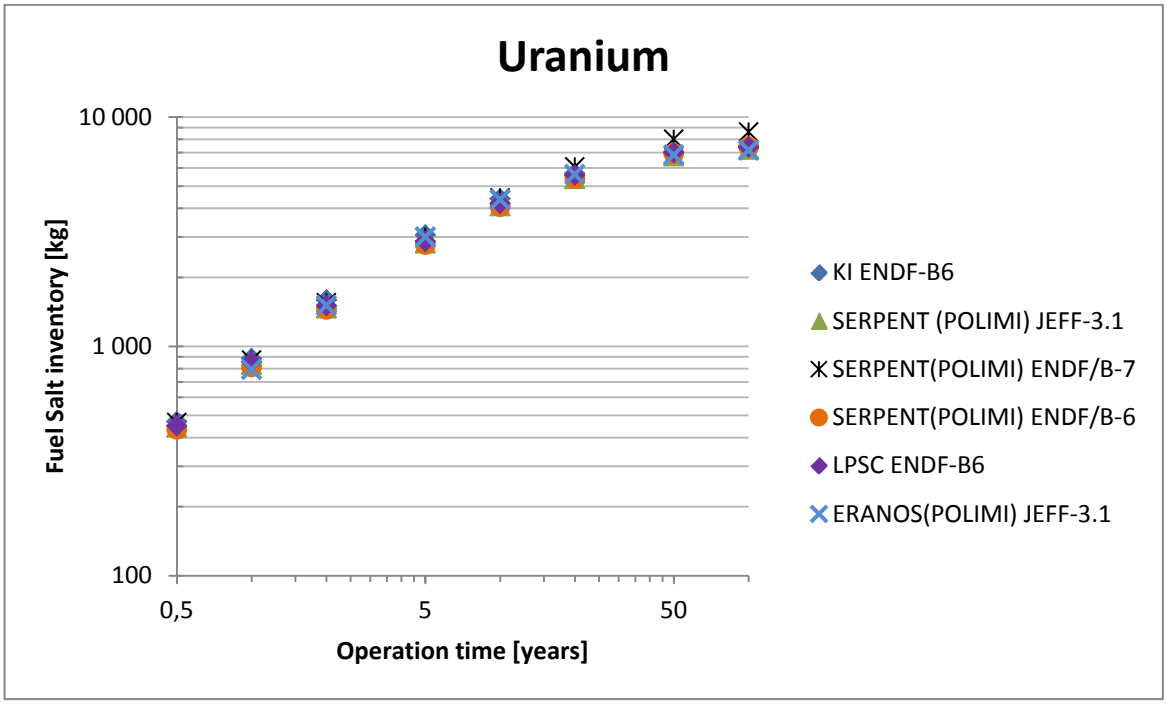

Figure 3.40: Fuel salt inventory in Uranium during reactor evolution

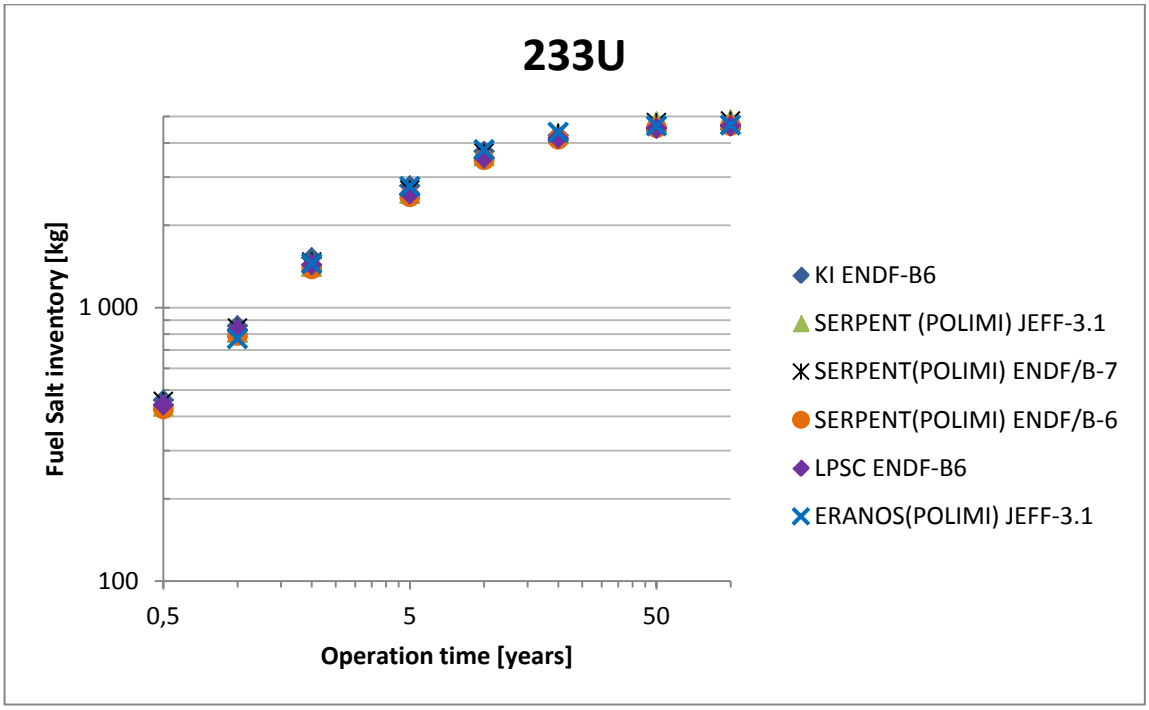

Figure 3.41: Fuel salt inventory in ^{233}U during reactor evolution

3.4.4. Evolution of the fission products composition

In order to compare the fission products extraction simulated in the various evolution codes, the total fission products inventory as a function of the operation time was calculated as shown in Figure 3.42. The values obtained at TU Delft, LPSC and Kurchatov Institute are in a very good agreement, while the ERANOS calculation leads to a fission products inventory reduced by a factor 2. This difference is due to the assumptions used in the ERANOS code evolution, namely some fission products are neglected in the inventory.

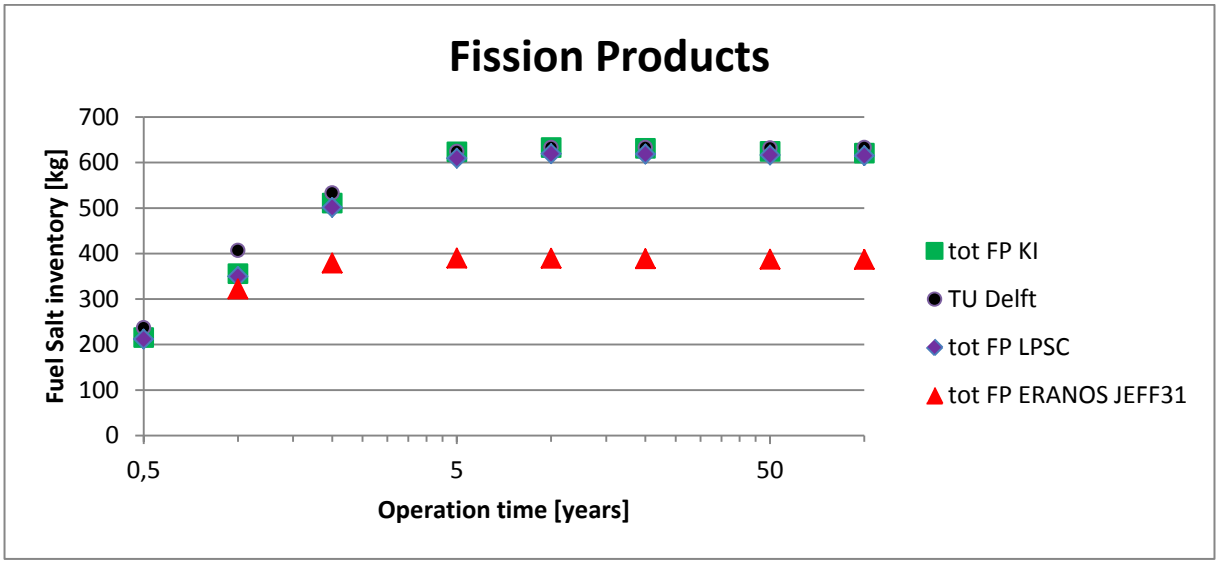

Figure 3.42: Evolution of the fission products content for in the fuel salt ^{233}U-started MSFR as a function of the operation time

3.4.5. Breeding gain and breeding ratio evolution

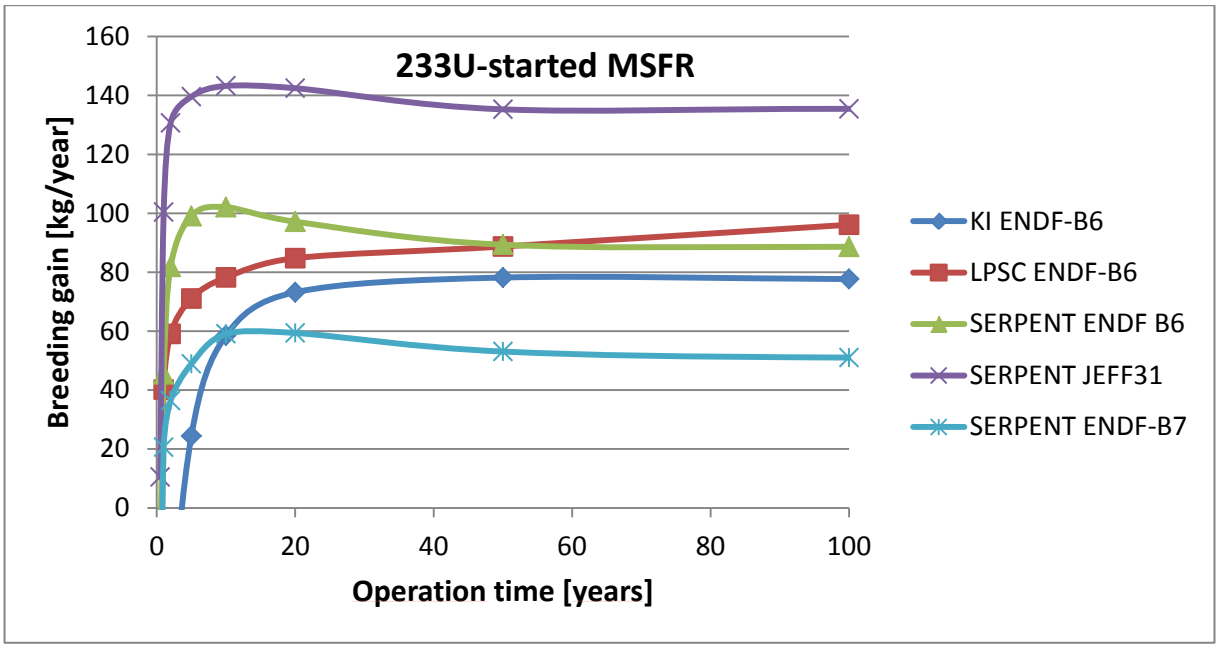

Figure 3.43: Evolution of breeding gain of the ^{233}U-started MSFR as a function of the operation time

The breeding gain was defined in the benchmark template as a balance of uranium in the core and the blanket, so that the uranium extracted from the blanket, uranium supply in the core has to be taken into account.

$$BG = \frac{Extraproducedfissilematerial}{Operationtime}$$ = Balance of ^{233}U (system: core + blanket)

The calculations of the breeding gain for the ^{233}U-started MSFR are presented in Figure 3.43. The values calculated by the different partners with the same database (ENDF/B-6) are very close, around 90 kg/year. While changing the database, this value can be increased up to 140 kg/year (JEFF-3.1) or decreased down to 50 kg/year (ENDF/B-7). The ENDF-B7 data seem to be the most pessimistic, and consequently the most conservative ones.

The same definition of the breeding gain was used for the TRU-started MSFR, as presented in Figure 3.44. The breeding gain after 100 years of operation is of about 140 kg/year, that is higher than the one obtained for ^{233}U-started MSFR. This difference may be explained by the fact that the TRU-started MSFR is using its load of minor actinides initially to produce power, the produced ^{233}U being stored; in the ^{233}U-started MSFR, a part of the produced ^{233}U is used to fission. A breeding gain taking into account a balance of all the fissile matters and not only ^{233}U would be more precise in the case of the TRU-started MSFR.

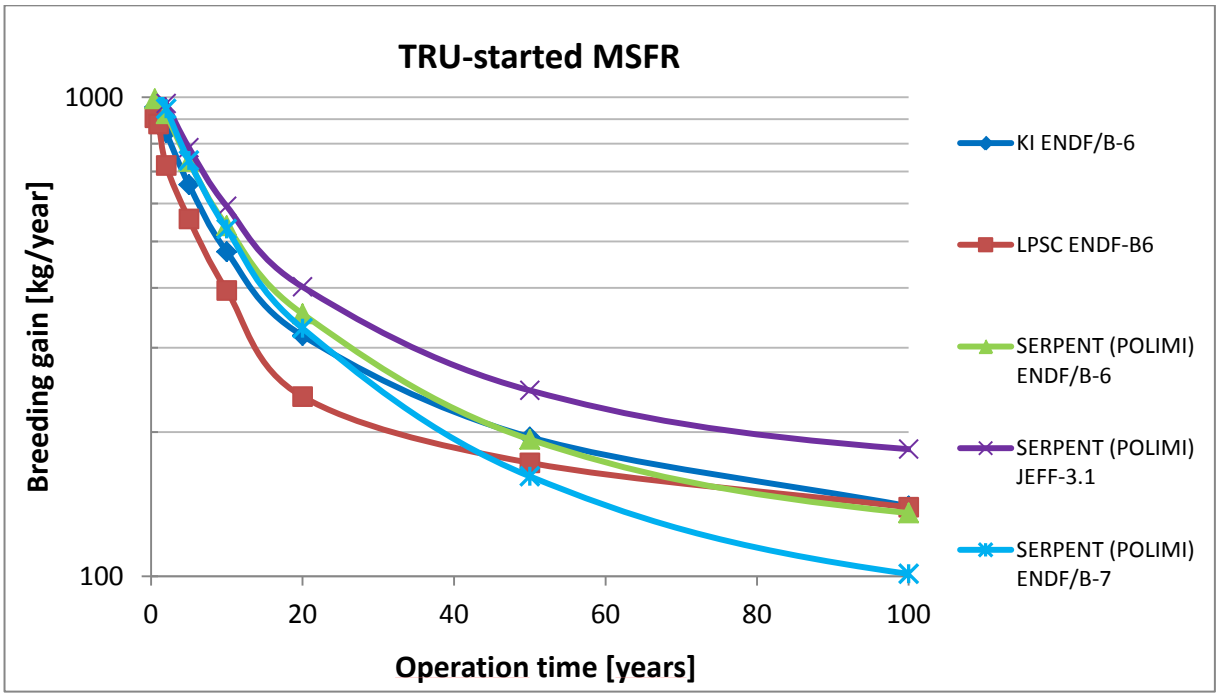

Figure 3.44: Evolution of breeding gain of the TRU-started MSFR as a function of the operation time

Similar conclusions may be observed concerning the impact of the database used: the different codes are in a good agreement especially at longer term when using the same database.

The breeding ratio of the MSFR, as described below, has also been evaluated:

$$BR = \frac{Decay rate of\ {}^{233}_{91}Pa}{Capture + Fission rate of\ {}^{233}_{92}U}$$

The results, listed in Table 3.24, are in good agreement when using the same database (see LPSC and KI calculations), except for the results provided by POLITO. Their definition of the breeding ratio is indeed different from than suggested in the template, corresponding to:

$$\boldsymbol{BR_{U233} = \frac{\text{Capture rate in } {}^{232}_{90}\text{Th}}{\text{Capture} + \text{Fission rate of } {}^{233}_{92}\text{U}}}$$

$$\boldsymbol{BR_{TRU} = \frac{\text{Capture rate in } {}^{232}_{90}\text{Th}}{\text{Capture} + \text{Fission rate in TRU}}}$$

This last definition relying on the capture rate of the ^{232}Th and not on the decay of the produced ^{233}Pa, the delay corresponding to the period of the ^{233}Pa is neglected, as for the possible parasitic captures on the ^{233}Pa. This leads to a light over-estimation of the breeding ratio, mainly at the beginning of life of the reactor.

BR (w/o units)	KI (ENDF/B-6)	LPSC (ENDF/B-6)	POLIMI SERPENT (JEFF-3.1)	POLIMI SERPENT (ENDF/B-7)	TU Delft (core only)	POLITO (JEFF3.1)
Steady state (^{233}U-started)	1.07	1.13	1.112	1.039	0.944	-
Steady state (TRU-started)	1.07	1.11	1.112	1.039	-	-
^{233}U-started initial composition	-	0.664 (6 months)	-	-	0.95 (6 months)	1.137
TRU-started initial composition	-	-	-	-	-	0.610

Table 3.34: Breeding ratio evaluation with different tools and databases

3.5. Conclusions

A large diversity of important neutronic parameters calculations performed by benchmark participants were compared, while using different tools, databases and methods. An overall good agreement could be observed for the static neutronic parameters as thermal feedback coefficients, delayed neutron fractions, generation times, neutron flux and initial critical composition calculations. Only small discrepancies were thereby observed for the evaluations based on different calculations tools, while the choice of the nuclear database has a more consequent impact on the results.

As mentioned above, during the initial reactor design studies, in particular those related to the neutronic calculations, the MSFR core was approximated as a single compact cylinder (2.25 m high x 2.25 m diameter). The next step is the thermal-hydraulics simulations benchmark. Preliminary thermal-hydraulics calculations performed in the frame of the EVOL project have shown that the simple design used for the first benchmark of neutronic calculations will induce very hot spot in the salt flow. Because it's not efficient to compare results too far from the working point of the MSFR, a more complex geometry has been designed for the thermal-hydraulics benchmark in order to obtain acceptable thermal-hydraulic performances, as presented in the next section.

4. Thermal-hydraulic benchmark of the MSFR

In order to get realistic results, the T&H benchmark is defined using a core cavity shape with curved inlet and outlet tubes and core walls. The geometries for the 2D and 3D T&H benchmarks of the MSFR core have been provided as *.stp format files (and *.dwg for the 2D one). These geometries are provided for two different fuel salt domains:

i. Partial fuel circuit: the fuel salt volume to be modeled includes the MSFR core cavity and upper and lower legs. In this case the fuel salt flow in the heat exchangers is not modeled (and thus it is not included in the fluid volume solved by the CFD code).

ii. Full fuel circuit: containing the core, upper and lower legs, and the heat exchangers.

In both cases, partial or full geometries, the flow rate and heat source distribution in the core shall be kept as described in the next sections.

4.1. Presentation of the 2D T&H benchmark (Axi-symmetrical benchmark)

4.1.1. Geometry

In the 2-D T&H benchmark, the core geometry is axi-symmetrical. The 2D benchmark can be performed using the full or the partial fuel circuit geometries (with or without the exchangers) which have been provided. As an example, the fluid domain corresponding to the model without the exchanger can be seen on the mesh example given in Figure 4.1.

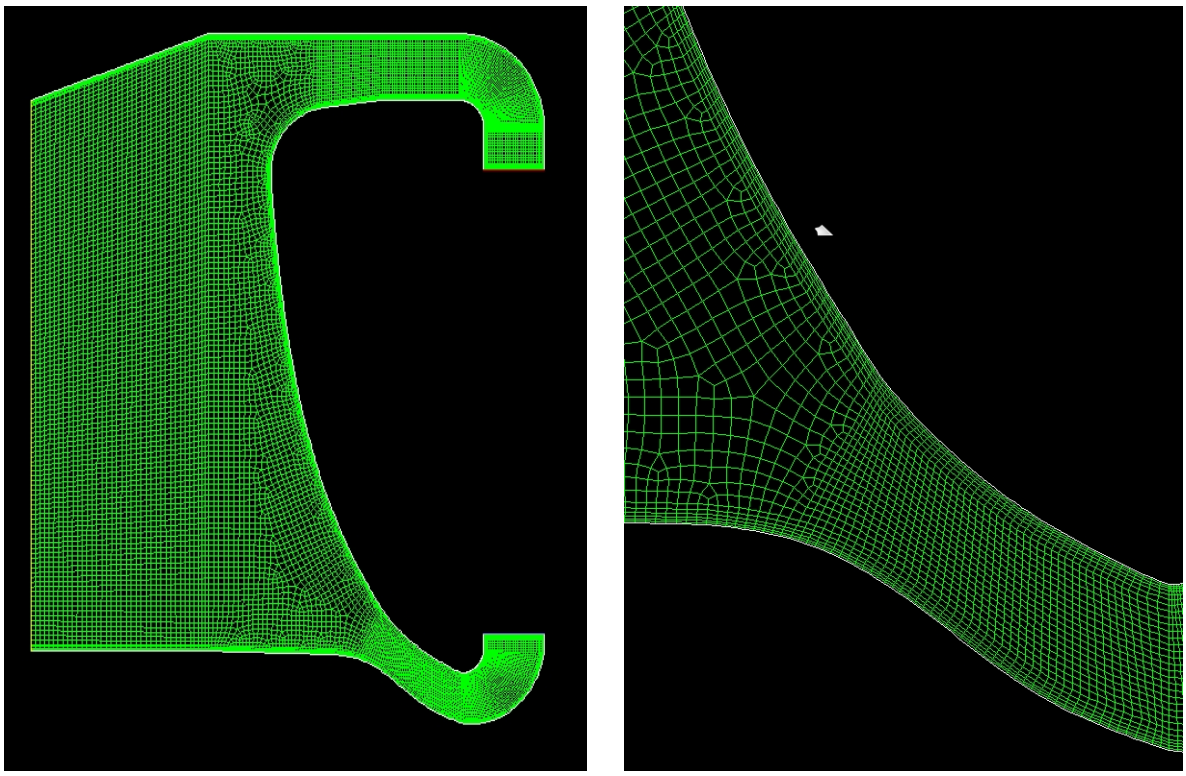

Figure 4.1: Mesh of the axi-symmetrical geometry (left, without exchanger part), and zoom on inlet part with mesh refinement near walls

The following parameters should be retrieved after reading geometry files:

- -1.36m < z < +1.12m
- On the axis (R=0): -1.095m < z < 0.884m
- The minimum radius of the core is 0.947m

- The core volume is 8.48m3
- The volume outside the core, including the exchanger shape of the full geometry, is also 8.48m^3. The upper and lower limits of the "core" are given on Figure 4.1 with the mesh view.

The mesh shown on Figure 4.1 is given only as an example. It is up to the benchmark participants to determine the optimal mesh for the T&H benchmark. This mesh will depend on the approximations made by the model and on the CFD code. However, the T&H benchmark results should not depends on the mesh characteristics. Some sensitivity studies should be done to verify this point.

4.1.2. Fluid model

The turbulent flow conservation equations to be solved in the T&H benchmark are:

- Mass conservation
- Linear Momentum (Navier-Stokes equations)
- Energy conservation

In order to facilitate the comparison between CFD codes, a classical k – epsilon turbulence model shall be used in the simulation. The k-epsilon model is available in most of the numerical CFD codes and in the range of Reynolds numbers found in the MSFR (between 10^6 and 2 10^6) can be considered as a good RANS model.

A more recent and efficient turbulent model such as the RNG k-epsilon turbulence model would be more appropriate however it may not be available in all codes. For this reason, a calculation using an advance turbulent model is left as an optional calculation in the benchmark.

4.1.3. Flow conditions and boundaries conditions

The total mass flow rate in the core is 18932.2 kg/s.

This flow rate shall be defined in the model as a:

- Momentum source in the heat exchanger (or top part or bottom part of the heat exchanger) in case of complete geometry,
- Mass flow rate, volume flow rate or velocity in case of fluid model without exchanger volume, depending on the software possibilities. The corresponding volume flow rate is 4.54m3/s at core inlet at 650°C and average velocity is 1.577m/s at 650°C at the inlet.

The cold temperature is 650°C.

This temperature may be defined in the model as:

- An appropriate negative heat source in the exchanger volume such as a temperature of 650°C is obtained at least on a point in the inlet zone in case of complete geometry.
- Fixed temperature of 650°C at the inlet in case of geometry without exchanger.

If necessary a relative pressure may be fixed to 0 on the outlet zone: exchanger inlet in case of the partial fuel circuit geometry.

The heat source is given by the following function, in W/m^3:

$$\textbf{source = A1 * cos(0.5 * PI * Rn/R10) * cos(PI * Z/Z10)}$$

with the normalization factor Rn given by:

$$\textbf{Rn = R*(1.0555+0.22896*Z)} \text{ for } \textbf{Z < 0.59}$$

and

$$\textbf{Rn= R*(1.40277-0.359622*Z)} \text{ for } \textbf{Z > 0.59}$$

and **A1 = 7.83816907e+08W/m3**.

The total heat source in the core is equal to 2.794 GW.

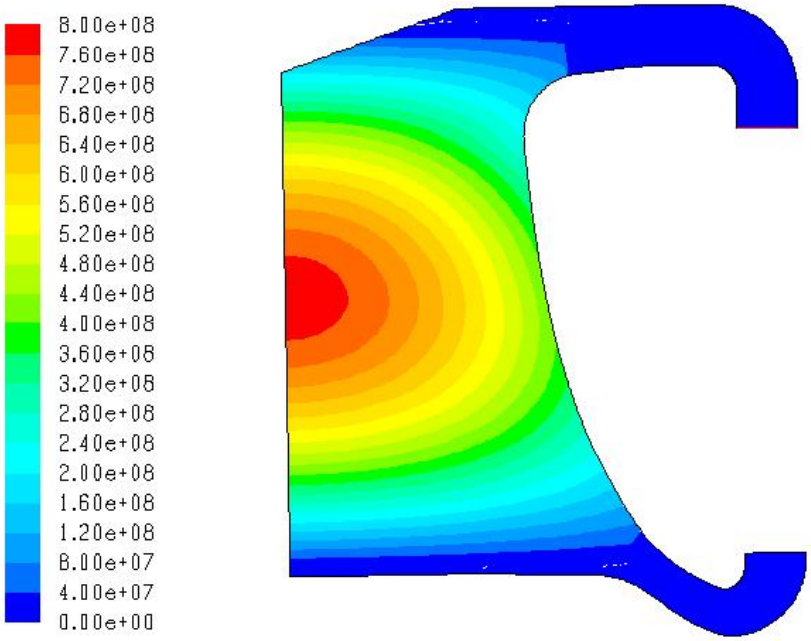

Figure 4.2: Heat source in the core (W/m^3)

On the symmetry axis: no stress and no heat flux. These conditions can be defined through the following boundary conditions:

- **dP/dR = 0**
- **dVz/dR=0**
- **Vr=0**
- **dT/dR = 0**

which may correspond to « symmetry » or « axis-symmetry » conditions depending of the CFD software.

On all other walls in contact with the fluid, the following flow and thermal conditions apply:

- A wall function depending on the turbulence model,
- An adiabatic thermal condition (no heat flux). Therefore for the purpose of this benchmark, the flux from the blanket is not taken in account because it has a negligible effect on core temperature.

This source term was used for every T&H simulations. Coupled simulation from KIT used the thermal source calculated by the coupled approach, slightly different from this one.

4.1.4. Data and results provided from the 2D T&H benchmark

The following data have been provided to the benchmark participants:

- Brief description of the CFD code used in the benchmark
- Numerical fluid mesh characteristics
- A temperature (°C) view, with iso-values ranging from 650°C to the maximum
- A velocity magnitude view (in m/s), with iso-values, from 0 to the maximum
- Two graphs of salt velocity (m/s) and temperature (°C) versus the radial positions for three axial elevations:

z = -1 m (~10cm above the low reflector)

z = 0 m (mid-core)

z = 0.8 m (~10 cm below the bottom reflector).

4.2. Presentation of the 3D T&H benchmark

4.2.1. Geometry and mesh

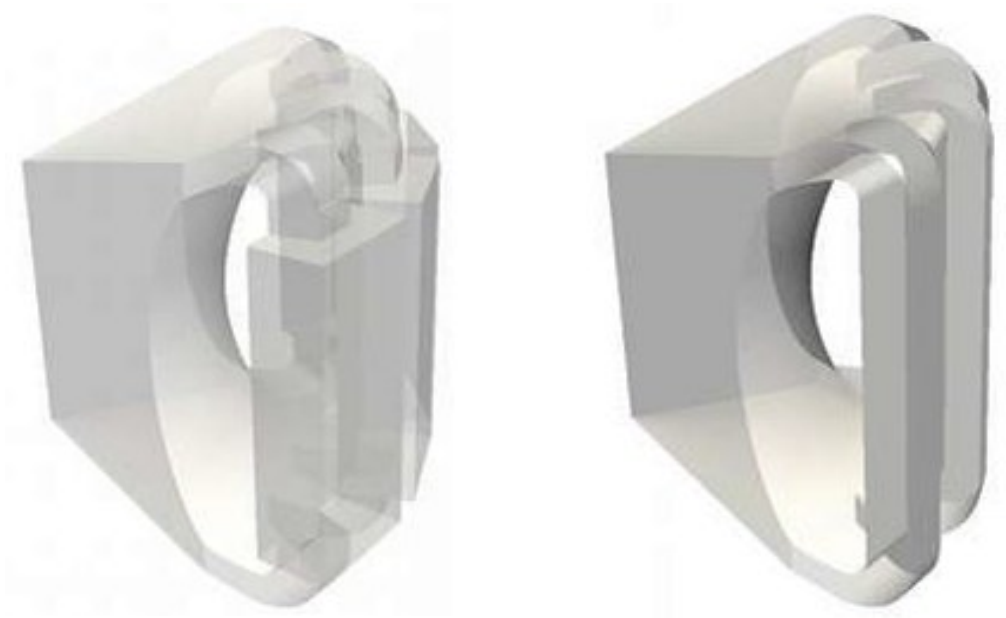

Figure 4.3: Optimal 3D geometry with full loops and exchanger (left) and 3D geometry of the final 3D benchmark (right) with more simple exchangers volume

The core geometry was changed from the one in the benchmark definition (Deliverable 2.1) and corresponds to the best optimized shape obtained. It has a symmetrical core-blanket wall but has same volume and dimensions. For the full core there are 16 heat exchangers (16 inlets and outlets pipes). For meshing convenience in the benchmark these tubes section are considered as having a rectangular section. The geometry is given as 3D step files for a quarter of the core. The benchmark has been done on 1/16 of the core and ¼ of the core for comparison purpose.

As previously discussed two fluid domains are possible depending on whether heat exchanger are modelled or not (partial or full fuel circuit models). We finally choose to do the optimization and the benchmark on the full geometry, including an arbitrary volume for the exchangers. The exchangers are modelled as simple volumes whose size is chosen to keep 8.48 m^3 outside the core. Core volume is fixed to 8.48 m^3. Selection of the turbulence model is left to the choice of the benchmark partners.

4.2.2. Fluid models

Similarly to the 2D benchmark, the turbulent flow conservation equations to be solved in the T&H benchmark are:

- Mass conservation
- Linear Momentum (Navier-Stokes equations)
- Energy conservation

On the contrary to the 2D T&H benchmark, in this case the participants have compared their results using the same turbulence model: k – epsilon realizable model. In addition two comparisons have been done:

- between two pressure interpolation method: a standard first order interpolation, and the “presto” pressure interpolation from Fluent,

- between k – epsilon realizable turbulence model and Reynolds stress model [Launder, 1975].

This last model called Reynolds stress involved five conservation equations to solved the turbulence effects instead of two. It is still a stationary model, but it may be seen as the less bad RANS (Reynolds Average Navier Stockes) model.

4.2.3. Flow and fluid boundaries conditions

The flow and the fluid boundaries conditions are the same as those defined in the 2D T&H benchmark, with two exceptions:

- The total flow rate is 18932.2 kg/s is now split in sixteen heat exchangers thus giving a 1183.3kg/s mass flow rate per loop. As before, this mass flow rate may be defined in the model as a:
- Momentum source in the heat exchanger (or top part or bottom part of the heat exchanger) in case of complete geometry,
- Mass flow rate, volume flow rate or velocity in case of fluid model without exchanger volume (partial fuel circuit), depending on the software possibilities. The corresponding volume flow rate is 0.28375 m^3/s at core inlet at a temperature of 650°C, and the average velocity is 3.987 m/s at 650°C at the inlet (inlets surface of 0.071164 m^2).

Axis-symmetrical conditions are not necessary is this case.

4.2.4. Results of the 3D T&H benchmark

The information and the results (and formats) required in the 3D T&H benchmark are the same as those required for the 2D benchmark (see the discussion in the section **Erreur ! Source du renvoi introuvable.**) with the following particularities. The results should be provided for the vertical plane corresponding to the center line of one of the inlet/outlets pipes (line AA' in Figure 4.4), and the same set of results may be provided for the vertical plane between two inlet/outlet pipes (line AA in Figure 4.4).

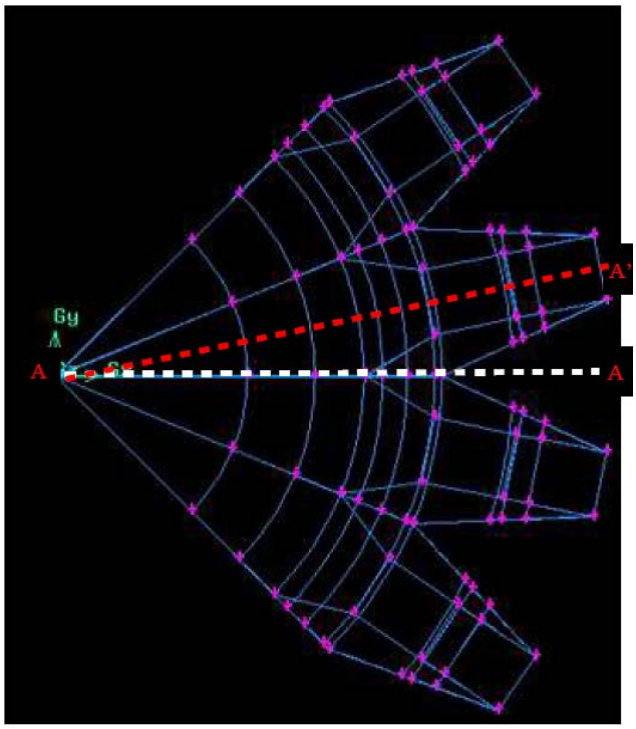

Figure 4.4: Top view of a quarter of the 3D geometry, with the two vertical planes (dashed lines) used to present qualitative results and to defined points for quantitative results

4.3. Results of the Thermal-Hydraulics benchmark

4.3.1. Presented results

The results of the benchmark we will compare are the following:

- 2D results from KIT using SIMMER for coupled simulation on simplified geometry,
- 2D results from INOPRO IAO using FLUENT for T&H simulation on the same geometry for comparison purpose,
- 2D results from INOPRO IAO with FLUENT on the bechmark 2D geometry
- 2D results from LPSC with OPENFOAM (for some turbulence models) on the benchmark 2D geometry for comparison purpose,
- 3D results from INOPRO IAO on FLUENT, on optimized geometry, using k – epsilon turbulence model [Shih, 1995] with standard pressure interpolation or "presto" [Patankar, 1980] pressure interpolation, and Reynolds stress model [Launder, 1989; Launder, 1975].
- 3D results from LPSC on OPENFOAM, on optimized geometry for comparison.

The benchmark results are then presented for three geometries. For comparison efficiency, the results corresponding to each geometry are presented in separated chapter and interpreted in the same section.

4.3.2. Simplified 2D geometry

Coupled calculations were performed by KIT using the code SIMMER. This code is able to do a coupled simulation between neutronic and thermal hydraulic, but is not able to deal with the real geometry of the benchmark. Then a simplified geometry was used. INOPRO IAO did a thermal hydraulic simulation on the same geometry (Figure 4.5) in order to include this two calculations in the benchmark, even if the geometry is not exactly the benchmark geometry.

Another difference between these two results is the heat source:

- in KIT case the heat source is calculated from the coupled calculation by SIMMER,
- In INOPRO IAO case the source term defined for the T&H benchmark was used.

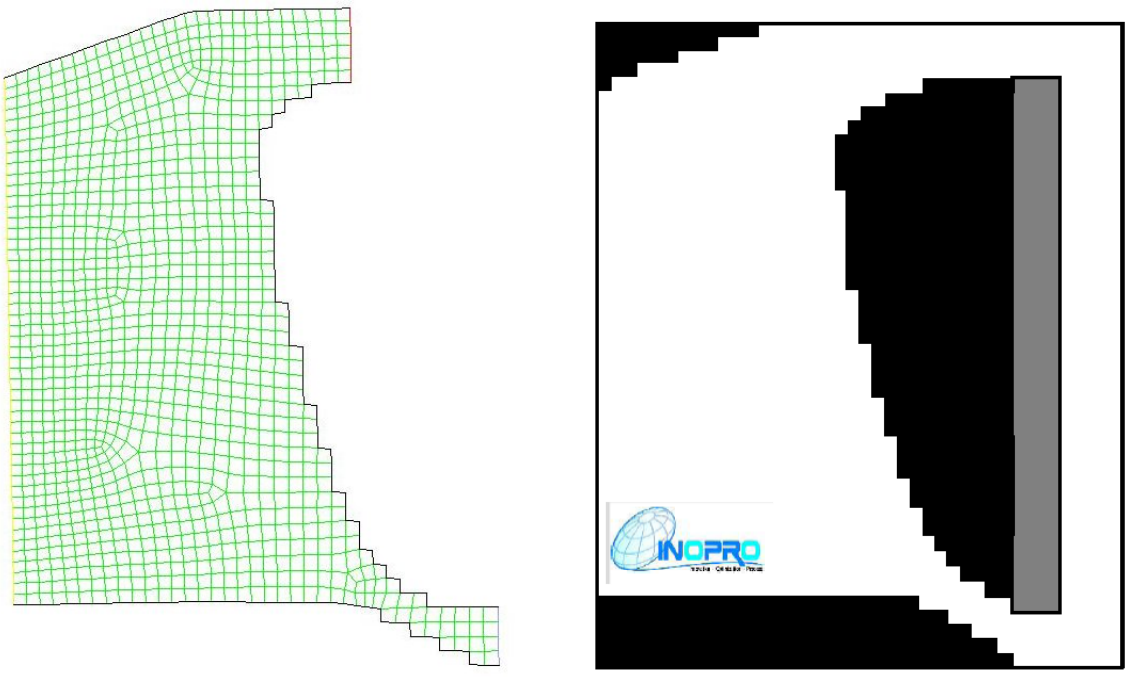

Figure 4.5: Geometry of KIT 2D simulation with SIMMER (right) and similar geometry and mesh used by INOPRO IAO for comparison purpose (left)

The geometries are not exactly same but are as close as possible for this level of precision (Figure 4.5). In both cases the precision (few centimetres) is the same, and the core shape are as close as possible to the 2D benchmark definition. In both cases also the turbulence model is the same : standard k-epsilon, and the source term of INOPRO IAO results has been adapted to fit the source term from coupled calculation done by KIT (Figure 4.6).

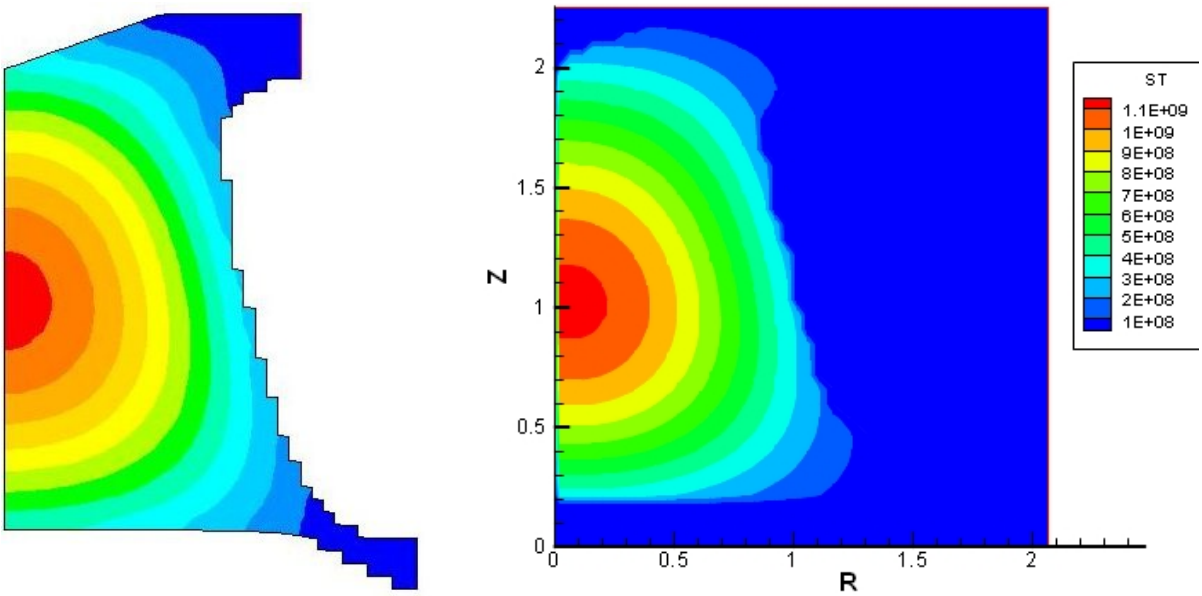

Figure 4.6: Heat source (W/m3) from KIT (right) coupled calculation, and adapted source (left) used by INOPRO IAO to fit the KIT source

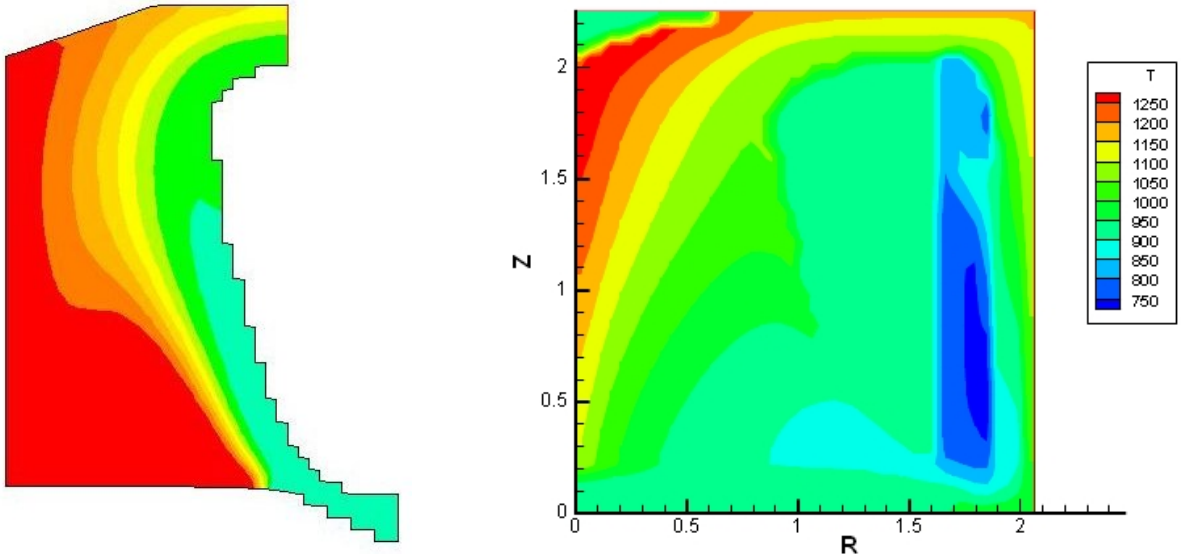

Figure 4.7: Temperature (K) from KIT (right), on approximate benchmark geometry and INOPRO IAO (left) simulations with similar mesh and model, and same scale

The temperature fields still includes hot region over 1000°C, but this is not the aim in this benchmark part of the project to discuss this fact. Using the benchmark shape the temperature level is kept in an acceptable range for the simulation tool. In both cases the highest zone is in the centre of the core and the blanket wall is cooled by the salt flux. KIT results show highest temperature is less than 1300K and is located in centre of the core close to the top reflector (Figure 4.7 left). In INOPRO IAO case the highest temperature is over 1300K and located close to bottom reflector (Figure 4.7 right). The hot spot in the bottom half of the core in INOPRO IAO case is clearly due to the recirculation of the flow going down along the axis of the core. In KIT case there is no recirculation, then no local hot region. This induces a large

temperature gap in bottom part of the core, but the temperature field in the top half of the core are almost same.

Then these differences are explained by looking at velocity fields (Figure 4.8): the flow is faster (2 to 3 m/s) and close to the core-blanket wall in the INOPRO IAO case, and with a recirculation inducing back flow in bottom centre of the core. It is much more homogeneous and then slower in KIT case.

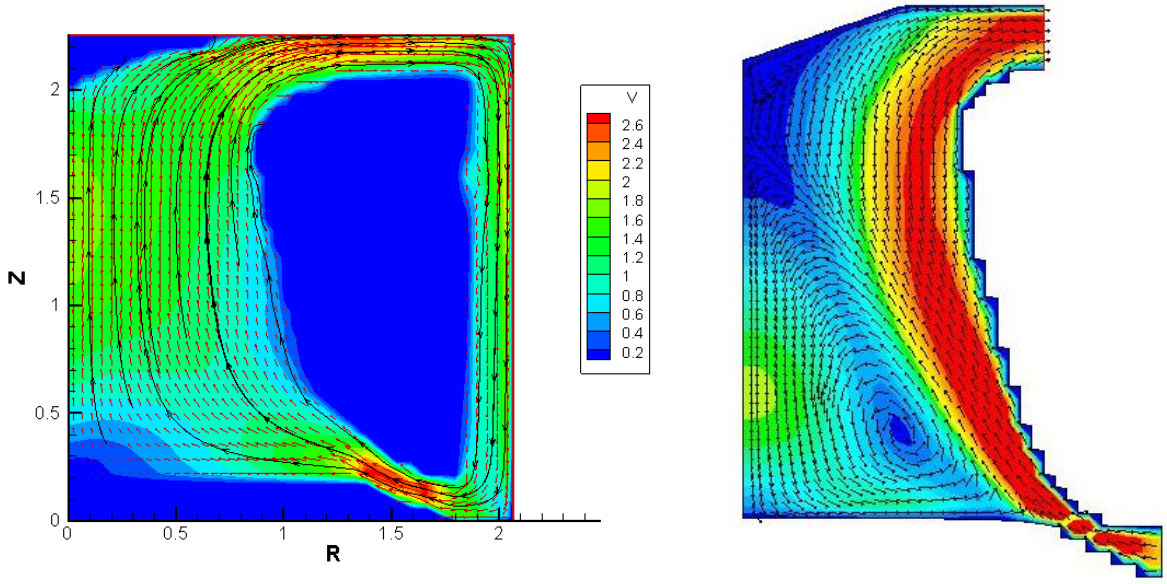

Figure 4.8: Velocity (m/s) from KIT simulation (left) and INOPRO IAO simulation on similar geometry and mesh (right)

In order to explain these differences, sensitivities to the mesh and interpolation scheme were done from INOPRO IAO simulations. These sensitivity studies have been done using the common source term (Figure 4.2) from LPSC calculation on a cylinder shape.

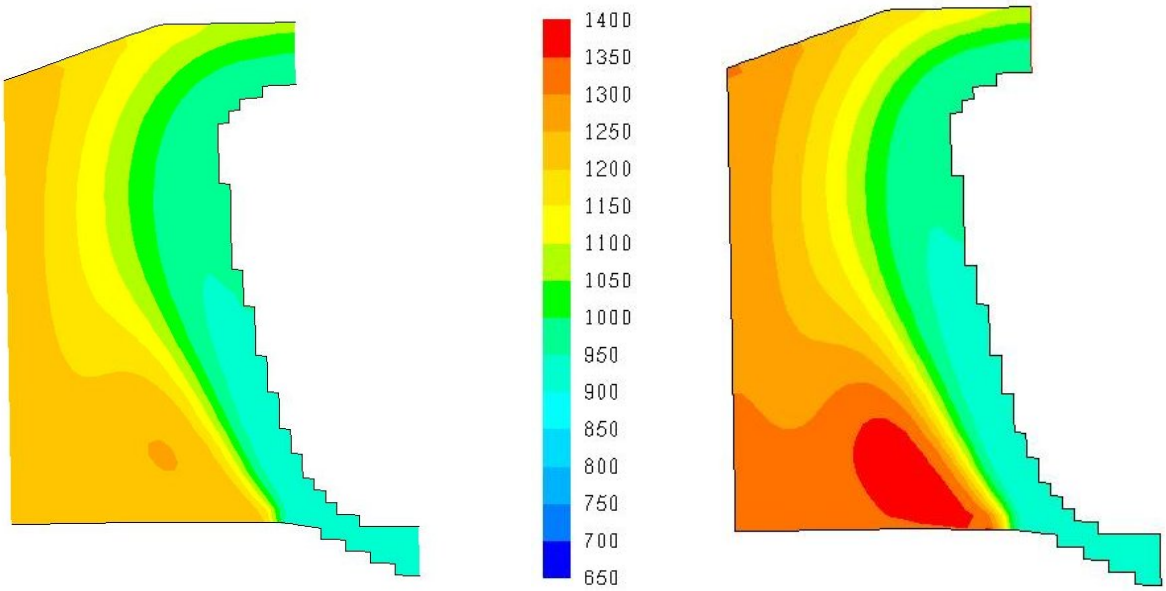

Figure 4.9: Temperature (in K, primary different scale) for initial source term from LPSC (left) and for source term from KIT (right) with all other parameter of the model are unchanged

We then start looking at the sensitivity to the heat source. The difference between the two source terms seems negligible (Figure 4.6) but it has a non-negligible effect on the temperature (Figure 4.9) with higher temperature in the recirculation and axis zone of the core

when using the source term from KIT coupled simulation. This comparison give an order of magnitude of the effect of the source term, with temperature differences of 100° in stagnation zones, but of course much less in the main salt flow. All other sensitivity studies have been done with the source term provided by LPSC (Figure 4.2).

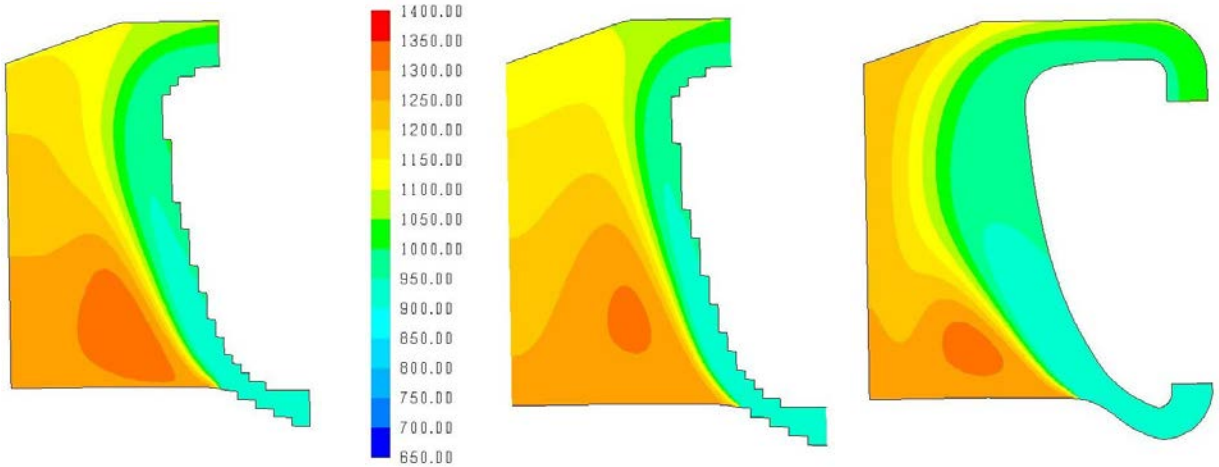

Figure 4.10: Temperature (in K, same scale) for finer mesh (2 time finer on left, 4 time finer on the middle), and exact geometry with optimal mesh and same turbulence model (right) than figure 4.8 on the right

Figure 10 summarizes the mesh sensitivity results done by mesh refinement in all the geometry: using this almost optimized geometry, the thermal field is not so sensible to the mesh thickness: the maximum temperature is inside the recirculation and the wall is well cooled with temperature gaps lower than 30° in all cases. Only the temperature near the top reflector depends on the mesh thickness with local gaps over 50°. We will learn from 3D results that it does not mean that thermal hydraulic calculations are precise using coarse mesh. But for this optimized geometry in 2D, the gap between thermal fields from different codes cannot be explain by the mesh precision.

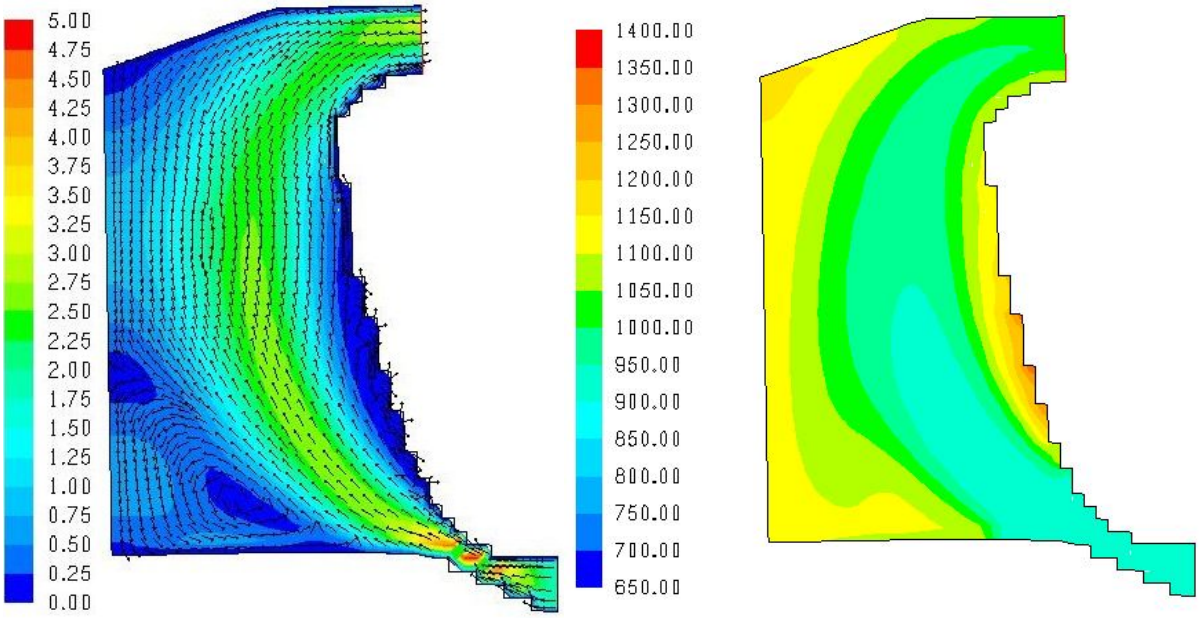

Figure 4.11: Velocity (m/s) and temperature (K, same scale than previous) with same model but with mesh refinement only near the wall

We also checked the effect of mesh refinement only near walls. The effect is to create a flow detachment which induces as usually a hot region (Figure 4.11). Another consequence of this detachment is to push the flow in the centre of the core and decrease the size of back flow.

Looking at the temperature the consequence is an increase of the hottest temperature close to the top reflector and a decrease of the hottest temperature near the bottom reflector. Despite the previous remark about the mesh sensitivity, this result show that the exact flow shape and temperature are still very sensible to shape and mesh definition especially close to the walls. Here “exact” mean at a local precision below 100° which is needed for any technological conclusion.

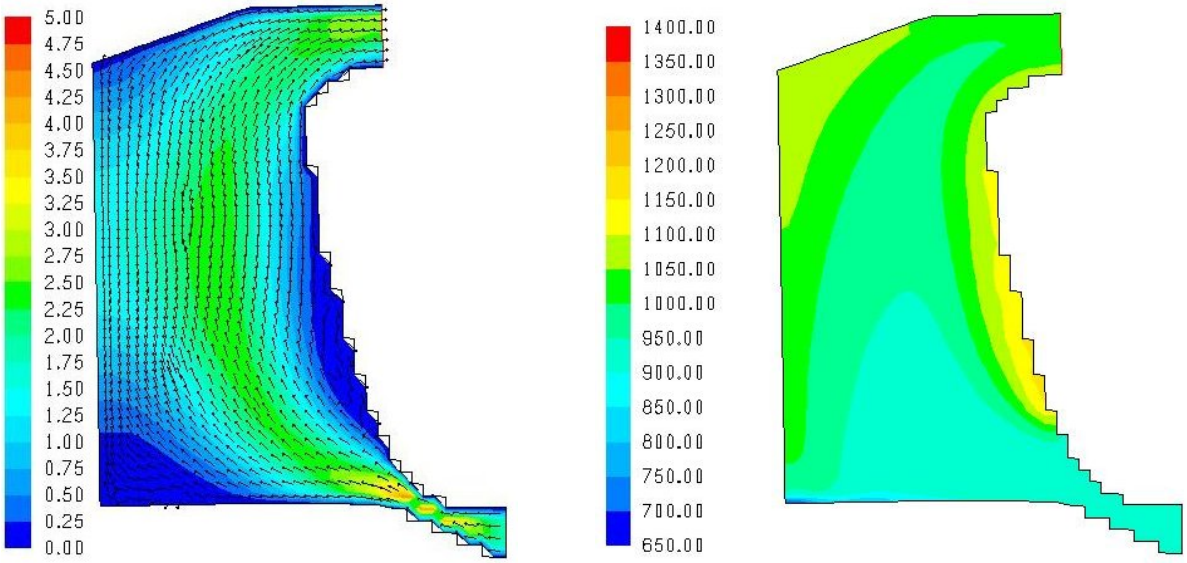

Figure 4.12: Velocity (m/s) and temperature (K, same scale than previous) with same model and mesh than results from KIT, and using « PRESTO » interpolation scheme for pressure

The last sensitivity test was done on pressure interpolation scheme. By changing only the pressure interpolation scheme and use the so call “PRESTO” method [Launder, 1989], which is similar to the staggered-grid schemes used with structured meshes, we get results (Figure 4.12) qualitatively close to KIT results. The flow rate is more homogeneous in the horizontal middle plane, with a much more smooth velocity and temperature repartition (much smaller gradients). The maximum temperature is close to the wall, which is not the case in KIT result, but on the axis of the core, the temperature increases from bottom to the top, with a highest value on top reflector like in KIT result. The quantitative differences between this last and KIT results, mainly the lower temperature in top region and outlet of the core may be due to a difference in the heat source.

Some other sensitivity studies have been done to compare standard and realizable k – epsilon models and k-omega turbulence model in next chapter. But in the present case the turbulence models are the same in both cases.

We can conclude from this first comparison that the differences are mainly due to the interpolation scheme and to the heat source. Temperature gap due to mesh thickness are not so high in this 2D case on a roughly optimized shape of the core.

4.3.3. Benchmark on the 2D geometry

The results obtained by LPSC and INOPRO IAO for the exact geometry of the 2D benchmark, and same heat source, are presented here.

On Figure 4.13 is presented an example of velocity field. This is a result obtain on the 2D benchmark geometry, by k-epsilon realizable turbulence model. This result, as well as all the other results in this section, doesn't depend on the cells thickness of the mesh. The main flow is going up close to the core wall, and a recirculation (the salt flow goes down) takes place in the bottom part of the centre of the core. As it was already emphasize, this is a bad design result. But the present results

and discussions are only for benchmark purpose. Then we will compare the results without taking care of the high temperature or recirculation phenomenon: this geometry is not optimum. The horizontal line corresponds to the axis along which are taken the temperature and velocities presented on the following graphs (Figure 4.14 et Figure 4.15).

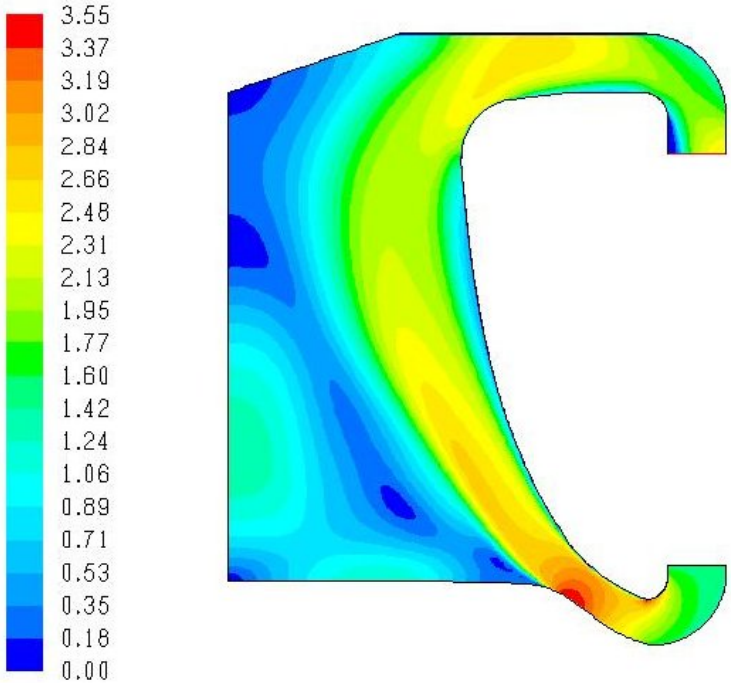

Figure 4.13: Velocity (m/s) from 2D benchmark simulation of INOPRO IAO

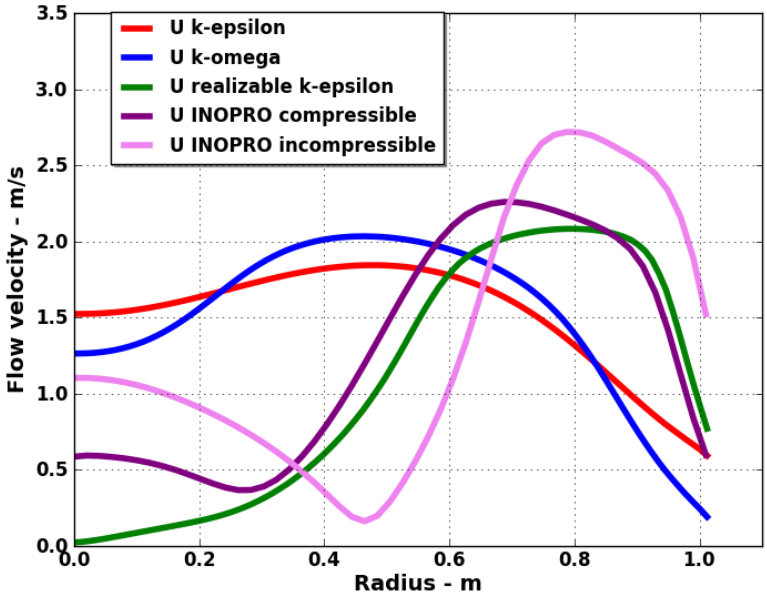

Figure 4.14: Velocities (m/s) along the axis of figure 4.12. Comparison of results from LPSC for standart k-epsilon model (red) for k-omega model (blue), and for realizable k-epsilon model (green), and INOPRO results for realizable k-epsilon using compressible density model (purple) and constant density (pink)

The results compared on the following figures are from:

- LPSC simulation using OpenFoam and standart k-epsion turbulence model (red)
- LPSC simulation using OpenFoam and standart k-omega turbulence model (blue)
- LPSC simulation using OpenFoam and realizable [Shih, 1995] k-epsilon turbulence model (green),

- INOPRO IAO Simulation using Fluent and realizable k-epsilon model with constant density (pink),
- INOPRO IAO Simulation using Fluent and realizable k-epsilon model with density depending on salt temperature (purple).

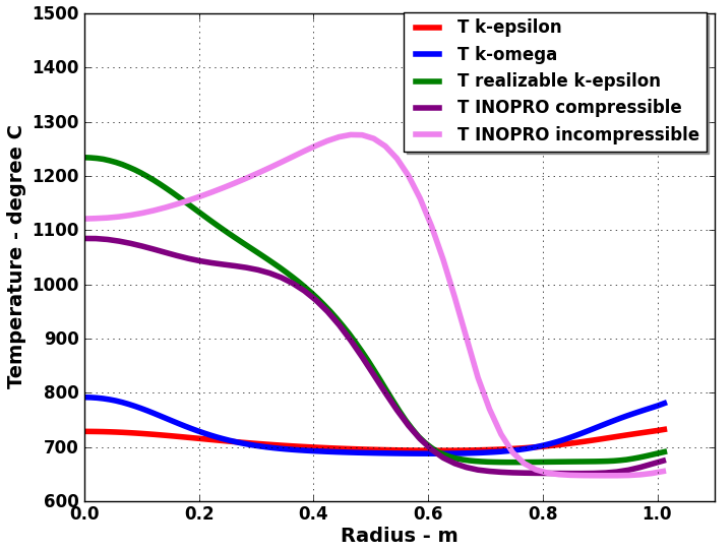

Figure 4.15: Temperature (°C) along the axis of figure 4.12. Comparison of results from LPSC for standard k-epsilon model (red) for k-omega model (blue), and for realizable k-epsilon model (green), and INOPRO results for realizable k-epsilon using compressible density model (purple) and constant density (pink)

The two comparable results from LPSC and INOPRO IAO use realizable k-epsilon which is the most precise model for these flow conditions, following previous benchmarking done for pressure drop inside tubes.

The dispersion of the results is quite large for temperatures as well as for velocities. But the results from the two realizable k-epsilon models, from LPSC and INOPRO IAO are similar. For these two results only:

- A difference takes place near the symmetry axis and is due to the exact position of the recirculation.
- In INOPRO IAO case the velocity on the axis (centre of the core) is not null because the recirculation is a bit higher, inducing higher temperature,
- In LPSC case the velocity is almost zero on the axis : the stagnation point corresponding to the top of the recirculation is located exactly on the horizontal axis,
- The temperatures near the core wall are exactly same,
- The velocities near the core wall are almost same.

In case of standard k-epsilon and standard k-omega model, the velocities are more homogeneous. Results for more viscous flow may be similar to these one. This induces a quite large temperature gap of 300° between standard turbulence models and realizable k-epsilon.

The effect of pressure interpolation on Fluent results has also been checked even it is not shown the graphs. With the fine mesh used for these last calculations, the pressure interpolation scheme has very small influence on the results. The purple curve of Figure 4.15 changes when using presto interpolation are less than 20°.

Our conclusions of these 2D benchmark are the following:

- By choosing this first roughly optimized curved shape of the core wall, there are still hot « spot ». But it was possible to compare the results from three teams using three different codes and more turbulence models,

- The change in heat source due to coupled calculation induce temperature gaps of 100° inside stagnation zone of the salt flow, but much less in main flow,
- The effect of mesh thickness seems low (local temperature gap of 50°, less in main flow), but this is a specific result obtained on this roughly optimized 2D geometry and it should not be generalized: a local mesh refinement induce large temperature gap near the blanket wall,
- The effects of turbulence model choice (standard k – epsilon or k- omega versus realizable k – epsilon) or pressure interpolation ("presto" versus standard order 2 interpolations) are a strong modification of the flow shape with or without a recirculation over the bottom reflector. Of course this change in flow velocities induces large temperature gap of more than 200° inside the recirculation and much lower gap in the main flow.
- The two results from LPSC and INOPRO IAO with realizable k – epsilon turbulence model were obtained on fine mesh: they are not sensible to the mesh size and interpolation scheme for pressure. Some local temperature gap of 100° still exists inside the flow recirculation. The differences are much lower in large zone especially on all the walls.

4.3.4. Benchmark on the 3D geometry

Two partners have performed calculations on the T&H 3D benchmark: LPSC and INOPRO IAO.

Following 2D benchmark results and preliminary 3D benchmark results on same geometry, some 3D instabilities in the flow were founded. These instabilities are transient, they then avoid any stationary comparison which are planned for the benchmark. As a consequence we had to performed more optimisation work to do the benchmark on a more optimized shape which allows a more stable salt flux. The final geometry of the 3D benchmark is the optimized geometry described in chapter 1.2.1 (Figure 4.3). In this geometry the curved wall of the core has an horizontal plane symmetry.

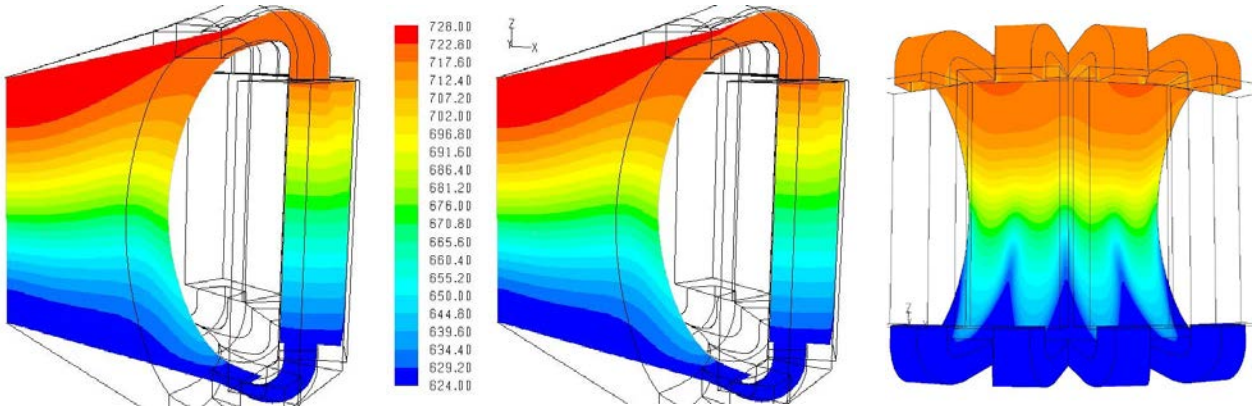

Figure 4.16: Temperature (°C) in vertical plane (left) and on core wall (right) for optimized solution

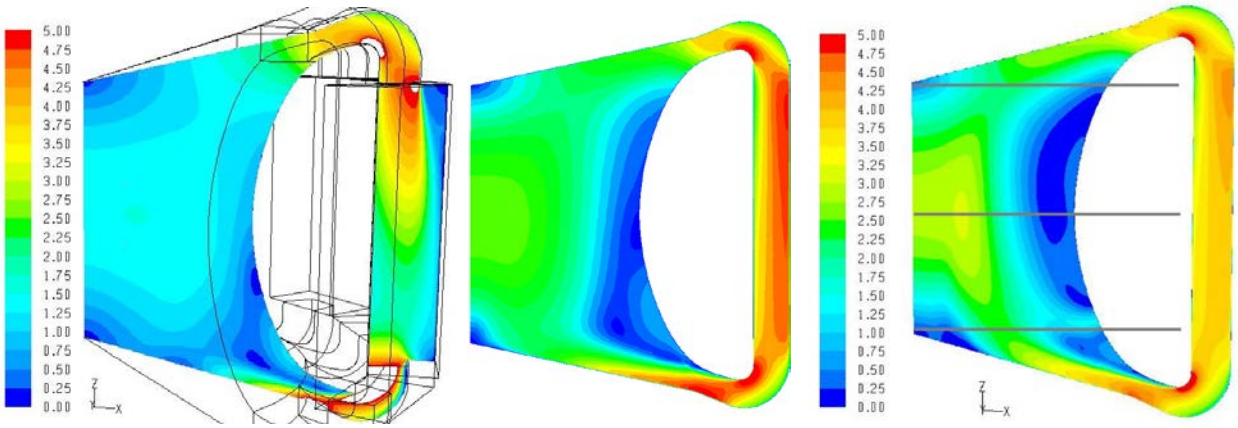

Figure 4.17: Velocities (m/s) in a vertical plane with the full exchanger (left) with simplified exchanger for the benchmark (middle from INOPRO IAO and right from LPSC)

The first results (Figure 4.16) correspond to the optimized shape with full heat exchangers (Figure 4.3 left). It is given to show the result of the optimization and will be discussed in another report dealing with the design.

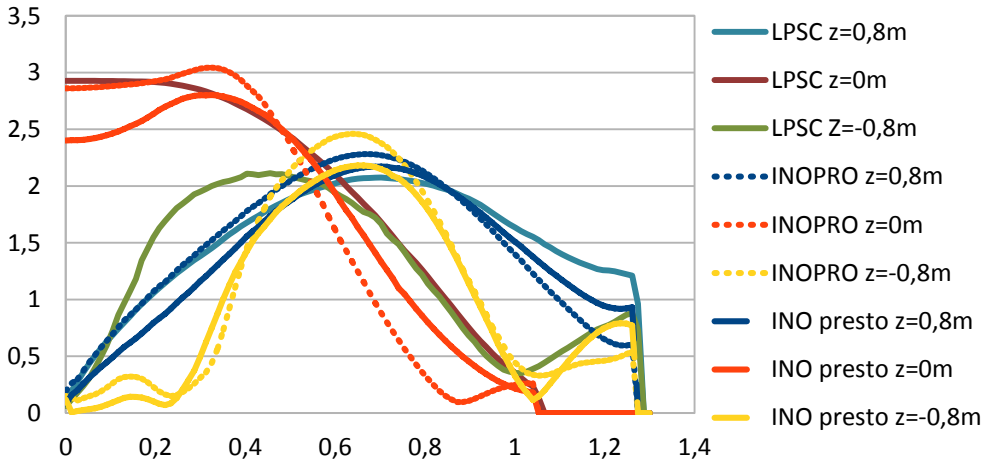

Figure 4.18: Velocities (m/s) along horizontal axis in plane AA' of figure 4 from INOPRO IAO with Fluent (dashed lines) and LPSC with OpenFoam (continuous lines)

The benchmark is done on the geometry with simplified exchanger zone (Figure 4.3 right). The flow is less homogeneous (Figures 4.16 and 4.17) showing the strong sensitivity to the inlet flow repartition, then to technological choices for exchanger or pumping. These results will also be discussed in the sensitivity studies of deliverable 2.3.

The benchmark results are given on Figure 17 middle and right for the qualitative comparison of flow velocities in vertical planes, but more quantitative comparisons are done on graphs (see Figures 4.18 and 4.19) along horizontal axis in the same plane at three vertical position (Figure 4.17 on the right).

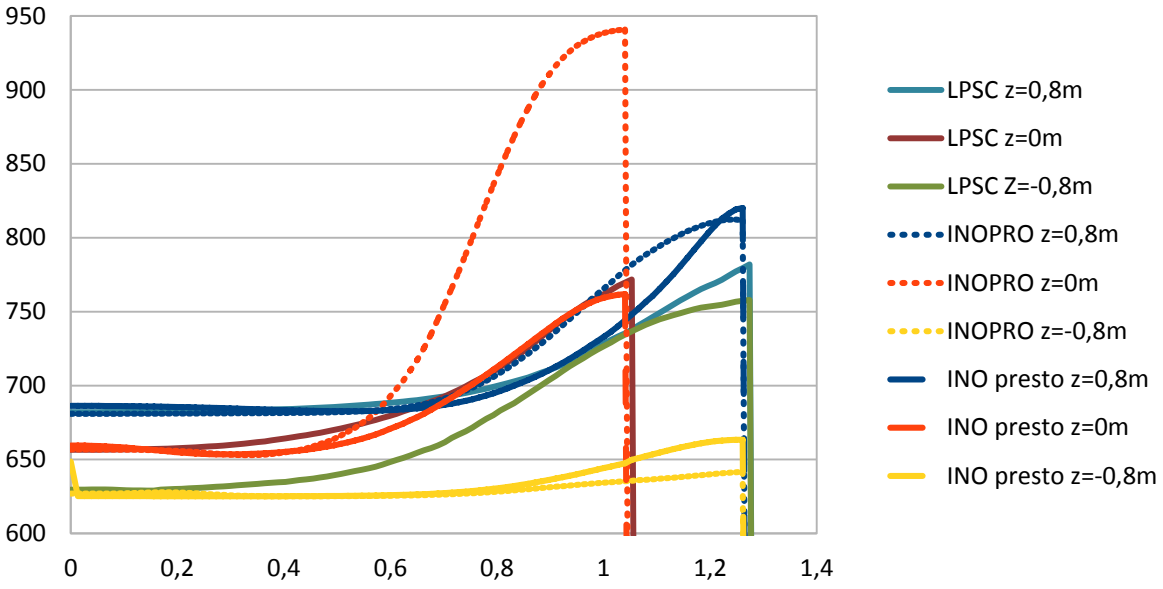

Figure 4.19: Temperature (°C) along horizontal axis in plane AA' of figure 4 from INOPRO IAO with Fluent (dashed lines) and LPSC with OpenFoam (continuous lines)

The main differences between the graphs of velocities are:

- The stagnation zone (low velocity) in the middle part of the core (left of the graph) along the bottom reflector (yellow curves for z=-0.8m) is larger in INOPRO IAO results,
- A flow more concentrated in the middle part of the core in INOPRO IAO results, inducing a larger stagnation zone along the blanket wall. We can see on orange graphs at "z=0m" that this difference is much lower between INOPRO results using presto pressure interpolation or Reynolds stress model and LPSC results.

The consequences on temperature fields are the following:

- Near the inlet (yellow curves) a temperature gap exists between INOPRO and LPSC results. It is due to a less stable flow in the LPSC result with more 3D effects inducing differences between the flow shape and recirculation in each injection.
- In the middle part of the core (orange curves), the stagnation zone close to the wall induce a local increase of temperature. There is a large temperature gap between INOPRO result with standard pressure interpolation and the other results from LPSC and INOPRO results with presto pressure interpolation or Reynolds stress model. The gap between these three last cases is almost null showing that the presto interpolation (INOPRO case with fluent) is probably better when recirculation and high temperature gradients appear in the flow.
- Everywhere else (centre, top and outlet of the core) the differences are smaller with temperature gaps lower than 50°C between all models.

The conclusions of the 3D benchmark are the following:

- The four results which had been compared were done with OpenFoam and Fluent. The results are qualitatively similar with a recirculation zone still existing near the wall and another stagnation zone in the bottom centre of the core.
- Near the inlets some differences exist in the velocity fields, inducing local temperature gaps. They are mainly du to 3D instabilities which are limiting the convergence of such stationary simulations. We have to note that the objectives of the design work are to avoid such instabilities.
- A large temperature gap near the blanket wall exists between one of the result, using k epsilon model with standard pressure interpolation and the other. The three other results from OpenFoam and fluent, and from two different models from fluent are very similar with almost no temperature gap.
- The choice of the benchmark geometry also shows that the flow is still very sensitive to the injection shape. Then it will be necessary to fixed technological choice of pumping and heat exchanger before working further on shape optimization. This point will be discussed in following report on design.

4.4. TH Benchmarks conclusions

The main conclusion of the benchmark is that the two different codes used to do both 2D and the 3D benchmarks give similar qualitative results, and quantitative results are very close outside the 3D instabilities. The temperature precision isn't good inside the instabilities, with temperature gaps as large as 100°, but quite good outside the instabilities with temperature gaps lower than 50° even inside stagnation zones. As soon as these instabilities are transient, it is normal that there are not well simulated using a stationary assumption. Then the main problem is the following: are we able to know, using such stationary simulations if some 3D transient instabilities exist or not in the calculated flow ? Buy looking at the benchmark results the answer may be positive: instabilities exist when and where there are gaps between the results from different models. But this can actually be checked only by transient LES simulation.

Another remark may be to keep in mind the final objectives of such simulation, which are core design to obtain a stable and homogeneous salt flow. In such case, when (and where in the benchmark results) there is no instabilities or recirculations, the three models give similar results. Then the main objective of the benchmark, before looking at precise temperature comparisons, is to check the existence and the position of recirculations. With this objective, the conclusions are the following:

- 2D results from KIT (on SIMMER) and INOPRO IAO (on FLUENT) are quite similar when using the same mesh, same heat source, and standard k – epsilon turbulence model, without any recirculation in core centre,
- A recirculation in core centre exists when using realizable k – epsilon turbulence model in any of the tested cases (LPSC with OpenFoam, INOPRO IAO with fluent, any size mesh and any pressure interpolation scheme), and doesn't exist when using standard k – epsilon model,
- Then, the choice of the turbulence model is important,
- Using Fluent, « presto » pressure interpolation or Reynolds stress model gives more precise results as soon as there are some recirculations,
- The two simulation using Fluent (from INOPRO IAO) and OpenFoam (from LPSC) give similar results in 2D and 3D outside local instabilities near injection.

The design results and the sensitivity to injection shape, working point of the core will be discussed in the following report.

5. Conclusions

To be completed

6. References

Alcaro F.,Dulla S.and Ravetto P., *"Neutronic Evaluations for the EVOL Molten Salt Reactor"*, Transactions of the American Nuclear Society, 108 (2013)

Aufiero M., A. Cammi, C. Fiorina, J. Leppanen, L. Luzzi, M.E. Ricotti, *"An extended version of the SERPENT-2 code to investigate fuel burn-up and core material evolution of the Molten Salt Fast Reactor"*, Journal of Nuclear Materials, http://dx.doi.org/10.1016/j.jnucmat.2013.06.026 (2013a)

Aufiero M., Brovchenko M., A. Cammi, Clifford I., Geoffroy O., Heuer D., Laureau A., Losaa M.,L. Luzzi, Merle-Lucotte E., M.E. Ricotti, Rouch H., *"Calculating the effective delayed neutron fraction in the Molten Salt Fast Reactor: analytical, deterministic and Monte Carlo approaches"*, submitted to Annals of Nuclear Energy (2013b)

Boussier H. et al., *"The Molten Salt Reactor in Generation IV: Overview and Perspectives"*, Proceedings of the Generation4 International Forum Symposium, San Diego, USA (2012)

Briesmeister J.F., *"MCNP4B-A General Monte Carlo N Particle Transport Code"*, Los Alamos Lab. report LA-12625-M (1997)

Brovchenko M. et al., *"Preliminary safety calculations to improve the design of Molten Salt Fast Reactor"*, Proceedings of the International Conference PHYSOR 2012 Advances in Reactor Physics Linking Research, Industry, and Education, Knoxville, Tennessee, USA (2012)

Doligez X. Heuer D., Merle-Lucotte E. et al., *"Numerical tools for Molten Salt Reactors simulations"*, Proceedings of the International Conference Global 2009 - The Nuclear Fuel Cycle: Sustainable Options & Industrial Perspectives, Paris, France (2009)

Doligez X., "*Influence du retraitement physico-chimique du sel combustible sur le comportement du MSFR et sur le dimensionnement de son unité de retraitement*", PhD Thesis Grenoble Institute of Technology (Grenoble INP), France (2010)

Dulla S., Ravetto P., and Rostagno M.M., "*Neutron kinetics of fluid–fuel systems by the quasi-static method*", Ann. Nucl. Energy, 31, 1709-1733 (2004) POLITO 6

Dulla S., "*Models and methods in the neutronics of fluid fuel reactors*", PhD Thesis, Politecnico di Torino (2005) POLITO 5

Eastwood J. W. and Morgan J. G., "*The FISPACT-II(12) Software Specification Document*", Technical Report CEM/100421/SD/2 Issue 4, Culham Electromagnetics Ltd (May 2011) POLITO 3

Fiorina, C., Cammi, A., Krepel, J., Mikityuk, K., Ricotti, M.E., 2012a. "Preliminary analysis of the MSFR fuel cycle using modified-EQL3D procedure", Proceedings International Conference ICONE, Anaheim, US, (2012)

Fiorina, C., Aufiero, M., Cammi, A., Guerrieri, C., Krepel, J., Luzzi, L., Mikityuk, K., Ricotti, M.E., 2012b. *"Analysis of the MSFR core neutronics adopting different neutron transport models"*, Proceedings International Conference ICONE, Anaheim, US, (2012)

Fiorina C., Manuele Aufiero, Antonio Cammi, Fausto Franceschini, Jiri Krepel, Lelio Luzzi, Konstantin Mikityuk, Marco Enrico Ricotti, *"Investigation of the MSFR core physics and fuel cycle characteristics"*, Progress in Nuclear Energy http://dx.doi.org/10.1016/j.pnucene.2013.06.006 (2013)

Forsberg C.W. et al., *"Liquid Salt Applications and Molten Salt Reactors"*, Revue Générale du Nucléaire N° 4/2007, 63 (2007)

Fridman E. and Leppanen J., "*On the Use of the Serpent Monte Carlo Code for Few-group Cross Section Generation*", Ann. Nucl. Energy, 38, 1399-1405 (2011)

Frima L.L.W., *"Burnup in the Molten Salt Fast Reactor (MSFR)"*, Master Thesis, Technical University of Delft (2013)

GIF (Generation IV International Forum), *"Annual report 2008"*, http://www.gen-4.org/PDFs/GIF_2008_Annual_Report.pdf, 36-41 (2008)

GIF (Generation IV International Forum), *"Annual report 2009"*, http://www.gen-4.org/PDFs/GIF-2009-Annual-Report.pdf, 52-58 (2009)

HELIOS Methods, Studsvik Scandpower (Nov. 2003)

Heuer D., Merle-Lucotte E. et al., *"Simulation Tools and New Developments of the Molten Salt Fast Reactor"*, Contribution A0115, Proceedings of the European Nuclear Conference ENC2010, Barcelona, Spain (2010) [ENC2010]

Ignatiev V., Feynberg O., Merzlyakov A. et al., "Progress in Development of MOSART Concept with Th Support", Proceedings of ICAPP 2012, Paper 12394 Chicago, USA (2012)

Leppanen J., "*Development of a New Monte Carlo Reactor Physics Code*", Ph.D. Thesis, Helsinki University of Technology, VTT Publications 640 (2007)

Launder B. E., Reece G. J., and Rodi W., "*Progress in the Development of a Reynolds-Stress Turbulence Closure*", J. Fluid Mech., 68(3):537-566 (April 1975)

Launder. B. E., "*Second-Moment Closure: Present... and Future?*", Inter. J. Heat Fluid Flow, 10(4):282-300 (1989)

Mathieu L., *"Cycle Thorium et Réacteurs à Sel Fondu: Exploration du champ des Paramètres et des Contraintes définissant le Thorium Molten Salt Reactor"*, PhD Thesis, Grenoble Institute of Technology, France – In french (2005)

Mathieu L., Heuer D., et al., *"The Thorium Molten Salt Reactor: Moving on from the MSBR"*, Prog in Nucl Eng, 48, 664-679 (2006)

Mathieu L., Heuer D., Merle-Lucotte E., et al., *"Possible Configurations for the Thorium Molten Salt Reactor and Advantages of the Fast Non-Moderated Version"*, Nucl. Sc. and Eng., 161, 78-89 (2009)

Merle-Lucotte E., Heuer D. et al., *"Introduction of the Physics of Molten Salt Reactor"*, Materials Issues for Generation IV Systems,NATO Science for Peace and Security Series - B, Editions Springer, 501-521 (2008)

Merle-Lucotte E., Heuer D. et al., *"Minimizing the Fissile Inventory of the Molten Salt Fast Reactor"*, Proceedings of the Advances in Nuclear Fuel Management IV (ANFM 2009), Hilton Head Island, USA -2009)

Merle-Lucotte E., Heuer D. et al., *"Optimizing the Burning Efficiency and the Deployment Capacities of the Molten Salt Fast Reactor"*, Proceedings of the International Conference Global 2009 - The Nuclear Fuel Cycle: Sustainable Options & Industrial Perspectives, Paper 9149, Paris, France (2009)

Nuttin A., *"Potentialités du concept de réacteur à sels fondus pour une production durable d''énergie nucléaire basée sur le cycle thorium en spectre épithermique"*, PhD Thesis, Université Joseph Fourier - Grenoble I, France – In french (2002)

Nuttin A, Heuer D., et al., *"Potential of Thorium Molten Salt Reactors"*, Prog. in Nucl. En., 46, 77-99 (2005)

Patankar S.V., "*Numerical Heat Transfer and Fluid Flow*". Hemisphere, Washington, DC (1980)

Rachamin, R.; Wemple, C.; Fridman, E., *"Neutronic analysis of SFR core with HELIOS-2, SERPENT, and DYN3D codes"*, DOI-Link: http://dx.doi.org/10.1016/j.anucene.2012.11.030, Annals of Nuclear Energy 55 (2013)

Renault C. et al., "The Molten Salt Reactor (MSR) in Generation IV: Overview and Perspectives", http://www.gen-4.org/GIF/About/documents/30-Session2-8-Renault.pdf, Proceedings of the GIF Symposium 2009, Paris, France (2009)

Rimpault, G., Plisson, D., Tommasi, J., Jacqmin, R., Rieunier, J., Verrier, D., Biron, D., *"The ERANOS code and data system for fast reactor neutronic analyses"*, Proceedings International Conference PHYSOR 2002, Seoul, Korea (2002)

Shih T.-H., Liou W. W., Shabbir A., Yang Z., and Zhu J., « A New k-epsilon Eddy-Viscosity Model for High Reynolds Number Turbulent Flows - Model Development and Validation » Computers Fluids, 24(3):227-238 (1995)

Van der Linden E. "*Coupled neutronics and computational fluid coupled neutronics and computational fluid dynamics for the Molten Salt Fast Reactor*", Master Thesis, Technical University of Delft (2012)

Villarino E.A., Stammler R.J.J., Ferri A. and Casal J.J., "*HELIOS: angularly dependent collision probabilities*", Nuclear Science and Engineering 112 (1992)

Warmoeskerken M.M.C.G. and Janssen L.P.B.M., "*Transport Phenomena Data Companion*", VSSD, Delft, Netherlands (2012)